Site M0059[1]

T. Andrén, B.B. Jørgensen, C. Cotterill, S. Green, E. Andrén, J. Ash, T. Bauersachs, B. Cragg, A.-S. Fanget, A. Fehr, W. Granoszewski, J. Groeneveld, D. Hardisty, E. Herrero-Bervera, O. Hyttinen, J.B. Jensen, S. Johnson, M. Kenzler, A. Kotilainen, U. Kotthoff, I.P.G. Marshall, E. Martin, S. Obrochta, S. Passchier, N. Quintana Krupinski, N. Riedinger, C. Slomp, I. Snowball, A. Stepanova, S. Strano, A. Torti, J. Warnock, N. Xiao, and R. Zhang[2]

Chapter contents

[1] Andrén, T., Jørgensen, B.B., Cotterill, C., Green, S., Andrén, E., Ash, J., Bauersachs, T., Cragg, B., Fanget, A.-S., Fehr, A., Granoszewski, W., Groeneveld, J., Hardisty, D., Herrero-Bervera, E., Hyttinen, O., Jensen, J.B., Johnson, S., Kenzler, M., Kotilainen, A., Kotthoff, U., Marshall, I.P.G., Martin, E., Obrochta, S., Passchier, S., Quintana Krupinski, N., Riedinger, N., Slomp, C., Snowball, I., Stepanova, A., Strano, S., Torti, A., Warnock, J., Xiao, N., and Zhang, R., 2015. Site M0059. *In* Andrén, T., Jørgensen, B.B., Cotterill, C., Green, S., and the Expedition 347 Scientists, *Proc. IODP,* 347: College Station, TX (Integrated Ocean Drilling Program).
doi:10.2204/iodp.proc.347.103.2015
[2] **Expedition 347 Scientists' addresses.**

Introduction

During Integrated Ocean Drilling Program (IODP) Expedition 347, cores were recovered from five holes at Site M0059 (Little Belt), with an average site recovery of 87.79%. The water depth was 37.1 m, with a tidal range of <10 cm. Existing data sets, including seismic reflection profiles, were evaluated prior to each site to guide the initial drilling with an anticipated lithologic breakdown. The total time spent on station was 12.05 days.

Operations

Transit to Hole M0059A

At 1615 h on 12 September 2013, the *Greatship Manisha* set sail from Kiel, Germany, and headed for the first Expedition 347 coring site (M0059) in Little Belt (proposed Site BSB-3). The vessel arrived on site at 0000 h on 13 September. Setup and preparation of the drill floor commenced and continued throughout the day until 1530 h, when coring operations began (Table **T1**).

Hole M0059A

The first piston corer system (PCS) core from Hole M0059A was recovered to deck at 1920 h on 13 September 2013. Piston coring was carried out using 3.3 m strokes. However, because of a dense sand lithology at 83.2 meters below seafloor (mbsf), it was necessary to switch from the PCS to the rotary extended coring system (ECS). Coring continued through 14 September. On core Run 29 (86.7 mbsf; 15 September), the lower section of the barrel was lost because of shearing of the spring spline. Attempts were made to recover the core barrel, unfortunately without success. The hole was terminated at 0900 h on 15 September.

Twenty-nine coring attempts were made in Hole M0059A to a maximum depth of 90.2 mbsf. Recovery for the hole was 94.68%.

Hole M0059B

The vessel moved under dynamic positioning (DP) with the drill string suspended in the water column to Hole M0059B, 20 m east-northeast of Hole M0059A, arriving on station at 1300 h on 15 September 2013. Operations commenced immediately. To create a

doi:10.2204/iodp.proc.347.103.2015

composite record with Hole M0059A, noncoring assembly (NCA) drilling was conducted to 60 mbsf (having recovered almost 100% in the upper section of Hole M0059A) before recommencing piston coring. Damage to seals was observed when recovering core Runs 1 and 5. American Petroleum Institute (API) pipe was tripped to identify and remove the source of seal damage. Coring then continued until the core barrel became stuck near the mud valve, which was not fully opening. Coring continued following repairs and alternated between the PCS, ECS, and rotating core barrel as high sand concentrations and varying lithologies were encountered.

Coring operations in this hole continued through 17 September. A harder till lithology was encountered, and the main polycrystalline diamond cutting bit was replaced with a six-cone Rock Roller core bit and tricone insert bit. Open holing continued until drilling parameters indicated softer lithologies. Where these softer lithologies were encountered, spot coring using the push coring assembly or hammer sampler (HS) was conducted. The hole was terminated at 204.03 mbsf at 1355 h on 18 September upon advancing into chalk basement, after which preparations were made for downhole logging.

Downhole logging operations were run by the Petrophysics Staff Scientist and the Weatherford Engineer and Technician. Operations commenced at 1811 h on 18 September using the compact gamma ray and compact induction tools. Because of loss of tension, the maximum depth reached was 72.5 mbsf. The tool string was then run up and reached the seafloor at 1840 h. After pumping, a second attempt was made. However, the depth reached was restricted to 58 mbsf as tension was again lost. Following this, the decision was made to run in with pipe to 175 mbsf and complete a wiper trip before tripping pipe to 90 mbsf. The tools were again run into the hole at 2305 h at a speed of 9 m/min. Tension was lost at 183.5 mbsf, and the up run began at 2340 h. The tools were recovered back to the rig floor at 0027 h on 19 September. As high tensions with up to 650 lb overpull were observed during the uplog, the decision was taken to set the pipe back to 20 mbsf and run in the hole with a second tool string. At 0207 h, a further run was attempted using the compact gamma ray, compact spectral gamma, and compact sonic tools. The string was run downhole at a speed of 10 m/min, reaching the end of the pipe at 0211 h and the total depth at 0222 h. Tension was lost at 73.5 mbsf, and the up run began at 0230 h. By 0248 h, the tools were recovered back to the rig floor, the drill string was pulled, and logging operations ended at 0320 h.

The drill floor was then prepared for transit, and the vessel departed for Hole M0059C at 0600 h.

A total of 30 coring attempts were made in Hole M0059B, extending to a maximum depth of 204.03 mbsf (including six open-holing runs covering 155.6 m). The recovery for this hole was 56.51%.

Hole M0059C

The vessel then moved 40 m west-northwest under DP to Hole M0059C on the morning of 19 September 2013, establishing position at 0620 h. During the short transit, work was undertaken to check and refit the transponder device on the seabed frame following failure in Hole M0059B (possibly as a result of sinking into the sediment/being covered in drill cuttings).

Following this, pipe was run at station in Hole M0059C, where an initial attempt at passing pipe through the seabed template resulted in a bent pipe. Following removal of this pipe, the vessel moved 5 m in order to enter the seabed template correctly and establish the hole. Coring operations on this microbiology-dedicated hole commenced with the first core recovered to deck at 0850 h. The coring rate was moderated following instructions from the microbiologists on shift to ensure appropriate time for processing the microbiology samples and ensure there was no backlog of cores waiting to be processed.

Coring operations continued through 20 September. During the first part of the day, the PCS was used to recover mud/clay lithologies. Upon completion of the microbiology sampling at 83 mbsf (at 1255 h on 20 September; dictated by lithology), the underlying till material was then sampled by drilling down using the NCA and HS to recover material for optically stimulated luminescence (OSL) samples at 3 m intervals. This approach was used through 22 September, with the drilling/coring approach driven by the material encountered.

On 21 September, microbiology samples were removed from the vessel by European Consortium for Ocean Research Drilling Science Operator personnel and transferred to shore on board the Danish Naval Homeguard Vessel (which brought visiting journalists).

Hole M0059C was terminated at 158.10 mbsf at 0535 h on 22 September.

A total of 84 coring attempts were made in Hole M0059C to a maximum depth of 158.10 mbsf. Twenty-four of these involved open holing, covering 52.91 m. Hole recovery was 97.82% with these open-holed sections discounted.

Transit to Site M0059 for second phase of sampling

Following completion of Hole M0067B, the vessel returned to Site M0059 to resample at this location to complement the samples already collected and improve recovery rates in the lower sections. The vessel arrived back at Site M0059 at 0340 h on 29 October 2013 and commenced coring operations.

Hole M0059D

Coring in Hole M0059D commenced at 0350 h on 29 October 2013 and ran smoothly throughout the day, with a total of 27 piston cores and one hammer sample recovered before midnight. On recovery of sand at the base of the hole (86.60 mbsf), the hole was ended and the drill floor was readied to bump over to Hole M0059E.

A total of 28 cores were recovered in Hole M0059D to a depth of 86.57 mbsf. Recovery for the hole was 99.9%.

Hole M0059E

Coring commenced in Hole M0059E on 30 October 2013 at 0028 h and continued successfully with good recovery of the mud lithology throughout the morning. At 1330 h, the wireline rope parted on retrieving the PCS. The barrel became jammed in the bottom-hole assembly because of a broken seal. Fishing attempts failed, and the pipe was tripped. The core was recovered to deck and operations recommenced with six more cores recovered before midnight.

On 31 October, PCS coring continued through the morning until Run 27 at 0415 h. The subsequent core Runs 28–37 used a combination of ECS and hammer sampling in an attempt to maximize recovery. The hole was terminated at 100.80 mbsf following issues with hole stability. This hole was considered an important logging target, so to minimize further damage to the hole it was terminated at this depth, and setup preparations for downhole logging commenced at 1700 h.

Logging operations started in Hole M0059E on 31 October at 1800 h with rigging up the Weatherford logging setup after the drill pipe was tripped to 15 mbsf. The first tool string comprising total gamma radiation and induction tools reached ~70 mbsf, from where an uplog was performed. The second tool string comprising total gamma radiation and microimager tools and the last tool string comprising total gamma radiation, spectral gamma radiation, and sonic tools reached 60 mbsf, from where an uplog was started. Logging operations were finished at 2130 h.

A total of 37 cores were collected in Hole M0059E to a depth of 100.80 mbsf. Hole recovery was 90.02%. Completion of this hole marked the end of coring operations for Expedition 347.

Lithostratigraphy

Cores were recovered from Holes M0059A–M0059E. The sediments are slightly disturbed in the uppermost 85 mbsf, and lithologic changes deeper than this point presented coring problems, resulting in major core disturbance and low core recovery (see **"Operations"**). These issues are in part due to piston coring for the uppermost 85 mbsf before a switch to a combination of open hole and hammer sampling because the piston corer could no longer penetrate the lithology, which consisted of successions of coarse-grained diamicton and gravely sands. Deeper than 169 mbsf, coring encountered limestone bedrock, and Hole M0059B was terminated (204 mbsf). The dominant lithofacies in the uppermost 80 mbsf are clay deposits with subordinate lithofacies that include laminated organic-rich clay, silty clay, and semivarved clay with downhole increases in silt and sand content as well as the rare occurrence of pebble-sized clasts.

Based on visual core descriptions and smear slide analyses, Site M0059 is divided into seven lithostratigraphic units (Fig. **F1**). Subunit Ia (0–47.1 mbsf; Hole M0059A) is composed of laminated, organic-rich biosiliceous clay, indicating a marine to brackish environment. The subunit is influenced by the effects of methane expansion. Subunit Ib (47.1–51.68 mbsf; Hole M0059A) is a downhole continuation of Subunit Ia, but silt in the biosiliceous clay and the presence of freshwater diatoms show a change to freshwater conditions. Unit II (51.68–51.73 mbsf; Hole M0059A) is a centimeter-scale silty sand unit that reveals an erosional unconformity. Unit III (51.73–82.20 mbsf; Hole M0059A) is characterized by rhythmites of clayey silt and silty clay with low organic content and a downhole increase of sand and rare dispersed gravel-sized clasts, which is evidence for ice rafting in a glaciolacustrine environment. Unit IV (82.20–93.12 mbsf; Hole M0059B), Unit V (93.12–99.12 mbsf; Hole M0059C), and Unit VI (99.12–169.03 mbsf; Hole M0059B) comprise a variety of gravel-bearing lithologies and interlayered glacial clays, proximal glacial sands, and diamicton indicative of a succession of repeated glaciations, followed by the final deglaciation that continues uphole in Unit III. Unit VII (169.03–204.03 mbsf; Hole

M0059B) is the lowermost unit at Site M0059, and despite very poor recovery, limestone with flint gravel, moderately consolidated, and rich in bioclastic material indicates penetration of Cretaceous limestone bedrock.

Unit I

Subunit Ia

Intervals: 347-M0059A-1H-1, 0 cm, to 15H-1, 60 cm; 347-M0059C-1H-1, 0 cm, to 17H-1, 0 cm; 347-M0059D-1H-1, 0 cm, to 16H-2, 56 cm; 347-M0059E-1H-1, 0 cm, to 15H-3, 0 cm

Depths: Hole M0059A = 0–47.10 mbsf; Hole M0059C = 0–50.12 mbsf; Hole M0059D = 0–50.06 mbsf; Hole M0059E = 0–46.20 mbsf

This uppermost subunit is composed of black to greenish black well-sorted clay. The subunit is mostly homogeneous with faint millimeter-scale lamination and minor bioturbation (Fig. F2). Some shell fragments and other bioclasts are present and increase in abundance in the lower half of the subunit. Core sections were generally well recovered with only slight to occasionally moderate disturbance.

It is estimated from smear slides that the major lithology is biosiliceous clay with 64%–89% clay minerals and 5%–27% biogenic silica (primarily diatoms, silicoflagellates, and sponge spicules).

The high biogenic and low terrigenous contents of the sediments in Subunit Ia indicate hemipelagic sedimentation in a high-productivity environment and/or a low terrigenous sediment supply. The fine lamination with an imprint of minor bioturbation and the generally homogeneous character of this black organic-rich clay are interpreted as strong evidence for the establishment of marine conditions, with low-oxygen bottom water during the Holocene referred to as the Littorina transgression (i.e., the marine transgression at the onset of the Littorina Sea stage of the Baltic Sea). Based on smear slide analysis, the isolated light-colored laminae noted within this subunit constitute fibrous diatomaceous mats interpreted to represent biosiliceous bloom events along with silicoflagellates, also indicative of a marine environment.

Subunit Ib

Intervals: 347-M0059A-15H-1, 60 cm, to 16H-2, 38 cm; 347-M0059C-17H-1, 0 cm, to 17H-2, 86 cm; 347-M0059D-16H-2, 56 cm, to 17H-2, 71 cm; 347-M0059E-15H-3, 0 cm, to 17H-1, 35 cm

Depths: Hole M0059A = 47.10–51.68 mbsf; Hole M0059C = 50.12–52.48 mbsf; Hole M0059D = 50.06–53.50 mbsf; Hole M0059E = 46.20–53.15 mbsf

This subunit contains greenish gray well-sorted silty clay and is generally well preserved with only slight disturbances. The subunit has more prominent pale green laminae that tend to occur over centimeter scales instead of the fine millimeter-scale lamination of the subunit above. This difference is due to a terrigenous silt component. Estimated from smear slides, the major lithology is biosiliceous silty clay with a quartz silt component. No bioturbation is visible in this subunit. Core disturbance is only slight with some degradation and oxidation along the core liner and ends.

Based on smear slides, freshwater diatoms are present in the main lithology but are more abundant in light green to pale brown mats composed of colonial diatom chain fragments, indicating diatom bloom and lake dump events (see **"Biostratigraphy"**). Coupling this observation with the nature of the fine-grained millimeter- to centimeter-scale color laminations suggests that, overall, Subunit Ib represents the establishment of a freshwater lake stage.

Unit II

Intervals: 347-M0059A-16H-2, 38 cm, to 16H-2, 43 cm; 347-M0059C-17H-2, 86 cm, to 17H-2, 90 cm; 347-M0059D-17H-2, 71 cm, to 17H-2, 78 cm; 347-M0059E-17H-1, 35 cm, to 17H-1, 38 cm

Depths: Hole M0059A = 51.68–51.73 mbsf; Hole M0059C = 52.48–52.52 mbsf; Hole M0059D = 53.50–53.57 mbsf; Hole M0059E = 53.15–53.18 mbsf

Unit II is a light yellowish brown, poorly sorted, centimeter-scale silty sand horizon (Fig. F3). Subangular and rounded quartz is present, acting as the grain support to the granule- to pebble-sized clasts of various lithologies, overall exhibiting inverse grading. More than 10 clasts >3 mm in length were counted in this small horizon, primarily at the upper contact.

Because of the sharp but irregular basal contact, indicative of a downward-cutting erosional surface that gradually increases in grain size toward the top, this unit marks a lithostratigraphic boundary. This horizon may represent an erosional unconformity, marking a potential lowstand.

Unit III

Intervals: 347-M0059A-16H-2, 43 cm, to 26H-1, 50 cm; 347-M0059B-1H-1, 0 cm, to 8H-1, 133 cm; 347-M0059C-17H-2, 90 cm, to 27H-1, 0 cm; 347-M0059D-17H-2, 78 cm, to end of hole; 347-M0059E-17H-1, 38 cm, to 27H-1, 66 cm

Depths: Hole M0059A = 51.73–82.20 mbsf; Hole M0059B = 60.00–84.43 mbsf; Hole M0059C = 52.52–82.23 mbsf; Hole M0059D = 53.57–86.57 mbsf; Hole M0059E = 53.18–86.46 mbsf

Unit III is greenish gray clay with centimeter-scale color banding and centimeter-scale laminations. Laminae consist of well-sorted quartz silt, which tends to increase in abundance toward the base of the unit. Millimeter- to centimeter-scale clasts of varying angularity are observed in intervals in the lower half of the unit. A generally fining-upward sequence is seen, based on an increase in silty fine sand laminations increasing in frequency toward the base of the unit. Evidence of convolute bedding and soft-sediment deformation is observed in the lower part of the unit. Estimated from smear slides, rare angular and subangular sand grains are present, as well as traces of broken diatoms and other siliceous debris.

The rhythmically banded clays are indicative of lake deposits. Observed subangular sand and centimeter-scale pebble grains are interpreted to be dropstones originating from ice rafting, which suggests that the unit most likely represents a late glacial ice lake. Traces of broken diatoms and other siliceous debris suggest reworking. The increased grain size and frequency of sand laminations in the lower sections (70.0–82.2 mbsf) suggest an ice-proximal location, with a gradual upward shift toward ice-distal facies at the top of the unit. The convolute bedding and soft-sediment deformation located in the lower part of the unit are suggestive of slumping; however, they also may not be primary sedimentary features. They may instead be the result of pressure differentials and fluid liberation within the waterlogged clays during drilling (Fig. **F4**).

Unit IV

Intervals: 347-M0059A-26H-1, 50 cm, to end of hole; 347-M0059B-8H-1, 133 cm, to 10X-1, 31 cm; 347-M0059C-27H-1, 0 cm, to 34H-1, 0 cm; 347-M0059E-27H-1, 66 cm, to 29H-1, 0 cm

Depths: Hole M0059A = 82.20–86.70 mbsf; Hole M0059B = 84.43–89.61 mbsf; Hole M0059C = 82.23–93.12 mbsf; Hole M0059E = 86.46–91.80 mbsf

Olive-gray silty clay occurs at the top of this unit and gradually grades downward into a series of centimeter-scale sandy laminations with increasing detritus toward the base as evidenced by more thickly bedded, poorly sorted sand units. Gray sand with silty clay intraclasts and a large bioclastic content is principally composed of mollusk, coral, and echinoderm fragments.

Both the sand laminae and the massive sand unit are moderately well sorted sand with quartz and feldspar supporting grains, with biotite, amphiboles, garnet, rounded glauconite, reworked foraminifers, diatoms, and other organic debris. A massive fine-grained horizon deeper in this unit is well-sorted silt with a minor sand fraction, which has very similar composition to the sands in this unit.

The variation between mature and less mature lithic-bearing sands with clay-rich horizons and reworking of material is suggestive of glacial outwash deposits. This variation may represent a braided outwash network accounting for shifts between sand- and silt-dominated horizons.

Unit V

Intervals: 347-M0059B-10X-1, 31 cm, to 19H-1, 0 cm; 347-M0059C-34H-1, 0 cm, to 38H-1, 0 cm; 347-M0059E-29H-1, 0 cm, to end of hole (microbiology hole with limited recovery)

Depths: Hole M0059B = 89.61–107.28 mbsf; Hole M0059C = 93.12–99.12 mbsf; Hole M0059E = 91.80–100.80 mbsf

Unit V is dark gray to dark grayish brown poorly sorted clast-poor to clast-rich muddy diamicton. This unit is highly consolidated. Core recovery in this unit was much lower than in the overlying units. However, based on core catcher descriptions coupled with intervals of recovered core, we interpret this interval as a massive diamicton unit.

The silt-sand matrix, the poor sorting, and the angularity of the clasts point to a diamicton, possibly representing a glacial till deposit, drawing associations between this and the last period of ice advance in the area.

Unit VI

Intervals: 347-M0059B-19H-1, 0 cm, to 27H-1, 0 cm; 347-M0059C-38H-1 to end of hole

Depths: Hole M0059B = 107.28 –169.03 mbsf; Hole M0059C = 99.12–158.08 mbsf

Core recovery in this unit was very poor, with few complete cores described. To fill in some of our missing intervals, core catcher observations were included to interpolate the variation within and boundaries of the unit. Based on the various data, the unit comprises a series of interbedded centimeter- to decimeter-scale silt-rich sequences, as well as coarse sands and horizons with a diamicton character.

Despite limited recovery in this unit, the unit is interpreted as an interbedded glacial deposit based on the variation between silt, sand, and diamicton-rich

horizons. The variation in lithology could be related to ice advance and subsequent deposition of coarse-grained, poorly sorted material during retreat or melting periods.

Unit VII

Interval: 347-M0059B-27H-1, 0 cm, to end of hole
Depth: Hole M0059B = 169.03–204.03 mbsf

Unit VII is limestone with flint gravel, moderately consolidated and rich in bioclastic material, including echinoderms, coral, and foraminifers.

Based on the findings of Cretaceous foraminifers with no apparent reworking, the unit consists of Cretaceous limestone.

Biostratigraphy

Diatoms

Holes M0059A and M0059C were analyzed for siliceous microfossils. Diatoms were identified to species level, and the occurrences of silicoflagellates, ebridians, and chrysophyte cysts were recorded. Qualitative analyses were carried out on every sample from the core section tops (~1.5 m between samples) to 58 mbsf and then every core top (~3.3 m between samples) to 84 mbsf in Hole M0059A and at every recovered core top between ~125 and 142 mbsf in Hole M0059C. Hole M0059C was almost barren (only a limited number of corroded diatom fragments were found, together with reworked Cretaceous coccoliths), and the siliceous microfossil record described in the rest of this section refers to Hole M0059A. The results of the qualitative diatom analysis for Hole M0059A are summarized in a graph showing the number of taxa found divided into different salinity affinities and life forms (planktonic/periphytic) (Fig. **F5**). A species list of all 144 recorded taxa from Hole M0059A is presented in Table **T2.** Diatoms were classified with respect to salinity tolerance according to the Baltic Sea intercalibration guides of Snoeijs et al. (1993–1998), which divide taxa into five groups: marine, brackish-marine, brackish, brackish-freshwater, and freshwater (Table **T3**). Diatom preservation in Hole M0059A can be regarded as good to moderate based on the ratio of heavily to finely silicified taxa and the degree of fragmentation (e.g., Koç and Scherer, 1996). More detailed preservational data will be compiled onshore (e.g., Warnock et al., 2007).

The results of qualitative analysis give a good overview of the diatom assemblages and paleoenvironmental changes downcore. The results must, however, be interpreted with caution because the graph (Fig. **F5**) is based only on qualitative analyses. Because each species was counted as only present or absent, a species represented by a single valve carries as much weight as a species dominating the assemblage.

Sections 347-M0059A-1H-1 through 15H-1; 0–46.5 mbsf

A relatively diverse brackish-marine diatom assemblage with 15–54 taxa per sample is recorded at 0–46.5 mbsf. The dominating planktonic taxa are *Thalassionema nitzschioides*, *Chaetoceros* spp. resting spores, *Thalassiosira oestrupii*, *Thalassiosira eccentrica*, and periphytic taxa *Paralia sulcata*, *Dimmeregramma minor*, *Hyalodiscus scoticus*, *Grammatophora oceanica*, and *Cocconeis scutellum*. This assemblage resembles that recorded in the more marine phase of the Litorina Sea stage of Baltic Sea history (e.g., Westman and Sohlenius, 1999; Andrén et al., 2000a, 2000b). Below is a description of the environmental requirements and geographic distribution of some key diatom taxa found in the sequence.

The very fine silicified vegetative valves of *Chaetoceros* are rarely recovered in sediments but occur very frequently in the photic zone (Snoeijs et al., 1993–1998). Fossil occurrences of *Chaetoceros* are instead often recorded as heavily silicified resting spores, which is consistent with the record from Hole M0059A. However, it should be noted that partial vegetative valves of *Chaetoceros* were found in many samples, indicating very high quality siliceous microfossil preservation in some intervals. Resting spores are difficult to separate at species level but contribute information on surface water salinity and nutrient availability. In the oceans, *Chaetoceros* resting spore sedimentation occurs in response to nutrient depletion at the termination of a phytoplankton bloom (Grimm and Gill, 1994). Leventer et al. (1996) concluded that environmental stress in the form of nitrogen deficiency results in the production of a *Chaetoceros* resting spore stage in the Antarctic region, and this conclusion has been further supported by experimental data (e.g., Oku and Kamatani, 1997). In the Baltic Sea, high resting spore abundance is recorded during the Holocene thermal maximum, Medieval Climate Anomaly, and the last ~50 y and used as an indicator of high-productivity events (Andrén et al., 2000a).

P. sulcata is a robust brackish-marine diatom with a wide ecological range. It is believed to live on sandy sediment bottoms and is easily lifted up into the plankton of the coastal waters (tychoplanktonic), particularly after winter storms (Hendey, 1964; Zong, 1997). The salinity reported is very broad, ranging from entirely marine conditions down to a salinity of 5, and *P. sulcata* seems to be very tolerant of fluc-

tuating water salinities when compared with other taxa (Zong, 1997). *P. sulcata* is a neritic species commonly found in near-continental marine sediments (e.g., on the continental margins of Norway) and is advantaged by warm Atlantic surface waters (Koç Karpuz and Schrader, 1990). The valves of *P. sulcata* are heavily silicified and resistant to breakage and dissolution, and it is often found as the dominant species in fossil assemblages (Stabell, 1985), which is consistent with the record in Hole M0059A to 46.5 mbsf.

T. nitzschioides is a common widely distributed marine neritic diatom species that often has massive blooms in the northern Atlantic area (Hendey, 1964; Hustedt, 1930). It is currently found from the Kattegat Sea to the southwest Baltic Sea around Bornholm in waters of salinity ranging between ~8 and 34 (Snoeijs and Vilbaste, 1994). In the Baltic Basin, this species is mainly recorded in the most marine phase of the Littorina Sea stage of Baltic Sea history (e.g., Witkowski, 1994; Sohlenius et al., 1996; Westman and Sohlenius, 1999; Andrén et al., 2000a, 2000b).

T. oestrupii is considered a cosmopolitan oceanic species that is occasionally found in coastal waters (Fryxell and Hasle, 1980). It does not live in the modern Baltic Sea (Snoeijs and Kasperoviciene, 1996), but it has been found in Littorina Sea stage sediments (e.g., Westman and Sohlenius, 1999; Andrén 2000a, 2000b). Koç Karpuz and Schrader (1990) found *T. oestrupii* and *T. nitzschioides* to be indicators of warm Atlantic surface water in the Greenland, Iceland, and Norwegian Seas.

Cyclotella choctawhatcheeana is a small pelagic taxon that is very common in the Baltic proper today (Håkansson et al., 1993; Snoeijs, 1993–1998). It blooms occasionally in the Baltic Sea in the summer when there is an upwelling event near the east coast of Sweden (Hajdu and Larsson, 1990). *C. choctawhatcheeana* is the most abundant taxon in Chesapeake Bay (USA) and is thought to be an indicator of anthropogenic perturbation in brackish water (Cooper, 1995). However, in a low-salinity environment such as the Gulf of Finland, there is no clear correlation between high nutrient availability and this taxon (Weckström and Juggins, 2006).

Besides a diverse diatom assemblage, the silicoflagellate *Dictyocha speculum* Ehrenberg was recorded at nearly all levels in the brackish-marine interval, and the ebridian *Ebria tripartita* (Schumann) Lemmermann was recorded at a few levels (Fig. **F5**).

Silicoflagellates are planktonic algae that are most abundant in areas of upwelling and in equatorial waters but are also abundant at high latitudes (McCartney, 1993). Silicoflagellates are exclusively marine, requiring a salinity of >20 (Tappan, 1980). However, they are found in the Straits of Denmark (Moestrup and Thomsen, 1990) and the Arkona Basin (Willén, 1995), and they live in the Black Sea, where salinities are as low as 10 (McCartney, 1993). The taxon found in Hole M0059A, *D. speculum* Ehrenberg, generally occurs in water cooler than 15°C and has an optimum temperature near 0°C (Tappan, 1980; McCartney, 1993).

Ebridians are marine planktonic organisms present in the neritic zone and near river mouths (Tappan, 1980). The ebridian recorded in Hole M0059A, *E. tripartita* (Schumann) Lemmermann, has an optimum temperature of ~10°C and is known in the North Sea and the Baltic Sea (Tappan, 1980; Willén, 1995). The presence of ebridians has been attributed to high availability of nutrients in studies of recent eutrophication in the Baltic Sea (e.g., Risberg, 1990; Witkowski and Pempkowiak, 1995; Andrén et al., 2000a).

Sections 347-M0059A-15H-2 through 16H-1; 48–51.3 mbsf

A lacustrine assemblage is recorded in this part of the core. The transition between the lacustrine and brackish-marine environment can be narrowed down to Section 347-M0059A-15H-1 between 46.5 and 48 mbsf. The assemblage indicates a large lake flora typical of the Ancylus Lake (e.g., Hedenström and Risberg, 1999; Ojala et al., 2005): *Aulacoseira islandica*, *Stephanodiscus neoastraea*, *Karayevia clevei*, *Martyana martyi*, *Ellerbeckia arenaria*, and *Diploneis mauleri*. In the lowermost sample at 51.3 mbsf, there are other taxa in addition to the large lake flora that indicate a small, more nutrient rich lake environment (Andrén, 1999; Ojala et al., 2005). This interval is dominated by *Aulacoseira granulata* and *Aulacoseira ambigua*.

In addition to the diverse freshwater diatom assemblage, chrysophyte cysts are recorded in this sequence. Chrysophyte cysts occur in both marine and freshwater environments (Lipps and McCartney, 1993; Duff et al., 1995; Wilkinson et al., 2001). The factors involved in inducing encystment are poorly understood, but freezing and ice formation and changes in nutrient stress have been implicated (Mitchell and Silver, 1982; Duff and Smol, 1988; Smol, 1988). An attempt to assign the cysts found in the Littorina Sea stage sediments to different salinity ranges has been made (Westman and Sohlenius, 1996), but in Hole M0059A, cysts were only recorded in the lacustrine environment (Fig. **F5**).

Sections 347-M0059A-16H-2 through 25H-1; 52.8–78.4 mbsf

The glacial clays deposited beneath the sandy layer at 51.7 mbsf are barren of siliceous microfossils. It has been suggested that the very low primary production in the ice lake dammed in front of the receding Scandinavian Ice Sheet was caused by poor light conditions in the water due to the heavy load of sediments discharging from the melting ice (Winterhalter, 1992). This environment with extremely high sedimentation rates would further dilute any traces of diatoms in the sediment.

Sections 347-M0059A-26H-1 through 28H-1; 81.7–84 mbsf

Below the glacial clays, the two samples from core tops contain diatoms and chrysophyte cysts. The assemblage is a mixture of freshwater and brackish-marine taxa with both pelagic and periphytic life forms.

Foraminifers

For foraminifers, results are summarized for samples taken offshore and onshore (i.e., samples taken from core catchers and sections, respectively). A total of 196 samples were processed and analyzed for abundance and diversity of benthic foraminiferal fauna (>125 µm size fraction) (Table T4). The low diversity of species at this site indicates that conditions were never fully marine in Little Belt, as they are today in the Kattegat/Skagerrak area with bottom water salinity >30. The abundance of foraminifers, however, varies significantly downcore, suggesting that large variations between nearly fresh and marine-brackish conditions occurred (Fig. F6). However, abundances can also be influenced by the large variations in lithology and/or sedimentation rates, which could have led to dilution of foraminifers with high sediment volume. For postcruise investigations, the volume of sediment used will need to be taken into account for quantifying number of specimens per unit of sediment.

Downcore abundance of foraminifers at Site M0059 can be divided into five major intervals.

In the first interval (0–48 mbsf; Cores 1H through 15H in Holes M0059A, M0059C, and M0059D), foraminifers continuously occur in relatively high abundances and decrease with depth (Fig. F6). Species diversity is low in the entire interval (Fig. F7). The assemblage is always dominated by *Elphidium* spp., especially *Elphidium excavatum clavatum* (60%–95%), along with *Elphidium excavatum selseyensis*, *Elphidium albiumbilicatum*, and *Elphidium williamsoni*. *Ammonia beccarii*, often the first foraminiferal species to appear in low-salinity environments (Kristensen et al., 2000), occurs occasionally in the deeper part. The predominance of *E. excavatum clavatum* indicates mainly brackish conditions (salinity < 22) with slightly fresher conditions occurring around 40 mbsf as indicated by the slight increase of *E. albiumbilicatum*, a low-salinity tolerant species (Kristensen et al., 2000).

The interval from 48 to 60 mbsf is barren with respect to foraminifers.

The third interval, 60 to ~87 mbsf, has a clear maximum in foraminifers between 81 and 86.5 mbsf (Cores 347-M0059A-25H through 27H, 347-M0059C-25H through 27H, and 347-M0059B-7H through 8H). *E. excavatum clavatum* and *E. albiumbilicatum* (up to 80%) are the predominant species in this interval, with the peak occurrence around 81 mbsf. Findings of *E. albiumbilicatum* and occasional tests of *Bucella frigida* indicate lower salinity and possibly colder conditions (Madsen and Knudsen, 1994). However, colder conditions in the shallow-marine setting can be caused by a relative sea level rise leading to increased water depth and thus lower bottom water temperature.

Between ~87 and 160 mbsf, the sediments do not contain Quaternary foraminifers.

The fifth interval covers the lowermost part of Site M0059 from 160 to 210 mbsf. Because of lower recovery in this interval, it was not possible to determine if a continuous record of foraminifers is present. The analyzed samples (Cores 347-M0059C-80S, 347-M0059C-84S, 347-M0059B-27X, and 347-M0059B-29P) only contained reworked foraminifers. Examples of reworked species include *Parasubbotina* sp. and *Globalomalina* sp., which are known from the Maastrichtian/Danian boundary at Stevns Klint (Rasmussen et al., 2005). Reworked foraminifers were identified as species that do not occur during the Quaternary and have a "frosty" appearance (Sexton et al., 2006). The sample from Core 347-M0059C-84S also included several agglutinated foraminifers.

Ostracods

Ostracods were examined from 195 samples (including 119 core catchers) from Site M0059 during the onshore phase of Expedition 347 at the Bremen Core Repository. Samples were studied entirely in the >125 µm fraction in order to achieve a higher number of ostracods. Ostracods were found in 62 samples (Table T5).

Ostracod abundance from the onshore samples was calculated per sediment volume and is similar among the different holes at the site (Fig. F8). Ostracods were recorded from 2 to 60 mbsf (Holes M0059A and M0059D) and from 76 to 86 mbsf

(Holes M0059A, M0059C, and M0059D). Ostracod abundance varies markedly but remains relatively low in most samples (10–20 valves/20 cm^3). Peaks of up to 40–50 valves/20 cm^3 are observed at 23 mbsf in Hole M0059D, at 41.5 mbsf in Hole M0059A, and at 52 mbsf in Hole M0059E (Fig. F8).

Preliminary taxonomic identifications revealed at least three different assemblages of ostracods. The upper ~50 m (Holes M0059A, M0059C, M0059D, and M0059E) contains marine and brackish-water ostracod taxa. A group of very shallow brackish-water and marine species is dominated by *Leptocythere* spp., *Cythere lutea*, *Hirshmania viridis*, and *Cytherura* spp. These taxa can tolerate decreased salinity to 6.5–10 and inhabit the shallow sublittoral zone (Frenzel et al., 2010). Two peaks in abundance are observed at 23 mbsf (Hole M0059A) and 41.5 mbsf (Hole M0059D). Both peaks are characterized by an increase in deeper water marine ostracods. The second group of marine species includes *Cytheropteron latissimum*, *Palmoconcha* spp., *Robertsonites tuberculatus*, and *Sarsicytheridea bradii*. *C. latissimum*, *R. tuberculatus*, and *S. bradii* are typical of open-sea conditions and are commonly found on Arctic shelves (e.g., Stepanova et al., 2007; Frenzel et al., 2010). In the Baltic Sea, *R. tuberculatus* and *S. bradii* inhabit the deeper parts (18–32 m) of the southern Baltic region where salinity is higher (Rosenfield, 1977).

At ~50 mbsf (Holes M0059A, M0059C, M0059D, and M0059E), the assemblage comprises the freshwater species *Cytherissa lacustris* and *Candona* spp. *C. lacustris* is commonly found in cold and well-oxygenated waters with salinity <1.5 (Frenzel et al., 2010). This interval is also characterized by a peak in abundance and a high juvenile to adult ratio, altogether indicating an in situ assemblage and a freshwater environment.

At ~80 mbsf (in Holes M0059A, M0059B, and M0059D), the assemblage comprises different ecological groups: freshwater, oligohaline, shallow-water marine, and redeposited pre-Quaternary valves. Together with the low percentage of juvenile valves, it likely indicates a high-energy environment in a very shallow near-shore location.

Palynological results

For Site M0059, palynological analyses focused on Holes M0059A and M0059C (lower part). Resolution of one sample per ~1.5 cores (2–5 m between samples) was used for pollen and one per two cores for dinoflagellate cysts. The majority of samples analyzed contained enough palynomorphs to generate statistically relevant results for low-resolution pollen profiles (Figs. F9, F10). For Site M0059, bisaccate pollen was included in the reference sum because it does not appear to be overrepresented as a result of transportation bias. The dinocyst content was variable depending on the type of sediment. Sediments with marine components (e.g., foraminifers) contained significant numbers of dinoflagellate cysts. Lacustrine sediments could be identified by the presence of freshwater algae and insect remains and the absence of marine dinocysts.

Hole M0059A

For Hole M0059A, 28 sediment samples were prepared for pollen analysis.

5.62–10.45 mbsf

Pollen spectra of this interval are dominated by broad-leaved tree pollen. Among these, *Fagus* pollen is the most characteristic for the interval 5.62–10.45 mbsf, with values ranging from 4.5% to 19%. Among other tree taxa, fairly high amounts of pollen were noted for *Quercus* (maximum of 29%), *Alnus glutinosa* type (22.5%), *Pinus sylvestris* type (17.5%), *Betula alba* type (13.5%), and *Carpinus* (3%). The presence of *Secale* type and *Plantago lanceolata* pollen is noteworthy, as they are an indication of human activity. Pollen data from 5.62 to 45.07 mbsf reveal a succession that is very similar to that known from pollen records from Denmark and northern Germany and Poland (e.g., Dörfler et al., 2012; Apolinarska et al., 2012). The high percentages of *Fagus* in the uppermost samples (Fig. F9) indicate an age younger than ~2200 y BP (sub-Atlantic) as previously recorded in the high-resolution, well-dated pollen record from Lake Belau (~80 km south of Site M0059; Dörfler et al., 2012). The presence of numerous microreticulate cysts of *Gymnodinium* (probably *G. nolleri*; Figs. F10, F11) in the uppermost 38 m at this site indicates a sub-Atlantic age (e.g., Harland and Nordberg, 2011), which is in accordance with the findings from the pollen record. *Gymnodinium* cysts were excluded from the dinoflagellate percentage calculations because of their extraordinary high occurrences in some samples (Fig. F10).

15.57–45.07 mbsf

Pollen of *Quercus* (maximum of 35%) and *A. glutinosa* type (maximum of 34%) dominate this interval. *Corylus avellana* pollen percentages vary between 4% and 27% in this interval, reaching peak abundances at 24.27 and 41.57 mbsf. No reworked Tertiary pollen and no *Pediastrum coenobia* were found, only sporadic occurrences of *Botryococcus* colonies. Dinoflagellate cysts are present in high quantities. This indicates a marine environment during sedimentation, and the interval most possibly covers Atlantic and Subboreal phases.

49.16–50.65 mbsf

In pollen spectra of this interval, *P. sylvestris* type pollen dominates, reaching up to 42%. *Quercus* (21%) and *C. avellana* (15%) also occur frequently. Pollen of *B. alba* type, *Ulmus*, and *Fraxinus* are present. A characteristic feature of this interval is the absence of dinoflagellate cysts and Tertiary reworked pollen, whereas freshwater green algae *Pediastrum* and *Botryococcus* are present (3% and 6.5%, respectively). Presence of pollen originating from reed swamp plant communities (*Phragmites* type included in Poaceae pollen) as well as from *Myriophyllum spicatum* (a freshwater vascular plant) implies that a freshwater environment prevailed during this interval. This implication is also supported by more frequent findings of aquatic insect remains (Fig. **F11**). The high *P. sylvestris* type pollen amount may suggest an early Boreal age of the sediments (Apolinarska et al., 2012). An interval of particularly high percentages of *Ulmus* pollen between 36.03 and 49.16 mbsf can probably be correlated with a similar interval, dated between 9500 and 6000 y BP, in the Lake Belau pollen record from Northern Germany (Dörfler et al., 2012).

54.42–83.40 mbsf

Samples from the depth interval 54.42–83.40 mbsf have a very low frequency of pollen. Only in samples at 54.42, 80.10, and 83.40 mbsf was sporomorph frequency high enough to calculate percentage pollen spectra (Fig. **F9**). The pollen spectra are characterized by high amounts of reworked Tertiary pollen (Fig. **F9**). Among the observed Quaternary pollen taxa that are considered in situ, pollen of *P. sylvestris* type and *B. alba* type dominate, reaching >30%. Pollen of *Picea* is present with up to 10% and *Juniperus* with 5%. Among broad-leaved trees, the highest pollen percentages were noted for *C. avellana* and *A. glutinosa* type pollen. Very characteristic is a high amount of freshwater green algae *Pediastrum* and *Botryococcus*. Additionally, the presence of some organic-walled dinoflagellate cysts may point to a brackish environment. The reworked pollen of Tertiary origin most probably indicates meltwater inflow with redeposition of Tertiary sediments.

Hole M0059C

Six samples were macerated for pollen analysis. To complement the pollen record from Hole M0059A, the samples were selected from the depth interval 80.27–141.72 mbsf. Only the sample from 80.27 mbsf contains an appropriate pollen frequency for obtaining a reliable pollen spectrum. This spectrum correlates very well with the lower part of the pollen diagram from Hole M0059A (Figs. **F9, F12**). The rest of the results are given in Table **T6** and PalyM0059.xls in PALYNOLOGY in **"Supplementary material"**). Dinocysts are frequently present in the analyzed samples, but many of the encountered specimens in the lower part of Hole M0059C appear to be reworked and probably belong to tertiary taxa. Based on pollen analysis results (mainly green algae), sediments from the interval 80.27–141.72 mbsf most likely have a brackish origin.

Geochemistry

Interstitial water

At Site M0059, freshwater and glaciolacustrine deposits are overlain by ~47 m of brackish-marine sediment (see **"Lithostratigraphy"**). The pore water composition at this site reflects the associated strong variations in bottom water salinity during the deposition of individual sediment units. The pore water composition also records large changes in the input and degradation of organic matter in the sediment and reveals associated changes in the dissolution and precipitation of minerals.

Salinity variations: salinity, chloride, and alkalinity

Concentrations of chloride (Cl^-), a conservative element in seawater (Fig. **F13A**), are high and relatively constant at ~380 mM in the upper 15 m of the sediment. This suggests relatively minor change in bottom water salinity during deposition of the more recent sediments. Cl^- concentrations then decline with depth to a minimum of 115 mM at 70 mbsf. This trend with depth is the net result of the increase in bottom water salinity associated with the transition from the freshwater to brackish-marine system and downward diffusion of Cl^- into the freshwater sediment. Deeper than 70 m, Cl^- concentrations rise again slightly, possibly suggesting a source of seawater from below.

Pore water salinity can be calculated from Cl^- concentrations (Table **T7**) when assuming that seawater with a salinity of 35 has a Cl^- concentration of 558 mM. Comparison of Cl^- based salinity to shipboard measurements of salinity analyzed with a refractometer (see **"Geochemistry"** in the "Methods" chapter [Andrén et al., 2015]) illustrates that dissolved salts other than those typically present in seawater contribute to salinity in the upper 50 m of the sediment (Fig. **F13B**). Deeper than 50 mbsf, Cl^- based salinity and shipboard measurements of salinity are largely similar. These results can be explained when considering that organic matter degradation and associated processes lead to enrichment of cations and alkalin-

ity in pore water (e.g., Wallmann et al., 2008). These ions contribute to the salinity of the pore water. At Site M0059, alkalinity is exceptionally high in the upper ~50 m of the sediment, with a broad maximum of 200 meq/L centered around 20–40 mbsf (Fig. F13C). Cl^- based salinity can be corrected for additional anions by assuming that HCO_3^- is the dominant anion contributing to alkalinity. The resulting "anion-based salinity" (Fig. F13D) is similar to shipboard measurements of salinity by refractometry (Fig. F13B). Thus, whereas Cl^- based salinity results from the bottom water salinity during deposition of the sediment and the subsequent diffusive modification, the actual salinity of the pore water at present is significantly higher because of sediment diagenesis.

Organic matter degradation: methane, sulfate, sulfide, ammonium, phosphate, iron, manganese, pH, bromide, and boron

Microbial mineralization of organic matter leads to distinct changes in the geochemistry of pore water, often reflecting a combination of primary water column geochemistry during deposition and both past and ongoing diagenetic sedimentary alterations. Because of the highly transient nature of diagenesis at this site, the sequence of appearance of solutes with sediment depth differs from that typically observed in marine surface sediments (Froelich et al., 1979). At present, methane occurs in the sediment from the uppermost depth of measurement at 1.5 mbsf to 84 mbsf (Fig. F14A; Table T8). The measured methane concentrations are, however, not representative of actual methane concentrations because of the extensive degassing during core collection. The effect of degassing is probably greatest for the upper 65 m of the profile, whereas the drop in concentration deeper than 70 mbsf is probably real. Most of the methane likely formed in the brackish-marine sediments and diffused downward into the glaciolacustrine sediments.

Sulfate concentrations decrease from near 1.5 mM in the uppermost section to below detection at 2.2 mbsf (Fig. F14B). In this uppermost section (<0.8 mbsf), hydrogen sulfide (H_2S) is also present in the pore water (up to 2.45 mM), indicating active sulfate reduction in the near-surface sediments (Fig. F14C). Deeper than this, H_2S was below detection. Sulfate concentrations sporadically increase to 1.71 mM until 80 mbsf and deeper than this depth are as high as 10 mM. The cause of these relatively high sulfate concentrations remains unclear, but they may indicate occasional contamination of the sediment by seawater and/or drill fluid penetration during drilling (Table T9).

Pore water profiles of ammonium (NH_4^+) and phosphate (PO_4^{3-}) (Fig. F14D–F14E) follow the general trend in alkalinity (Fig. F13D) with higher concentrations in the upper 50–60 mbsf. Both NH_4^+ and PO_4^{3-} are products of organic matter degradation. Similar to alkalinity, they were largely formed in the brackish-marine sediments and diffused down into the glaciolacustrine sediments.

Pore water concentrations of dissolved iron (Fe^{2+}) and manganese (Mn^{2+}) vary strongly throughout the sediment column (Fig. F14F–F14G). Dissolved Fe^{2+} concentrations are elevated in the glaciolacustrine sediments (up to 1500 µM) deeper than 47 mbsf, whereas Mn^{2+} pore water concentrations are highest in the upper 47 m of the sediment, which represents the brackish-marine interval. Deeper than 47 mbsf, two distinct zones in the Mn^{2+} concentration profile are distinguished: (1) 50–60 mbsf, where pore water Mn^{2+} concentrations are very low (a few micromolar), and (2) deeper than 60 mbsf, where Mn^{2+} concentrations are again slightly elevated. The exact processes leading to the production of dissolved Fe^{2+} and Mn^{2+} in these sediments remain to be explored.

Pore water pH can be of value for the identification of the various diagenetic processes active in sediments (Soetaert et al., 2007). At this site, pore water pH varies greatly between holes. However, pore water pH is generally higher in the brackish-marine sediments than in the underlying freshwater and glaciolacustrine sediments (Fig. F14H).

Mineral reactions

Bromide, boron, sodium, potassium, magnesium, and calcium

Comparison of profiles of the major and minor ions to those for Cl^- can provide insight into the role of reactions in the sediment versus changes in contributions from seawater. Ratios of these ions to Cl^- are particularly useful because elevated (or depleted) ratios relative to those for seawater are directly indicative of production (or removal) of ions. The depth profile of dissolved bromide (Br^-) (Fig. F15A) does not follow the exact trend of Cl^- (Fig. F13A) but instead is rather similar to that of salinity (which includes the ionic products of organic matter degradation). The Br/Cl ratios indeed indicate excess Br^- in the upper 70 m of the sediment column relative to seawater (Fig. F15B). Bromide is known to be incorporated in marine organic matter, and thus the excess Br^- is likely released from organic matter during degradation. The boron (B) profile (Fig. F15C) largely resembles that of alkalinity (Fig. F13C). Ratios of B/

Cl reveal that, similar to Br^-, there is evidence for release of B in the brackish-marine sediments (Fig. F15D).

Sodium (Na^+), potassium (K^+), magnesium (Mg^{2+}), and calcium (Ca^{2+}) are all major components of seawater. Their concentrations in pore water may be altered by processes such as ion exchange, mineral weathering, and formation of new minerals. Trends in Na^+, K^+, and Mg^{2+} with depth resemble those of Cl^-, indicating the influence of seawater on the pore water chemistry in the upper ~50 mbsf (Fig. F16A–F16C). The Ca^{2+} profile is distinctly different and shows a concentration maximum deeper than 50 mbsf where the other profiles are at minima (Fig. F16D).

Ratios of the four cations to Cl^- indicate that their concentrations are all impacted by reactions in the sediment. In the upper 50–60 mbsf of the profile, ratios of Na/Cl, K/Cl, and Mg/Cl are elevated relative to those of seawater (Fig. F16E–F16G). This indicates release of Na^+, K^+, and Mg^{2+} from the sediment, possibly through desorption and exchange with pore water NH_4^+ and through weathering of silicate minerals (e.g., Wallmann et al., 2008). Deeper than 50–60 mbsf, ratios of Na/Cl, K/Cl, and Mg/Cl are lower than those in seawater, suggesting removal to solid phases. Possible reactions include ion exchange and, for K^+ and Mg^{2+}, removal through formation of new clay minerals. The profile of rubidium (Rb), a trace element in the pore water that may be released from sediment solids through ion exchange, is very similar to that of K^+ (Table T9).

Ratios of Ca/Cl in the pore water are always equal to or higher than those measured in the seawater (Fig. F16H). Two distinct zones of net production of Ca^{2+} can be distinguished. The first, less prominent zone occurs in the upper 15 m of the sediment, whereas the second zone is found at 40–80 mbsf, where Na/Cl and Ca/Cl profiles show opposite trends. Concentrations of Ca^{2+} in the upper 50 m of the sediment may be controlled by a combination of ion exchange, mineral precipitation, and dissolution reactions. In sediment deeper than 47 mbsf, the release of Ca^{2+} is possibly due to cation exchange with seawater Na^+. In freshwater sediments, Ca^{2+} is typically the dominant adsorbed ion on clay particles, and exposure to seawater is known to lead to exchange with Na^+ (e.g., Burdige, 2006).

Silica, lithium, barium, and strontium

Dissolved silica (H_4SiO_4) is typically released to pore water through dissolution of diatoms and silicate minerals. Lithium (Li^+) is also released through mineral weathering and may be removed through formation of authigenic mineral phases and adsorption to sediment particles. Concentrations of both H_4SiO_4 and Li^+ are elevated in the upper ~50 m of the sediment (Fig. F17A–F17B), but the shapes of the profiles are very different. Dissolved H_4SiO_4 is highest (~1500 µM) near the sediment surface and then is largely constant at ~1100 µM throughout the brackish-marine sediments, likely suggesting that H_4SiO_4 is released to the pore water through dissolution of diatoms present in the sediment (see "Biostratigraphy"). The depth trend in dissolved Li^+ in the upper 50 mbsf is similar to what is observed for the major cations Na^+, K^+, and Mg^{2+} (Fig. F16A–F16C). Deeper than ~50 mbsf, concentrations of dissolved H_4SiO_4 and Li^+ are typically lower, with distinct minima around 60 mbsf.

Dissolved barium (Ba^{2+}) in pore water is often the result of the dissolution of barite (barium sulfate mineral). It can also be released from minerals through dissolution or ion exchange. Pore water concentrations of Ba^{2+} are relatively low in the upper 50 m of the sediment column, mainly varying from 5 to 10 µm (Fig. F17C). A sharp peak in Ba^{2+} concentrations is observed between 50 and 60 mbsf, followed by a decline at greater depths. This profile may indicate release of Ba^{2+} from minerals linked to the intrusion of seawater into the former freshwater sediments. Similarly, pore water concentrations of strontium (Sr^{2+}) are relatively constant throughout the upper ~50 m with a first maximum between 50 and 60 mbsf (Fig. F17D), possibly also reflecting release from solid phases. However, in contrast to Ba^{2+}, there is also a strong increase in dissolved Sr^{2+} deeper than 75 mbsf. Again, analyses of the solid phases are necessary to elucidate the processes responsible for these trends with depth.

Sediment

Carbon content

The amount of total carbon (TC) in the sediment at Site M0059 is high throughout the profile (Fig. F18A; Table T10). In the brackish-marine sediments, total organic carbon (TOC) is the dominant form of carbon, with values up to 8 wt% (Fig. F18B). These high TOC values suggest high primary productivity at the time of deposition, high sedimentation rates, and/or low oxygen concentrations in the bottom water, all of which promote organic matter burial (Canfield, 1994). At ~52 mbsf, coinciding with the first downcore occurrence of the greenish gray clays of Unit III (see "Lithostratigraphy"), TOC values significantly decrease, and they remain low (<0.5 wt%) throughout the remainder of the profile.

The amount of total inorganic carbon (TIC) averages 1.2 wt% in the organic-rich sediments deposited under brackish-marine conditions (Unit I) but significantly increases to a maximum of 4.6 wt% in the greenish gray clays deposited under freshwater conditions (Fig. F18C). At 203 mbsf in Hole M0059B, TIC values reach 11.8 wt%, equivalent to ~98 wt% of calcium carbonate (Table T10). This is in good agreement with the sedimentologic observation indicating the presence of chalk at ~200 m (see "Lithostratigraphy").

Sulfur content

Similar to TOC, total sulfur (TS) contents are high in the uppermost part of the investigated sediment sequence, with values ranging between 1.1 and 1.9 wt% (Fig. F18D). At ~48 mbsf, TS sharply decreases to <0.4 wt% and remains low downcore. Such a change from low to high TS values is typical for a transition from a freshwater to a brackish-marine environment where, given sufficient TOC input, sulfate reduction will become quantitatively more important (Berner and Raiswell, 1983). Contents of TOC and TS in the upper 48 m of the sediment correlate positively, and TOC/TS weight ratios are in the typical range for marine sediments overlain by oxygenated bottom waters (Berner and Raiswell, 1983). Much of the sulfur is likely present in the form of Fe sulfide minerals (see "Lithostratigraphy").

Physical properties

This section summarizes the primary physical property results, focusing on the higher quality data sets obtained from cores with good recovery in the upper ~90 m of Site M0059, which are best expressed in Hole M0059D (Fig. F19). Although all physical property measurements described in "Physical properties" in the "Methods" chapter (Andrén et al., 2015) were conducted at Site M0059, whole-round core shipboard *P*-wave data appear highly affected by artifacts related to inconsistencies in core volume (e.g., space between sediment and the core liner), likely as a result of coring disturbances. Discrete *P*-wave and thermal conductivity data are too sparsely distributed to exhibit any discernible downcore trend, and color reflectance and noncontact electrical resistivity data show little variability.

Natural gamma ray

The high-resolution natural gamma ray (NGR) data increase from core-top values of ~2.5 to ~5 cps at ~51 mbsf (Fig. F19). These generally low NGR values are interpreted as a result of high water content within organic-rich muds (Subunit Ia; see "Lithostratigraphy"). At the Subunit Ia/Ib boundary and into Unit II, NGR values decrease. This decrease reflects an increase in quartz and silt content within lithostratigraphic Subunit Ib and Unit II (see "Lithostratigraphy"). A pronounced stepwise increase to ~10 cps occurs at ~55 mbsf in all holes from Site M0059. This is interpreted to indicate a significant increase in clay content and corresponds to the lithostratigraphic Unit II/III boundary (see "Lithostratigraphy"). Meter-scale peaks throughout Unit III likely correspond to intervals of reduced grain size. NGR values drop to near zero at ~85 mbsf.

Density and porosity

A similar trend is expressed by the lower resolution discrete dry density and porosity data that were calculated from moisture and density measurements (Fig. F19). Dry density and porosity are highly correlated (r^2 = 0.99). Deeper than ~55 mbsf, significantly increased clay content within lithostratigraphic Unit III results in reduced porosity and increased density.

Gamma density was measured at 2 cm intervals during the offshore phase of Expedition 347. Values exhibit the same trend as the physical properties described in the previous section (Fig. F20), except for spurious results of ~4 g/cm^3 for the entirety of Core 347-M0059D-2H. Discrete bulk density measurements conducted during the Onshore Science Party (OSP) correlate well with shipboard measurements (r^2 = 0.94; Fig. F21).

Paleomagnetism

In accordance with the main objectives of the OSP paleomagnetic work, magnetic susceptibility measurements and rudimentary analyses of natural remanent magnetization (NRM) were made on discrete specimens of known volume and mass (see "Paleomagnetism" in the "Methods" chapter [Andrén et al., 2015]). The sediment samples recovered from Site M0059 display a wide range of magnetic properties. Magnetic susceptibility varies by approximately an order of magnitude and includes one diamagnetic sample recovered from the Cretaceous limestone (Unit VII). The response of pilot samples to sequential alternating field (AF) demagnetization reflects, to a large degree, the variation in magnetic susceptibility and indicates that a combination of low-, medium-, and high-coercivity minerals at this site contribute to the total magnetization and that some samples contain at least two overlapping components. Some samples recovered from Subunits Ib and Ia acquired a gyroremanent magnetization (GRM) during sequential AF demagnetization, which is

characteristic of, but not exclusive to, diagenetic greigite (Fe_3S_4). The majority of paleomagnetic samples recovered from Units VI–III carried a normal polarity magnetization, but the average inclination is ~30°–40° shallower than the 71° predicted by a geocentric axial dipole (GAD) model at the site latitude. The paleomagnetic samples recovered from Subunits Ib and Ia carry normal polarity NRMs that vary approximately ±10° around the GAD model prediction, with the exception of some shallow or reversed samples that are associated with sediment disturbance and/or samples taken from core catchers. Cores were not oriented with respect to an azimuth, and the relatively low density of sampling restricted the utility of the horizontal component of the NRM vector (declination).

Discrete sample measurements

A total of 454 discrete samples were obtained from Site M0059. Samples were recovered at intervals of ~50 cm from inside and outside the site splice to obtain denser coverage. The sample set consisted of 118 samples from Hole M0059A, 56 from Hole M0059B, 162 from Hole M0059C, 114 from Hole M0059D, and 4 from Hole M0059E.

Magnetic susceptibility

Magnetic susceptibility results are shown in Figure F22. Magnetic susceptibility (χ, which is normalized to sample mass) ranges between -4.7×10^{-9} m^3/kg (the sample of Cretaceous limestone at the base of Hole M0059B) and 0.6×10^{-6} m^3/kg (Sample 347-M0059B-25P-1, 20 cm). This section, which is between 117.3 and 117.9 mbsf in Unit VI, is considered to have been disturbed by coring and may not be in situ (see "Lithostratigraphy" for further details).

Samples taken from the bottom of Unit III between 83.2 and 80 mbsf have relatively high χ, which is followed by a general declining trend to the top of this unit. This trend is in agreement with the upward fining of this gray clay. The general trend of an uphole decrease in χ continues in Subunit Ia, although the interval between the bottom of Subunit Ib and a depth of 21 mbsf is characterized by frequent peaks in χ, which are shared between samples taken from different holes.

Sediment wet density and χ are positively related (Fig. F22), but there is considerable scatter in the data set. This scatter suggests that sediment consolidation and dilution of one ferrimagnetic component are not the only determinants of χ. It is most likely that variations in χ reflect sediment provenance and magnetic grain size and/or postdepositional precipitation of ferrimagnetic minerals.

Natural remanent magnetization and its stability

Results of the pilot sample demagnetization (e.g., Fig. F23) indicate that an AF of 5 mT is sufficient to remove a weak viscous remanent magnetization (VRM). After removal of this overprint, the pilot samples displayed varied responses to the sequential demagnetization, with three principal categories. Category 1 indicates the presence of a NRM carried by a mineral with high coercivity (median destructive field of NRM > 60 mT) and is characteristic of Unit III. The magnetization vector trends toward the origin after the 5 mT step, and 50% of the NRM intensity is removed at an AF of 80 mT. Category 2 indicates the presence of a mineral with low coercivity (median destructive field of NRM = 20–25 mT) and is characteristic of Unit III through Subunit Ia. After removal of a weak overprint by the 5 mT AF treatment, the magnetization vector trends toward the origin and the NRM intensity is reduced to <5%. Category 3 is characteristic of samples in Subunits Ib and Ia that have relatively high χ (between 51.68 and 16.00 mbsf). In this category the median destructive field of NRM is ~45 mT, and almost 20% remains after the application of an 80 mT AF. In addition, the magnetization vector trends toward the origin up to 40 mT AF, after which it veers into a plane that is perpendicular to the last applied demagnetization axis. This behavior is characteristic of the acquisition of a GRM, which can be indicative of the presence of diagenetic greigite (Fe_3S_4) in the samples.

After removal of the viscous overprint, the NRM intensity of the samples recovered from Site M0059 lies in the range between 0.07×10^{-3} and 120×10^{-3} A/m, and there is a positive relationship with χ in Subunits Ib and Ia (Fig. F22). The relationship between NRM intensity and χ is less obvious in Unit III, in which large peaks in NRM intensity are not reflected in the χ data.

Paleomagnetic directions

Palaeomagnetic samples recovered from Unit VI (between 149 and 123 mbsf) have inclinations that are widely scattered around 0°, and these are associated with high magnetic susceptibility and low NRM intensity. These data suggest that the paleomagnetic field has not been reliably recorded by these sediments. Similarly, the majority of samples recovered from Unit III, which is composed of laminated clay, show strong evidence of inclination shallowing. Some samples, however, show steep inclinations close to the GAD prediction.

The significant change in lithology that marks the bottom of Subunit Ib is accompanied by inclinations

that vary within 10° either side of a GAD prediction. The absence of independent time control points, however, does not allow for a detailed comparison to the FENNOSTACK regional master curve (Snowball et al., 2007). On the other hand, it may be possible that the interval of steepest inclinations between ~18 and 16 mbsf corresponds to the period of steep inclination experienced in Fennsocandia between 3090 and 2590 cal y BP, which is delimited by inclination features ε and ε^1, respectively, in FENNOSTACK.

Microbiology

Two holes, M0059C and M0059E, were drilled specifically for microbiology, interstitial water chemistry, and unstable geochemical parameters at Site M0059. Counts of microbial cells were made on board the ship by fluorescence microscopy using acridine orange direct counts (AODC) and by flow cytometry (FCM) using SYBR green I DNA stain. Additional AODC were also made during the OSP. Further counts by fluorescence microscopy will be done after the OSP using both acridine orange and SYBR green I staining.

Hole M0059C

Microbial cells were enumerated at 29 depths from independently taken samples for FCM (28 samples) and AODC (16 samples), both on the ship and during the OSP (Table T11). Microbial cell abundance in the clay of possible Holocene age (0 to ~50 mbsf) was very high (~10^8 to 10^9 cells/cm^3), with a maximum value of 1.15 × 10^9 cells/cm^3 at 4.53 mbsf (Fig. F24). There was only a small decrease in numbers until ~35 mbsf, below which cell numbers decreased more steeply. The change at 35 mbsf does not appear to be related to any lithologic change, as this depth is well within the clay interval (Fig. F24). Interestingly, there was also no abrupt change in cell abundance between the organic-rich Holocene sequence and the organic-poor glacial clay at ~51 mbsf. Cell numbers reached a minimum of 4.16 × 10^7 cells/cm^3 at 68.15 mbsf. A small increase in cell numbers in the lower two samples of this hole was detected by both methods.

The cell count profiles have some resemblance to the salinity profile, which also shows an overall decrease with depth (Fig. F24). The small increase in salinity at the base of Hole M0059C replicates the increase in total cell numbers. The alkalinity profile, indicative of bacterial mineralization of organic matter, appears less related to the cell count profile.

Cell concentrations measured in Hole M0059C were extremely high, with all data values above the upper prediction limit of the global regression of prokaryotes cells with depth (Fig. F24). The maximum deviation from the global regression occurred at 20–30 mbsf, where cell numbers were ~40 times greater than the global regression.

Hole M0059E

Microbial cell numbers were enumerated at 24 sediment depths from samples taken for FCM (9 samples) and AODC (19 samples), both offshore and during the OSP (Table T12). Microbial cell abundance in the upper Holocene clay was very high (~10^8 to >10^9 cells/cm^3), with a maximum value of 4.35 × 10^9 cells/cm^3 at 1.52 mbsf (Fig. F25). There was a hiatus in count data between 18 and 49 mbsf. Although samples were taken for this interval, they have proven difficult to count because of the clumped nature of the prokaryotic cells around organic particles. A different approach to sample processing will need to be developed for these samples before counting can be achieved. In order to check whether there was a distinct change in cell abundance from the Holocene sequence to the late glacial clay, detailed sampling was made across this lithologic boundary (~51 mbsf). A drop in cell numbers (Fig. F25) was observed below the transition from the Holocene organic-rich clay to the late glacial clay.

Similar to Hole M0059C, the cell count profile is similar to the salinity profile in this hole (Fig. F25). More importantly, the higher cell numbers in the Holocene sequence coincide with the zone of enhanced alkalinity production and, thus, of organic matter mineralization. The minimum cell count was 2.29 × 10^7 cells/cm^3 at 84.02 mbsf.

Similar to Hole M0059C, all cell abundances measured in this core were extremely high with almost all data values above the upper prediction limit of the global regression of prokaryotic cells with depth (Fig. F25). The maximum deviation occurred around 8 mbsf, where cell numbers based on cytometer counts were ~88 times greater than the global regression.

Cell counts were made by both AODC and FCM at the same sediment depths in 15 samples from Hole M0059C and 6 samples from Hole M0059E. Separate paired sample t-tests on these two data sets showed no significant difference between the two techniques (t = 1.633; degree of freedom [df] = 14 [not significant]; t = 2.031; df = 5 [not significant]) for Holes M0059C and M0059E, respectively. In Figure F26,

FCM counts are plotted against AODC counts from the same depths for both holes combined. The calculated regression of this data set shows strong agreement between the two techniques, and a slope test showed no significant deviation from a slope of 1 ($t = 0.0024$; $df = 19$ [not significant]).

High throughput cell counting by FCM has previously been attempted using samples from IODP Expeditions 329 and 337. This application was not successful, however, because of the extremely low cell abundance in sediments from both these expeditions.

Figure F27 shows fluorescence microscopic images of cells from Hole M0059C (1.53 mbsf) stained by SYBR green I. Figure F27A shows the microscopic image without any treatment to detach cells or remove particles. Compared to no treatment, sonication detached cells from large particles of diatoms and sediments enabling improved cell visualization (Fig. F27B). Further treatment with hydrofluoric acid cleared the background by removing clay minerals and other fluorescing particles and facilitated cell counting (Fig. F27C).

In order to assess potential contamination during the coring operation, measurements of the microbial loading of drilling fluid were made in Hole M0059E (Table T13). Cell numbers in the drilling fluid varied little over time: a maximum of 1.11×10^6 cells/mL when coring at 3 mbsf and a minimum of 5.14×10^5 cells/mL when coring at 26 mbsf. Average cell numbers in the drilling fluid were 7×10^5 cells/mL.

Perfluorocarbon tracer (PFC) for contamination testing was detected in the liner fluid and exteriors of all cores, indicating continuous PFC delivery into the borehole. An example is shown from Hole M0059E (Table T14). Liner fluid PFC concentrations at this site fluctuated over more than two orders of magnitude (Fig. F28A), indicating variations in the rates of PFC delivery and mixing into the drilling fluid stream. Generally, the measured PFC concentrations were considerably below the target concentration of 1 mg PFC/L. Despite the fluctuations, PFC was above detection in the vast majority of core halfway and interior sections (Fig. F28B). No clear depth-related trends in contamination are apparent, except that the two uppermost cores (347-M0059C-1H and 2H) show the highest level of contamination of interior parts of all cores sampled at this site (Fig. F28C). Similarly, there was no clear trend in relation to lithology, which consisted of organic-rich black clays and varved green clays throughout the hole (Fig. F25). In addition to Cores 347-M0059C-1H and 2H, Core 13H shows a high level of contamination in the interior. Cores 1H, 2H, and 13H may each potentially have 10^3–10^4 contaminant cells/cm^3 of sediment within their interiors (Fig. F28D). This, however, is still only ~0.001% of the indigenous community cell numbers (cf. Fig. F25).

Apart from these highly contaminated cores, numerous cores were potentially contaminated to a much smaller degree (~100 cells/cm^3 or less) in the interior. These include Cores 347-M0059C-6H, 7H, 11H, 15H, 17H, and 21H. No contamination was detected in the interiors of Cores 4H, 5H, 8H, 10H, 19H, and 25H (Fig. F28D). Taken together, these results indicate that 12 of the 18 cores sampled for PFC show very moderate to no evidence of contamination with foreign microbes from drilling fluid.

Stratigraphic correlation

Magnetic susceptibility, NGR, and gamma ray attenuation (GR) density data collected from Holes M0059A–M0059E were used to correlate between each hole and to construct a composite section for Site M0059 (Figs. F29, F30). The meters composite depth (mcd) scale for Site M0059 was based primarily on correlation of magnetic susceptibility between holes. NGR and GR density data provided confirmation of the correlation in some intervals and were used as constraints in other intervals where the magnetic susceptibility was low or lacked correlative features. All magnetic susceptibility data were cleaned for the top of each section, removing any outliers. The depth offsets (the affine table) that define the composite section for Site M0059 are given in Table T15.

The magnetic susceptibility anomalies could be well correlated to ~87 mcd. The uppermost ~27 mcd, however, has some uncertainties, which were reevaluated using cyclic variations in the NGR data (Fig. F30). At ~27 mcd, there is a prominent spike in susceptibility data. However, this spike is not associated with a definitive lithologic change. The next prominent feature in the susceptibility data is at 47 mcd, reflecting a sequence boundary (see "Lithostratigraphy"). A general increase in susceptibility values at ~53 mcd is coincident with a lithologic change from silty clays to laminated clays.

After constructing the composite depth section for Site M0059, a single spliced record from 0 mcd (top of Section 347-M0059D-1H-1) to 87 mcd (bottom of Core 347-M0059D-27H) was made from the aligned core intervals from all five holes (Table T16). If possible, cores that had been disturbed by the coring process (e.g., significantly compressed or expanded) were not used for the splice. Deeper than 87 mcd, Site M0059 relies on cores from only Hole M0059C. Therefore, Cores 347-M0059C-28S through 84S were appended to the record. Deeper than 87 mcd, coring

gaps occur between each core, as well as larger sections with no recovery.

No correction factor was applied to any of the data to allow for localized compression or expansion, so any offset within each core was equal at all points. Therefore, some features do not appear to align between holes. Because of this, the meters composite depth values will approximately, but not precisely, correspond to the same stratigraphic horizons in adjacent holes.

To test the robustness of the spliced record, the NGR core data from Holes M0059A and M0059E were compared with the logging total spectral gamma ray (HSGR) data of Hole M0059E (Fig. F31). Because of its relatively low resolution (~20 cm or less), all NGR measurements in both holes were included and plotted on the meters below seafloor depth scale using a five-point moving average. Hole M0059A core data were used as the primary reference, as sediments from Hole M0059E were almost completely sampled for microbiology, resulting in reduced core lengths for later NGR measurement. HSGR data were plotted on the logging meters below seafloor scale, which was directly derived from the tool string. Characteristic trends within both records between 0 mbsf (top of the logging operations) and 57 mbsf correlate well to one another, suggesting that the spliced core data contains an almost continuous stratigraphic succession of the uppermost 57 mbsf.

Seismic units

Seismic sequence boundaries were identified by onlap, downlap, and erosional truncation of reflectors. Seismic sequence boundary-sediment core correlations are shown in Figure F32. Correlation is based on the integration of seismic data and lithostratigraphy (see "Lithostratigraphy"). Two-way traveltime values were calculated for each lithostratigraphic unit boundary using sound velocity values measured offshore and during the OSP (see "Physical properties"; Table T17). Cores and/or logs were examined at these calculated depths to define the extent of agreement between seismic boundaries and actual lithologic or log disconformable surfaces. Uncertainties in the time-depth function have resulted in minor inconsistencies between sedimentological observations from cores, seismic features, and the multisensor core logger, as well as downhole logs.

Seismic Unit I

Two-way traveltime: 0.110 ms
Lithology: organic-rich clay (lithostratigraphic Subunit Ia)
Depth: 0–47 mcd

This relatively structureless seismic unit in the uppermost part of the seismic profile correlates to lithostratigraphic Subunit Ia.

Seismic Unit II

Two-way traveltime: 0.115 ms
Lithology: silty clay (lithostratigraphic Subunit Ib)
Depth: 47–52 mcd

The seismic profile shows relatively strong parallel structures in the lowermost part of this unit, suggesting a possible unconformity/erosional contact between seismic Units II and III. That horizon could be a silty sand unit described in "Lithostratigraphy".

Seismic Unit III

Two-way traveltime: 0.155 ms
Lithology: clayey silt and silty clay with a downhole increase of sand (lithostratigraphic Unit III)
Depth: ~52–82 mcd

This seismic unit, which correlates to lithostratigraphic Unit III, shows a slightly irregular internal structures.

Seismic Unit IV

Two-way traveltime: 0.164 ms
Lithology: clay, silt, and sand (lithostratigraphic Unit IV)
Depth: 82–93 mcd

This seismic unit, which correlates to lithostratigraphic Unit IV, shows a slight parallel structure in the seismic profile.

Seismic Unit V

Two-way traveltime: 0.174 ms
Lithology: diamicton (lithostratigraphic Unit V)
Depth: 93–99 mcd

This seismic unit shows strong irregular internal structures.

Seismic Unit VI

Two-way traveltime: 0.244 ms
Lithology: silt, sand, and diamicton (lithostratigraphic Unit VI)
Depth: 99–169 mcd

This seismic unit shows strong irregular internal structures but also some strong parallel reflectors. The very strong parallel reflector occurring in the middle of this unit might suggest a possible unconformity/erosional contact. Therefore, it might be possible to divide seismic Unit VI into subunits. Because of the very poor core recovery within this unit, it was difficult to make reliable seismic sequence boundary-sediment core correlations.

The bedrock surface was found at 169.03 mbsf (two-way traveltime = 0.257 ms), at approximately the same depth at which the seismic data show a very strong parallel reflector. Overall, the sedimentary sequence was shorter than expected, most likely because of the thick organic-rich clay unit (~0–47 mcd) containing high concentrations of gas, which likely resulted in a slower attenuation of seismic waves.

Downhole measurements

Hole M0059B logging operations

Hole M0059B was drilled with an 210 mm (8½ inch) rotary coring bit (Rock Roller) from the seafloor to 204.03 m drilling depth below seafloor (DSF). In preparation for logging, the hole was circulated, the drill string was pulled back in the hole to 20 m wireline log depth below seafloor (WSF), and rig up of the Weatherford equipment began.

The gamma ray tool (MCG)/array induction tool (MAI), measuring NGR and electrical resistivity, was the first tool string to be run and reached 72.5 m WSF, where an uplog was started. Then the drill pipe was run again to 204 m DSF and set at 87 m WSF, and the MCG/MAI tool string was deployed again in order to log the bottom part of the hole. The tool string reached 186.4 m WSF, where an uplog was started. While pulling out of the hole, an overpull was observed, and the decision was made to set the pipe again at ~20 m WSF and deploy the MCG/spectral gamma ray tool (SGS)/sonic sonde (MSS) tool string, measuring total gamma ray, spectral gamma ray, and compensated sonic velocity. This tool string was run to 72.5 m WSF, and an uplog was started.

Hole M0059B logging units

Hole M0059B is divided into six logging units on the basis of the logs (Fig. **F33**). The uplog was used as the reference to establish the wireline log depth below seafloor depth scale. Total gamma ray values from the different tool strings correlate well. The olive-green total gamma ray was measured from 0 to 87 m WSF through pipe. The compensated sonic log remains relatively constant downhole, with some paired aberrations probably due to unwanted environmental effects such as hole rugosity.

Logging Unit 1: base of drill pipe to 50 m WSF

This logging unit is characterized by constant gamma ray values and dominated by thorium and uranium and extremely low potassium values. Electrical resistivity slightly increases because of increasing compaction. This corresponds to lithostratigraphic Subunit Ia (see **"Lithostratigraphy"**).

Logging Unit 2: 50–57 m WSF

Logging Unit 2 is characterized by a sudden drop in both NGR and electrical resistivity, which again increase through this unit. This shows a lithostratigraphic boundary from clay to silty clay with quartz silt. The separation of the different investigation depths (shallow, medium, and deep) of resistivity values show that the formation is permeable.

Logging Unit 3: 57–72.5 m WSF

In logging Unit 3 from 55 m WSF to the deepest part of this logging unit, NGR values are high again and slightly increase. The electrical resistivity data also slightly increase with some fluctuations.

Logging Unit 4: 88.5–145 m WSF

Logging Unit 4 is characterized by a decrease in NGR from ~80 to <40 gAPI and by a decrease in resistivity. Deeper than 125 m WSF, resistivities at different investigation depths are separated again, showing water infiltration into the formation. Fluctuations are observed in resistivity between 90 and 110 m WSF. They might be due to poor borehole conditions, but no caliper data are available for this hole.

Logging Unit 5: 145–164 m WSF

In logging Unit 5, an increase in NGR and an increase in electrical resistivity between 145 and 157 m WSF are observed. As no caliper data are available and core recovery was very low, it is difficult to deduce whether this corresponds to an interbedded glacial deposit or poor borehole conditions.

Logging Unit 6: 164–185 m WSF

Logging Unit 6 is marked by a sudden drop in NGR values at 164 m WSF to values <20 gAPI. Resistivity slightly decreases to very low values. This decrease corresponds to lithostratigraphic Unit VII, limestone with flint gravel (see **"Lithostratigraphy"**).

Hole M0059E logging operations

Hole M0059E was drilled with a 210 mm (8½ inch) rotary coring bit (Rock Roller) from the seafloor to 100.8 m DSF. In preparation for logging, the hole was circulated, the drill string was pulled back in the hole to 15 m WSF, and rig up of the Weatherford equipment began.

The first tool string was the MCG/MAI tool string, with total gamma ray and induction tools; it reached ~70 m WSF, where an uplog was performed. The second tool string was the MCG/microimager (CMI) tool string, with a total gamma ray tool and a microimager; it reached 59 m WSF. The last tool string was

the MCG/SGS/MSS, with total gamma ray, spectral gamma ray, and sonic tools; it also reached 59 m WSF, where an uplog was started.

Hole M0059E logging units

Hole M0059E is divided into two logging units on the basis of the logs (Fig. F34). The uplog was used as the reference to establish the wireline log depth below seafloor depth scale. Total gamma ray values from the different tool strings correlate well. Resistivity shows a general increase downhole because of increasing compaction.

Logging Unit 1: base of drill pipe to 52 m WSF

The upper logging unit is characterized by slightly increasing gamma ray values and dominated by thorium and uranium and extremely low potassium values. Electrical resistivity slightly increases, with oscillations between 15 and 35 m WSF corresponding to an increased borehole diameter (cf. caliper log). This corresponds to logging Unit I in Hole M0059B. The sonic log increases from ~620 to 630 µs/m at 26 m WSF and then remains constant throughout this unit. The paired aberrations between 34 and 35 m WSF and 43 and 44 m WSF are due to unwanted environmental effects.

Logging Unit 2: 52–70 m WSF

Logging Unit 2 is characterized by an increase in NGR to high natural gamma ray values of 100 gAPI. The electrical resistivity data increase, with some fluctuations and separated logs for the different investigation depths (shallow, medium, and deep) indicating infiltration. This unit corresponds to logging Unit 3 from Hole M0059B.

References

Andrén, E., 1999. Changes in the composition of the diatom flora during the last century indicate increased eutrophication of the Oder estuary, southwestern Baltic Sea. *Estuarine, Coastal Shelf Sci.,* 48(6):665–676. **doi:10.1006/ecss.1999.0480**

Andrén, E., Andrén, T., and Kunzendorf, H., 2000a. Holocene history of the Baltic Sea as a background for assessing records of human impact in the sediments of the Gotland Basin. *Holocene,* 10(6):687–702. **doi:10.1191/09596830094944**

Andrén, E., Andrén, T., and Sohlenius, G., 2000b. The Holocene history of the southwestern Baltic Sea as reflected in a sediment core from the Bornholm Basin. *Boreas,* 29(3):233–250. **doi:10.1111/j.1502-3885.2000.tb00981.x**

Andrén, T., Jørgensen, B.B., Cotterill, C., Green, S., Andrén, E., Ash, J., Bauersachs, T., Cragg, B., Fanget, A.-S., Fehr, A., Granoszewski, W., Groeneveld, J., Hardisty, D., Herrero-Bervera, E., Hyttinen, O., Jensen, J.B., Johnson, S., Kenzler, M., Kotilainen, A., Kotthoff, U., Marshall, I.P.G., Martin, E., Obrochta, S., Passchier, S., Quintana Krupinski, N., Riedinger, N., Slomp, C., Snowball, I., Stepanova, A., Strano, S., Torti, A., Warnock, J., Xiao, N., and Zhang, R., 2015. Methods. *In* Andrén, T., Jørgensen, B.B., Cotterill, C., Green, S., and the Expedition 347 Scientists, *Proc. IODP,* 347: College Station, TX (Integrated Ocean Drilling Program). **doi:10.2204/iodp.proc.347.102.2015**

Apolinarska, K., Woszczyk, M., and Obremska, M., 2012. Late Weichselian and Holocene palaeoenvironmental changes in northern Poland based on the Lake Skrzynka record. *Boreas,* 41(2):292–307. **doi:10.1111/j.1502-3885.2011.00235.x**

Berner, R.A., and Raiswell, R., 1983. Burial of organic carbon and pyrite sulfur in sediments over Phanerozoic time: a new theory. *Geochim. Cosmochim. Acta,* 47(5):855–862. **doi:10.1016/0016-7037(83)90151-5**

Burdige, D.J., 2006. *Geochemistry of Marine Sediments:* Princeton, NJ (Princeton Univ. Press).

Canfield, D.E., 1994. Factors influencing organic carbon preservation in marine sediments. *Chem. Geol.,* 114(3–4):315–329. **doi:10.1016/0009-2541(94)90061-2**

Cooper, S.R., 1995. Diatoms in sediment cores from the mesohaline Chesapeake Bay, U.S.A. *Diatom Res.,* 10(1):39–89. **doi:10.1080/0269249X.1995.9705329**

Dörfler, W., Feeser, I., van den Bogaard, C., Dreibrodt, S., Erlenkeuser, H., Kleinmann, A., Merkt, J., and Wiethold, J., 2012. A high-quality annually laminated sequence from Lake Belau, northern Germany: revised chronology and its implication for palynological and tephrochronological studies. *Holocene,* 22(12):1413–1426. **doi:10.1177/0959683612449756**

Duff, K.E., and Smol, J.P., 1988. Chrysophycean stomatocysts from the postglacial sediments of a High Arctic lake. *Can. J. Bot.,* 66(6):1117–1128. **doi:10.1139/b88-160**

Duff, K.E., Zeeb, B.A., and Smol, J.P., 1995. *Atlas of Chryosphycean Cysts* (Vol. I)*:* Dordrecht, The Netherlands (Kluwer Academic Publ.).

Frenzel, P., Keyser, D., and Viehberg, F.A., 2010. An illustrated key and (palaeo)ecological primer for postglacial to Recent Ostracoda (Crustacea) of the Baltic Sea. *Boreas,* 39(3):567–575. **doi:10.1111/j.1502-3885.2009.00135.x**

Froelich, P.N., Klinkhammer, G.P., Bender, M.L., Luedtke, N.A., Heath, G.R., Cullen, D., Dauphin, P., Hammond, D., Hartman, B., and Maynard, V., 1979. Early oxidation of organic matter in pelagic sediments of the eastern equatorial Atlantic: suboxic diagenesis. *Geochim. Cosmochim. Acta,* 43(7):1075–1090. **doi:10.1016/0016-7037(79)90095-4**

Fryxell, G.A., and Hasle, G.R., 1980. The marine diatom *Thalassiosira oestrupii*: structure, taxonomy and distribution. *Am. J. Bot.,* 67(5):804–814. **doi:10.2307/2442672**

Grimm, K.A., and Gill, A.S., 1994. Fossil phytoplankton blooms and shellfish genes: the ecological and evolutionary significance of *Chaetoceros* resting spores in laminated diatomaceous sediments. *Geol. Soc. Am. Abstr. Prog.,* 26:A170–A171.

Hajdu, S., and Larsson, U., 1990. Spatial and temporal patterns in succession of pelagic diatoms in a brackish water coastal area [paper presented at the 11th International Symposium on Living and Fossil Diatoms, San Francisco, 13–17 August 1990].

Håkansson, H., Hajdu, S., Snoeijs, P., and Loginova, L., 1993. *Cyclotella hakanssoniae* Wendker and its relationship to *C. caspia* Grunow and other similar brackish water *Cyclotella* species. *Diatom Res.,* 8(2):333–347. **doi:10.1080/0269249X.1993.9705266**

Harland, R., and Nordberg, K., 2011. The identification, occurrence and importance of microreticulate dinoflagellate cysts in the latest Holocene sediments of the Skagerrak and Kattegat, west coast of Sweden. *Rev. Palaeobot. Palynol.,* 164(1–2):84–92. **doi:10.1016/j.revpalbo.2010.11.009**

Hedenström, A., and Risberg, J., 1999. Early Holocene shore-displacement in southern central Sweden as recorded in elevated isolated basins. *Boreas,* 28(4):490–504. **doi:10.1111/j.1502-3885.1999.tb00236.x**

Hendey, N.I., 1964. *Fishery Investigations, Series 4: An Introductory Account of the Smaller Algae of British Coastal Waters* (Part 5) Bacillariophyceae *(Diatoms):* London (HMSO).

Hustedt, F. 1930: Die Kieselalgen Deutschlands, Österreichs und der Schweiz mit Berücksichtigung der übrigen Länder Europas sowie der angrenzenden Meresgebiete, 7/1, 8/2. *In* Rabenorst, L. (Ed.), *Kryptogamen-Flora von Deutschland, Österreich und der Schweiz:* Leipzig, Germany (Akademische Verlagsgesellschaft).

Koç, N., and Scherer, R.P., 1996. Neogene diatom biostratigraphy of the Iceland Sea Site 907. *In* Thiede, J., Myhre, A.M., Firth, J.V., Johnson, G.L., and Ruddiman, W.F. (Eds.), *Proc. ODP, Sci. Results,* 151: College Station, TX (Ocean Drilling Program), 61–74. **doi:10.2973/odp.proc.sr.151.108.1996**

Koç Karpuz, N., and Schrader, H., 1990. Surface sediment diatom distribution and Holocene paleotemperature variations in the Greenland, Iceland and Norwegian Sea. *Paleoceanography,* 5(4):557–580. **doi:10.1029/PA005i004p00557**

Kristensen, P., Gibbard, P., Knudsen, K.L., and Ehlers, J., 2000. Last interglacial stratigraphy at Ristinge Klint, South Denmark. *Boreas,* 29(2):103–116. **doi:10.1111/j.1502-3885.2000.tb01204.x**

Leventer, A., Domack, E.W., Ishman, S.E., Brachfeld, S., McClennen, C.E., and Manley, P., 1996. Productivity cycles of 200–300 years in the Antarctic Peninsula region: understanding linkages among the sun, atmosphere, oceans, sea ice, and biota. *Geol. Soc. Am. Bull.,* 108(12):1626–1644. **doi:10.1130/0016-7606(1996)108<1626:PCOYIT>2.3.CO;2**

Lipps, J.H., and McCartney, K., 1993. Chrysophytes: crysophyte cysts. *In* Lipps, J.H. (Ed.), *Fossil Prokaryotes and Protists:* Cambridge, MA (Blackwell Sci. Publ.), 141–143.

Madsen, H.B., and Knudsen, K.L., 1994. Recent foraminifera in shelf sediments of the Scoresby Sund fjord, East Greenland. *Boreas,* 23(4):495–504. **doi:10.1111/j.1502-3885.1994.tb00617.x**

McCartney, K., 1993. Chrysophytes: silicoflagellates. *In* Lipps J.H. (Ed.), *Fossil Prokaryotes and Protists:* Cambridge, MA (Blackwell Sci. Publ.), 143–154.

Mitchell, J.G., and Silver, M.W., 1982. Modern archaeomonads indicate sea-ice environments. *Nature,* 296(5856):437–439. **doi:10.1038/296437a0**

Moestrup, Ø., and Thomsen, H., 1990. *Dictyocha speculum* (Silicoflagellata, Dictyochophyceae), studies on armoured and unarmoured stages. *Biol. Skr.—K. Dan. Vidensk. Selsk.,* 37:1–37.

Ojala, A.E.K., Heinsalu, A., Saarnisto, M., and Tiljander, M., 2005. Annually laminated sediments date the drainage of the Ancylus Lake and early Holocene shoreline displacement in central Finland. *Quat. Int.* 130(1):63–73. **doi:10.1016/j.quaint.2004.04.032**

Oku, O., and Kamatani, A., 1997. Resting spore formation of the marine planktonic diatom *Chaetoceros anastomosans* induced by high salinity and nutrient depletion. *Mar. Biol.,* 127(3):515–520. **doi:10.1007/s002270050040**

Rasmussen, J.A., Heinberg, C., and Håkansson, E., 2005. Planktonic foraminifers, biostratigraphy and the diachronous nature of the lowermost Danian Cerithium limestone at Stevns Klint, Denmark. *Bull. Geol. Soc. Den.,* 52(2):113–131. **http://2dgf.dk/xpdf/bull52-2-113-131.pdf**

Risberg, J., 1990. Siliceous microfossil stratigraphy in a superficial sediment core from the northwestern part of the Baltic Proper. *Ambio* 19(3):167–172.

Rosenfeld, A., 1977. Die rezenten Ostracoden-Arten in der Ostsee. *Meyniana,* 29:11–49.

Roussel, E.G., Bonavita, M.-A.C., Querellou, J., Cragg, B.A., Webster, G., Prieur, D., and Parkes, R.J., 2008. Extending the subseafloor biosphere. *Science,* 320(5879):1046. **doi:10.1126/science.1154545**

Sexton, P.F., Wilson, P.A., and Pearson, P.N., 2006. Microstructural and geochemical perspectives on planktic foraminiferal preservation: "glassy" versus "frosty." *Geochem., Geophys., Geosyst.,* 7(12):Q12P19. **doi:10.1029/2006GC001291**

Smol, J.P., 1988. Chrysophycean microfossils in paleolimnological studies. *Palaeogeogr., Palaeoclimatol., Palaeoecol.,* 62(1–4):287–297. **doi:10.1016/0031-0182(88)90058-2**

Snoeijs, P., and Kasperovicienè, J. (Eds.), 1996. *Intercalibration and Distribution of Diatom Species in the Baltic Sea* (Vol. 4): Uppsala, Sweden (Opulus Press).

Snoeijs, P., and Vilbaste, S. (Eds.), 1994. *Intercalibration and Distribution of Diatom Species in the Baltic Sea* (Vol. 2): Uppsala, Sweden (Opulus Press).

Snoeijs, P., Vilbaste, S., Potapova, M., Kasperoviciene, J., and Balashova, J. (Eds.), 1993–1998. *Intercalibration and Distribution of Diatom Species in the Baltic Sea* (Vol. 1–5): Uppsala, Sweden (Opulus Press).

Snowball, I., Zillén, L., Ojala, A., Saarinen, T., and Sandgren, P., 2007. FENNOSTACK and FENNORPIS: varve dated Holocene palaeomagnetic secular variation and relative palaeointensity stacks for Fennoscandia. *Earth Planet. Sc. Lett.,* 255(1–2):106–116. **doi:10.1016/j.epsl.2006.12.009**

Soetaert, K., Hofmann, A.F., Middelburg, J.J, Meysman, F.J.R., and Greenwood, J., 2007. The effect of biogeochemical processes on pH. *Mar. Chem.,* 106(1–2):380–401. (Reprint) **doi:10.1016/j.marchem.2007.06.008**

Sohlenius, G., Sternbeck, J., Andrén, E., and Westman, P., 1996. Holocene history of the Baltic Sea as recorded in a sediment core from the Gotland Deep. *Mar. Geol.,* 134(3–4):183–201. **doi:10.1016/0025-3227(96)00047-3**

Stabell, B., 1985. Diatoms in upper Quaternary Skagerrak sediments. *Nor. Geol. Tidsskr. (1905–2000),* 65(1–2):91–95.

Stepanova, A., Taldenkova, E., Simstich, J., and Bauch, H.A., 2007. Comparison study of the modern ostracod associations in the Kara and Laptev Seas: ecological aspects. *Mar. Micropaleontol.,* 63(3–4):111–142. **doi:10.1016/j.marmicro.2006.10.003**

Tappan, H., 1980. *The Paleobiology of Plant Protists:* San Francisco (W.H. Freeman).

Wallmann, K., Aloisi, G., Haeckel, M., Tishchenko, P., Pavlova, G., Greinert, J., Kutterolf, S., and Eisenhauer, A., 2008. Silicate weathering in anoxic marine sediments. *Geochim. Cosmochim. Acta,* 72(12):2895–2918. **doi:10.1016/j.gca.2008.03.026**

Warnock, J., Scherer, R., and Loubere, P., 2007. A quantitative assessment of diatom dissolution and late quaternary primary productivity in the eastern equatorial Pacific. *Deep-Sea Res., Part II,* 54(5–7):772–783. **doi:10.1016/j.dsr2.2007.01.011**

Weckström, K., and Juggins, S., 2006. Coastal diatom–environment relationships from the Gulf of Finland, Baltic Sea. *J. Phycol.,* 42(1):21–35. **doi:10.1111/j.1529-8817.2006.00166.x**

Westman, P., and Sohlenius, G., 1996. Chrysophyte cysts and diatom flora of a Littorina Sea sediment sequence from the northwestern Baltic proper. *PACT,* 50:175–184.

Westman, P., and Sohlenius, G., 1999. Diatom stratigraphy in five offshore sediment cores from the northwestern Baltic proper implying large scale circulation changes during the last 8500 years. *J. Paleolimnol.,* 22(1):53–69. **doi:10.1023/A:1008011511101**

Wilkinson, A.N., Zeeb, B.A., and Smol, J.P., 2001. *Developments in Hydrobiology* (Vol. 157): *Atlas of Chrysophycean Cysts* (Vol. II): Dordrecht, The Netherlands (Kluwer Academic Publ.).

Willén, T., 1995. Växtplankton i Östersjön 1979–1988. *Naturvårdsverket Rapp.,* 4288. (in Swedish with abstract in English)

Winterhalter, B., 1992. Late-Quaternary stratigraphy of Baltic Sea basins—a review. *Bull. Geol. Soc. Finl.,* 64:189–194.

Witkowski, A., 1994. *Bibliotheca Diatomologica* (Vol. 28): *Recent and Fossil Diatom Flora of the Gulf of Gdansk, Southern Baltic Sea:* Berlin (J. Cramer).

Witkowski, A., and Pempkowiak, J., 1995. Reconstructing the development of human impact from diatoms and ^{210}Pb sediment dating (the Gulf of Gdansk—southern Baltic Sea). *Geogr. Pol.,* 65:63–78. **https://www.geographiapolonica.pl/article/item/7900.html**

Zong, Y., 1997. Implications of *Paralia sulcata* abundance in Scottish isolation basins. *Diatom Res.,* 12(1):125–150. **doi:10.1080/0269249X.1997.9705407**

Publication: 20 February 2015
MS 347-103

Figure F1. Graphic lithology log summary of composite splice, Site M0059.

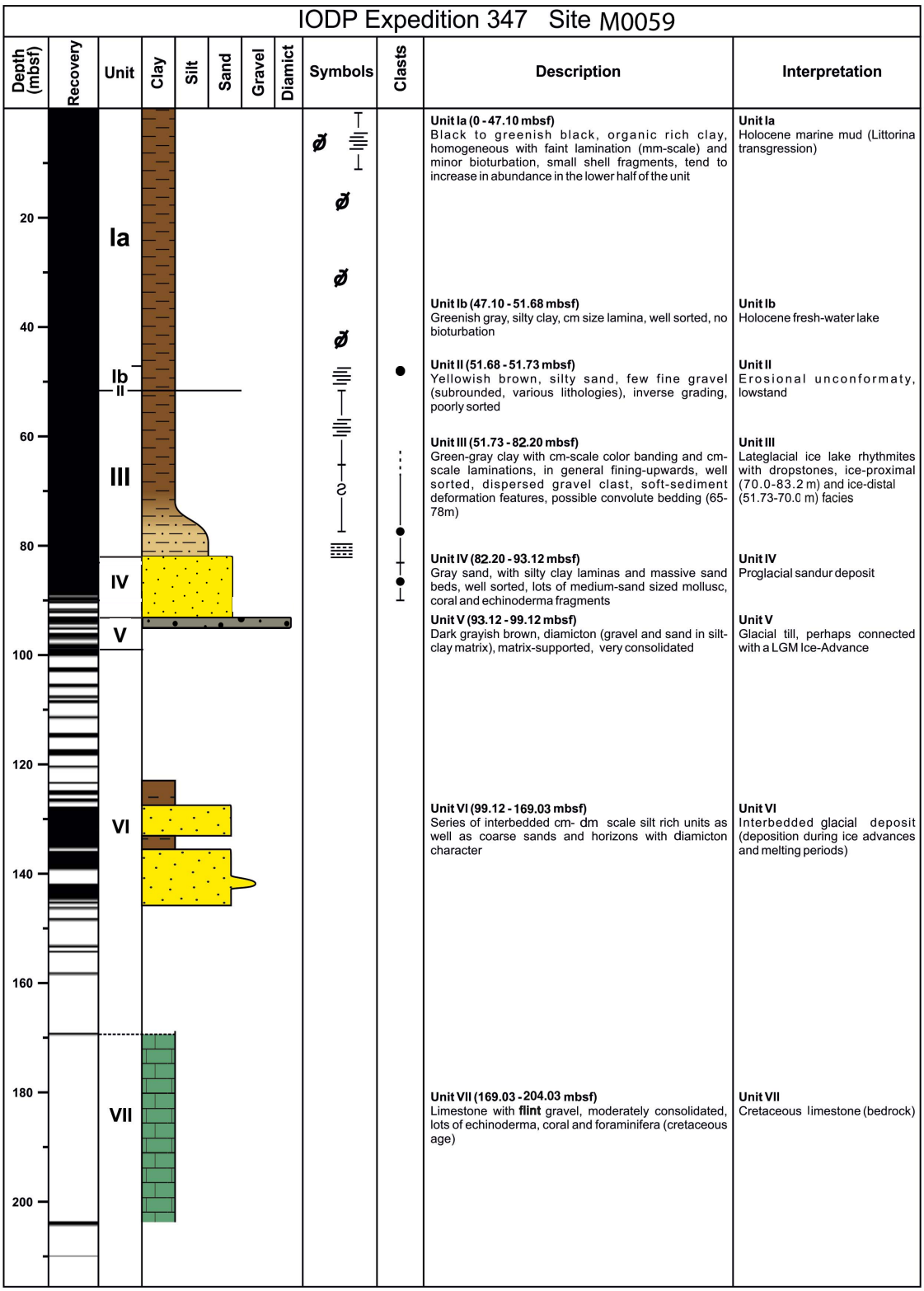

Figure F2. Example of black, homogeneous clay of Subunit Ia, with shell fragments and oxidized olive parts at the bottom (interval 347-M0059A-11H-1, 46–70 cm).

Figure F3. Example of transition from laminated black organic-rich clay of Subunit Ib (Section 347-M0059A-16H-2) through hiatus sand horizon of Unit II and into the varved clay sequence (Unit III). Inset: close-up of the coarse grained, poorly sorted sand hiatus marking a lowstand.

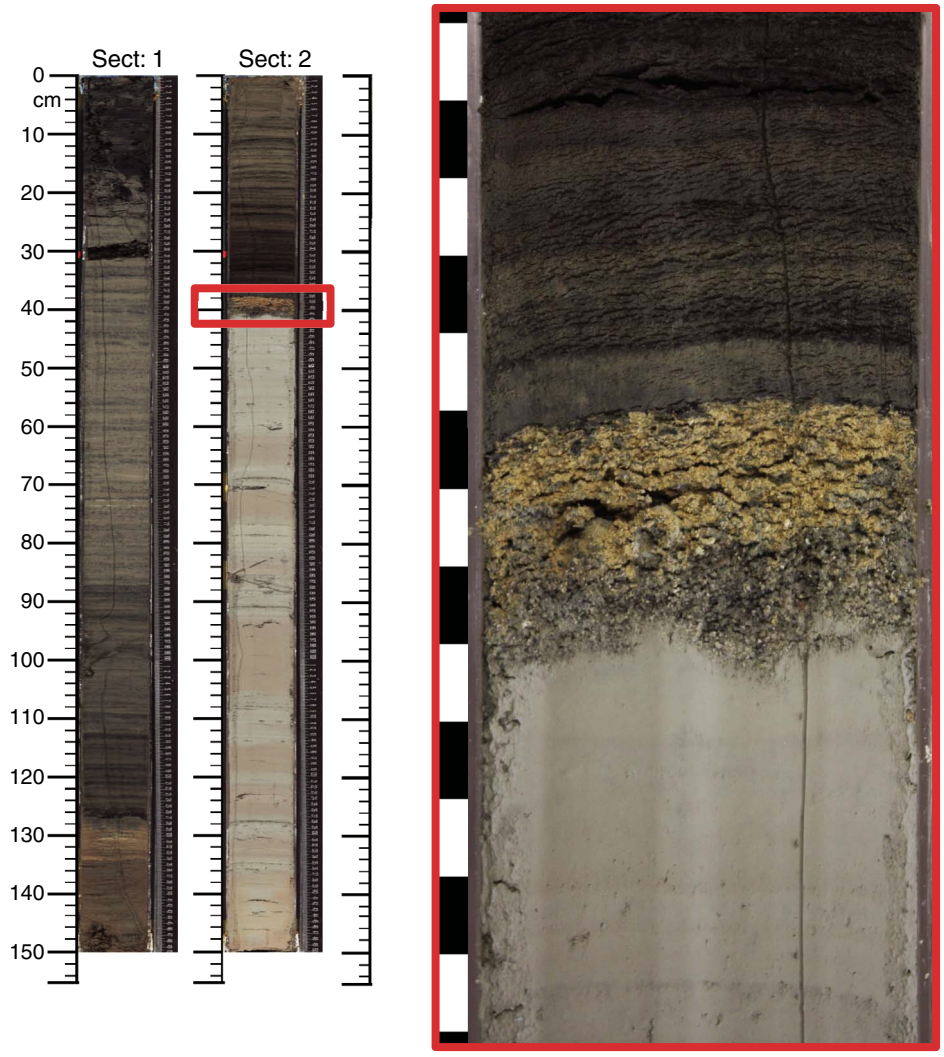

Figure F4. Example of core disturbance caused by drilling in glacial clays (Section 347-M0059C-22H-2).

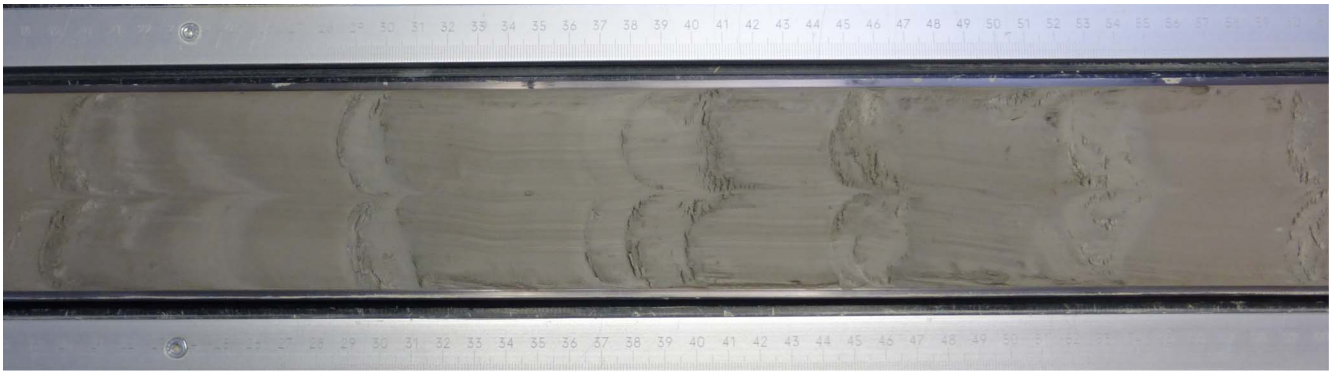

Figure F5. Analyzed levels and the proportion of diatom taxa showing different salinity affinities, Hole M0059A. The total number of diatom taxa recorded is plotted, as well as the number of taxa associated with planktonic and periphytic life forms. Red dots = other siliceous microfossils recorded in the cores.

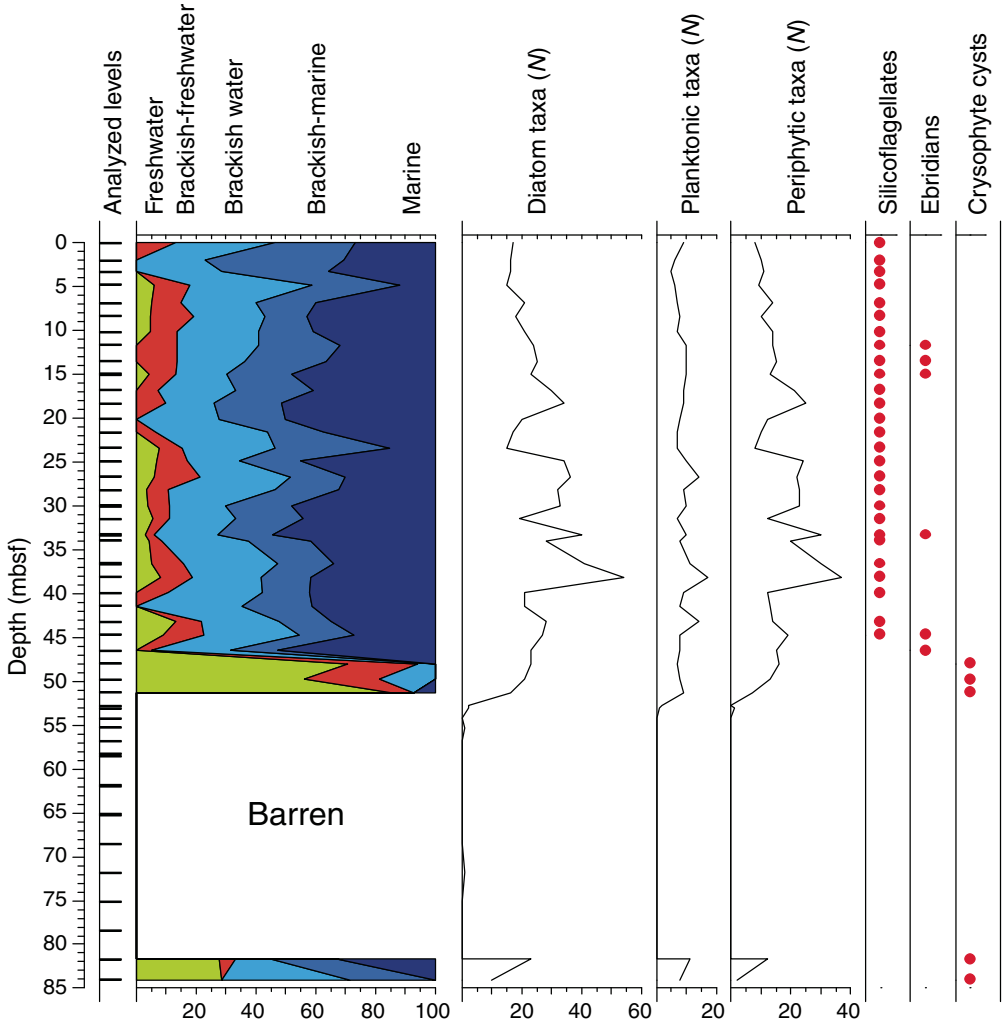

Figure F6. Abundance of benthic foraminifers based on the abundance classification defined in the "Methods" chapter (Andrén et al., 2015), Site M0059. A running average over five samples is plotted onto single data points. Increased shading indicates abundances sufficient for faunal and/or geochemical analyses.

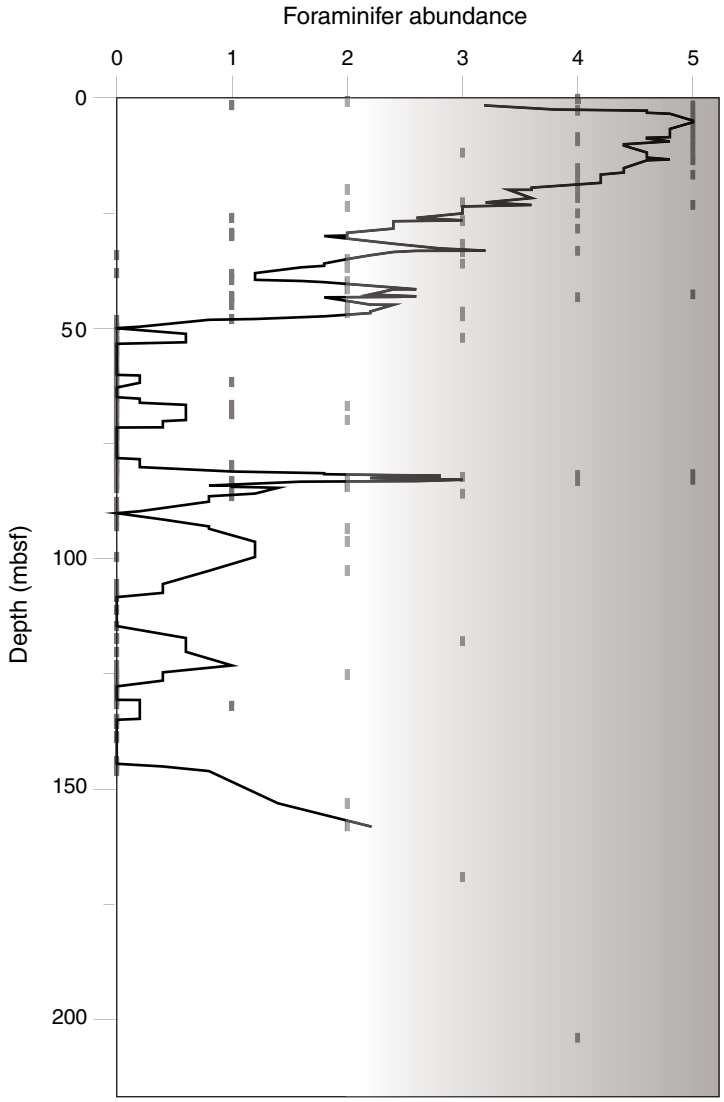

Figure F7. Diversity of benthic foraminifers based on the diversity classification defined in the "Methods" chapter (Andrén et al., 2015), Site M0059. A running average over three samples is plotted onto single data points.

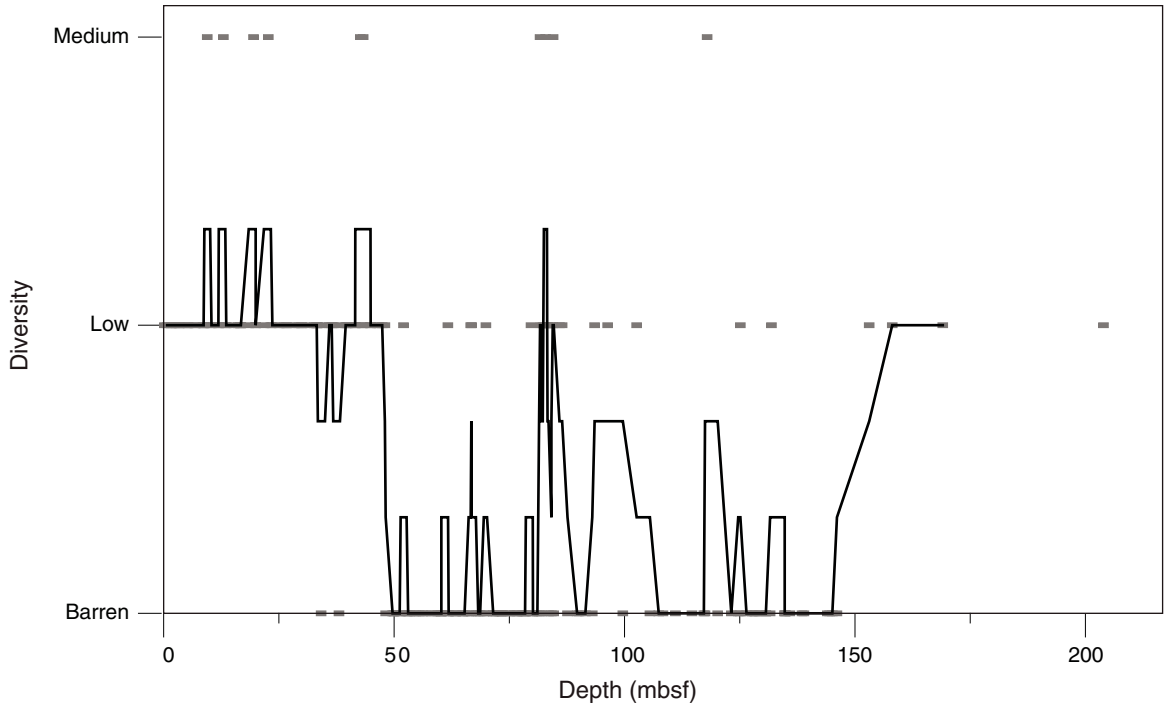

Figure F8. Plots of ostracod total abundance and ecological group distribution, Site M0059. Abundance is shown per sediment volume.

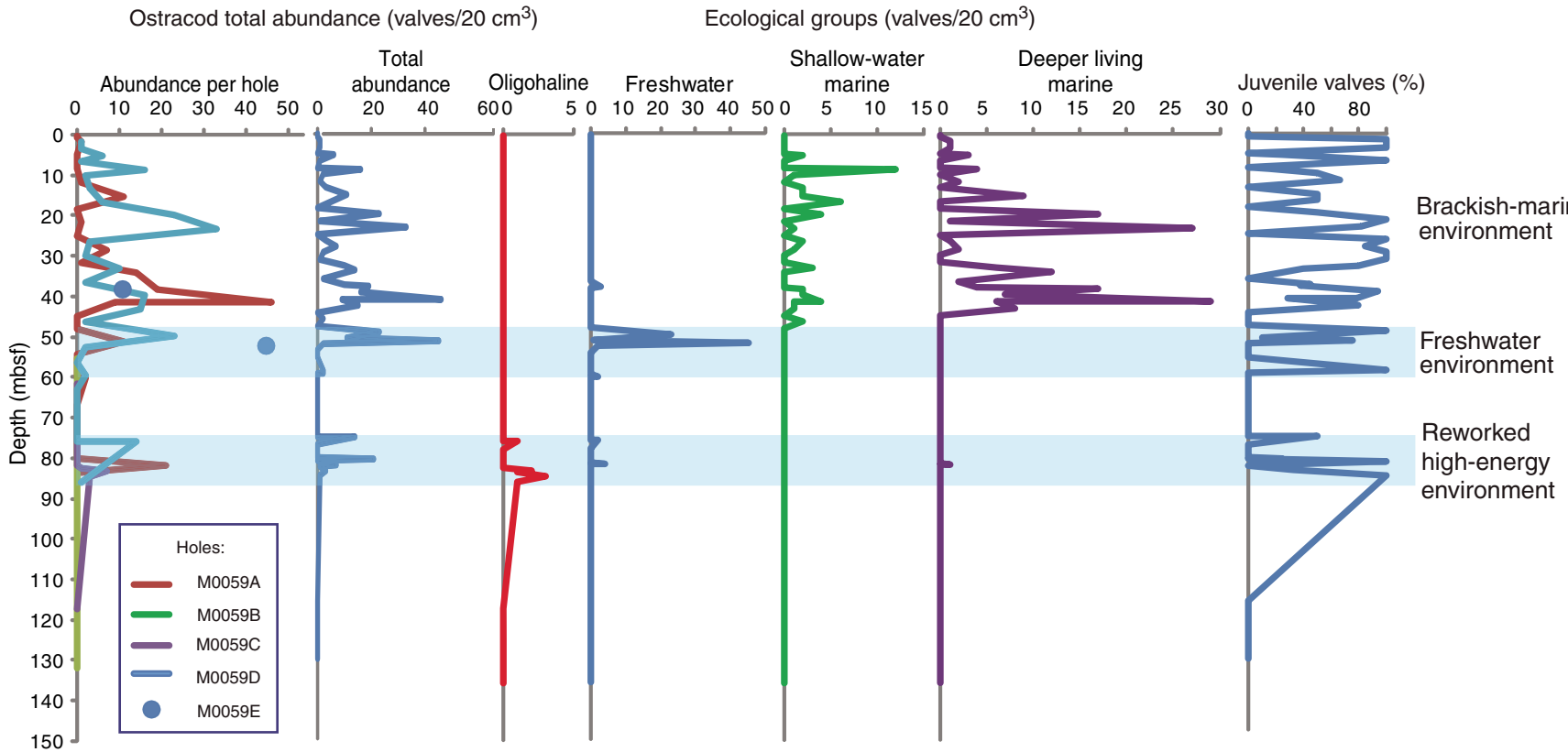

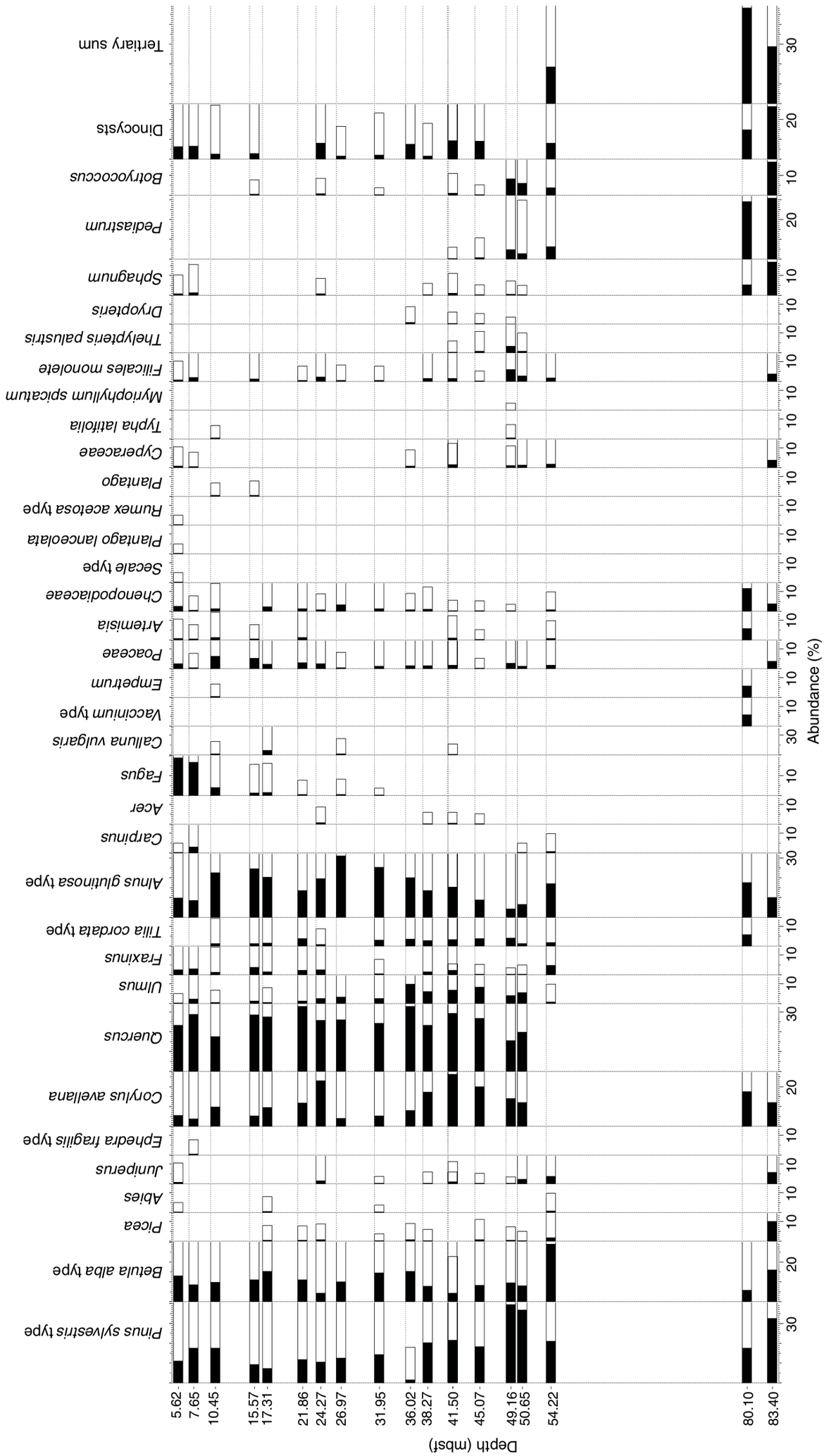

Figure F9. Pollen diagram with bisaccate pollen included in the reference sum, Hole M0059A. For most samples, between 100 and 300 grains were counted.

Figure F10. Diagram showing depth distributions of major pollen types and organic-walled dinocysts, Site M0059. The organic-walled-dinoflagellate-cyst/terrestrial-pollen ratio (*) could not be calculated in samples where in situ dinocysts were absent.

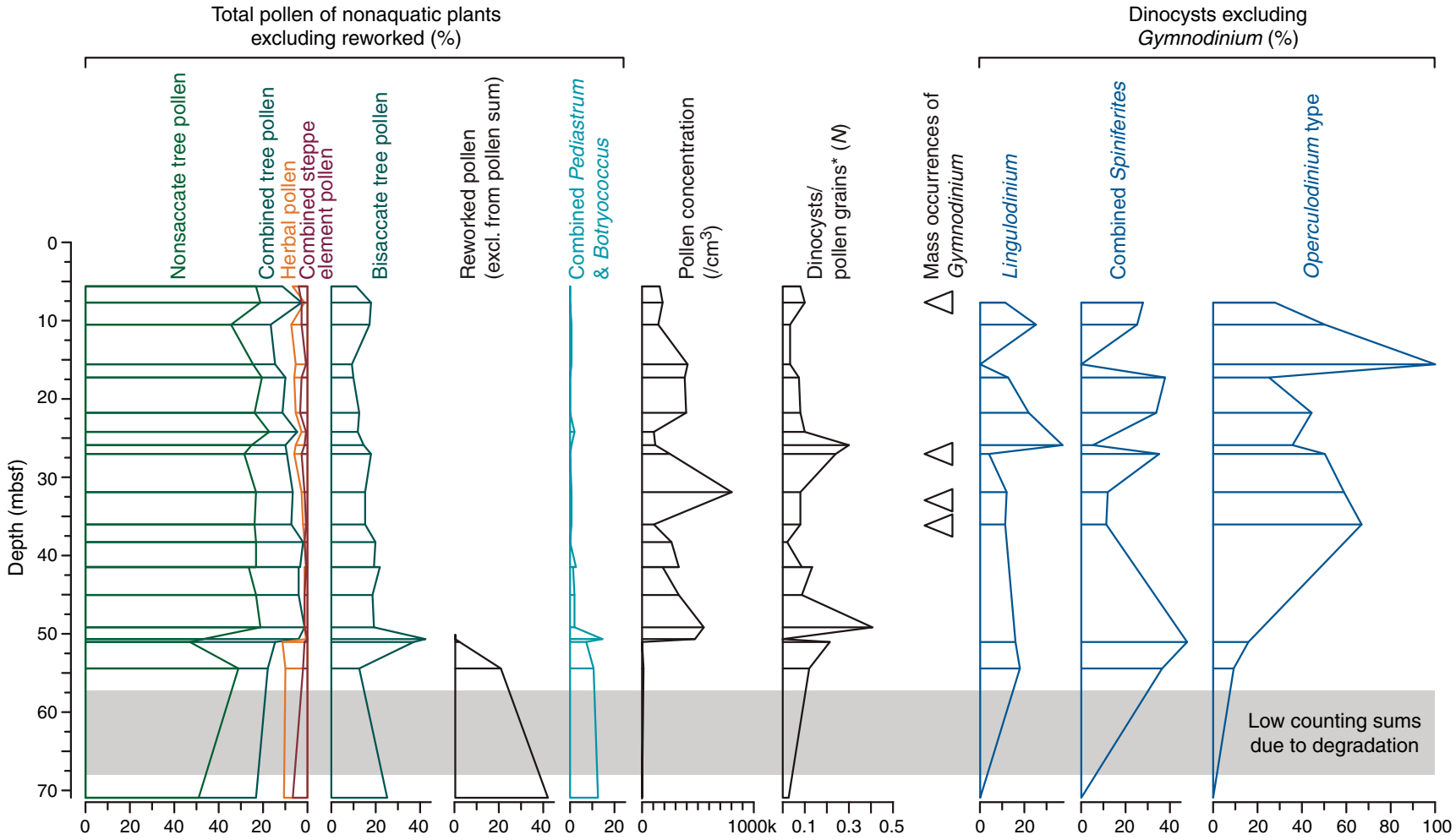

Figure F11. Palynomorphs, Hole M0059A. **1–3.** Pollen grains, (1) *Fagus* (beech, Core 347-M0059A-3H), (2) *Secale* (rye, Core 347-M0059A-3H), (3) *Quercus* (oak, Core 347-M0059A-11H). **4, 5.** Organic-walled dinoflagellate cysts, (4) *Lingulodinium* (Core 347-M0059A-3H), (5) *Gymnodinium* (Core 347-M0059A-4H). **6.** Arthropod mandible, probably larval Odonata (Core 347-M0059A-24H). Scale bars = 20 µm.

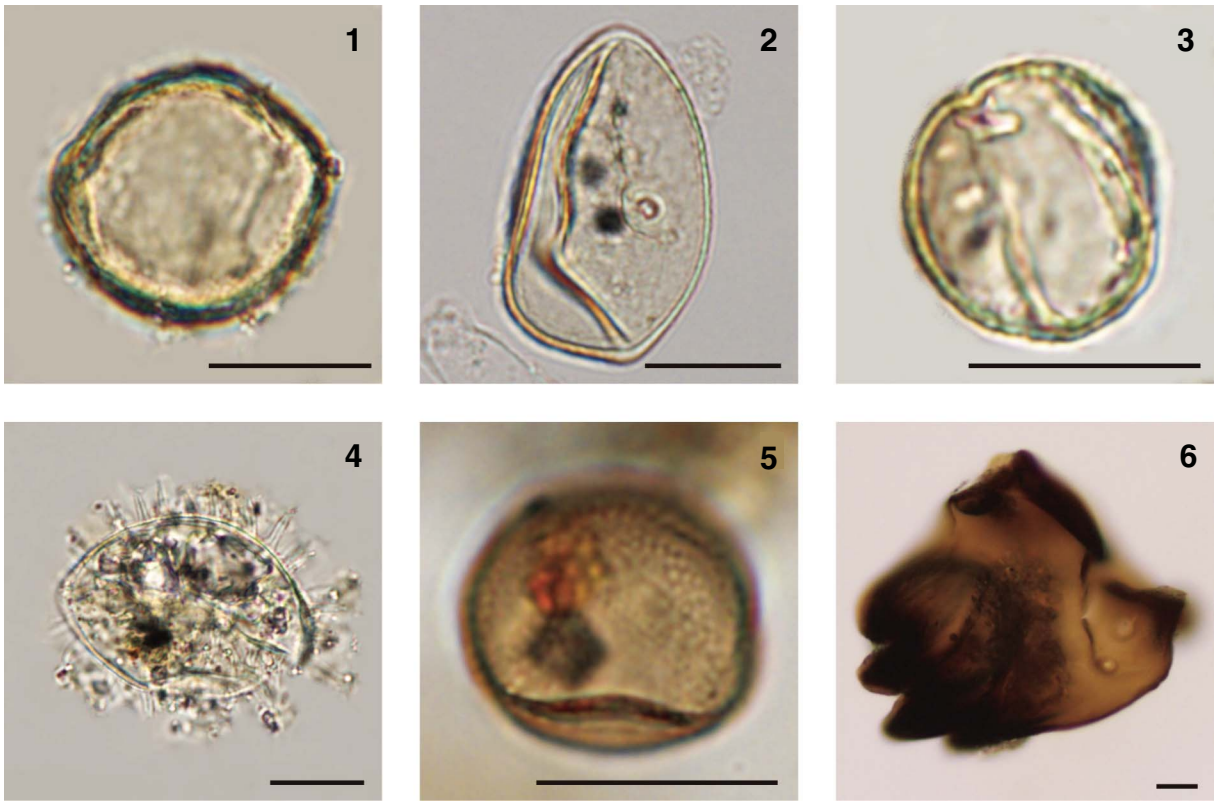

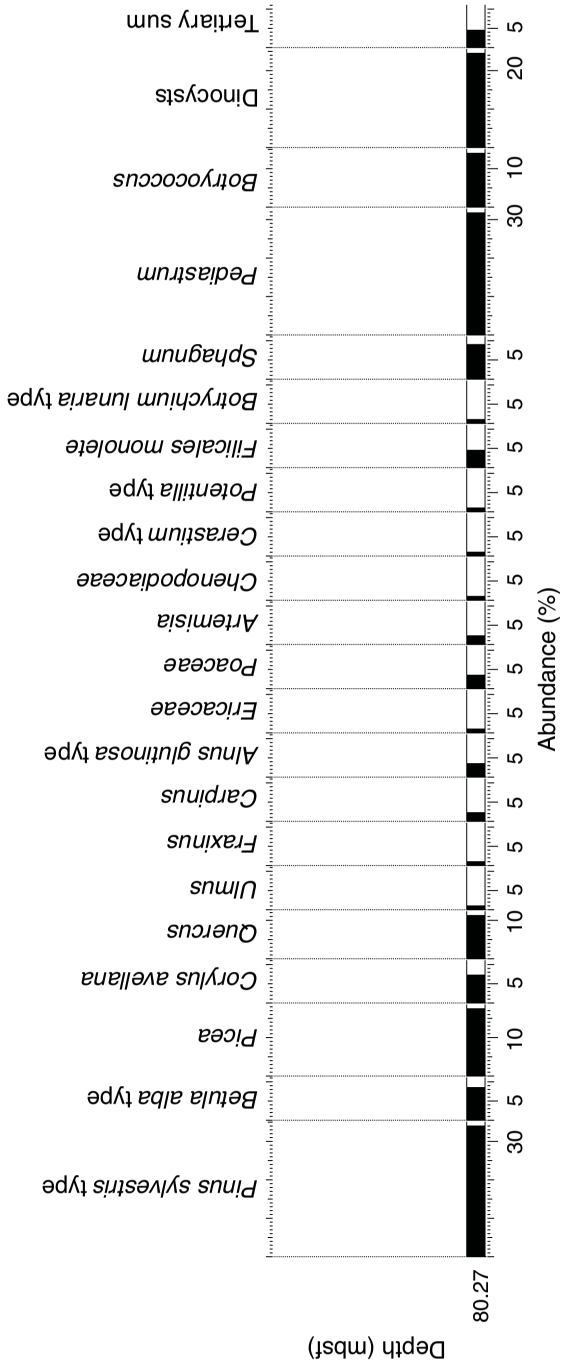

Figure F12. Pollen spectrum for one sample from Hole M0059C.

Figure F13. Concentrations of (**A**) chloride, (**B**) salinity by refractometer (black symbols) and chloride-based salinity (gray symbols), (**C**) alkalinity, and (**D**) anion-based salinity in interstitial water samples, Site M0059.

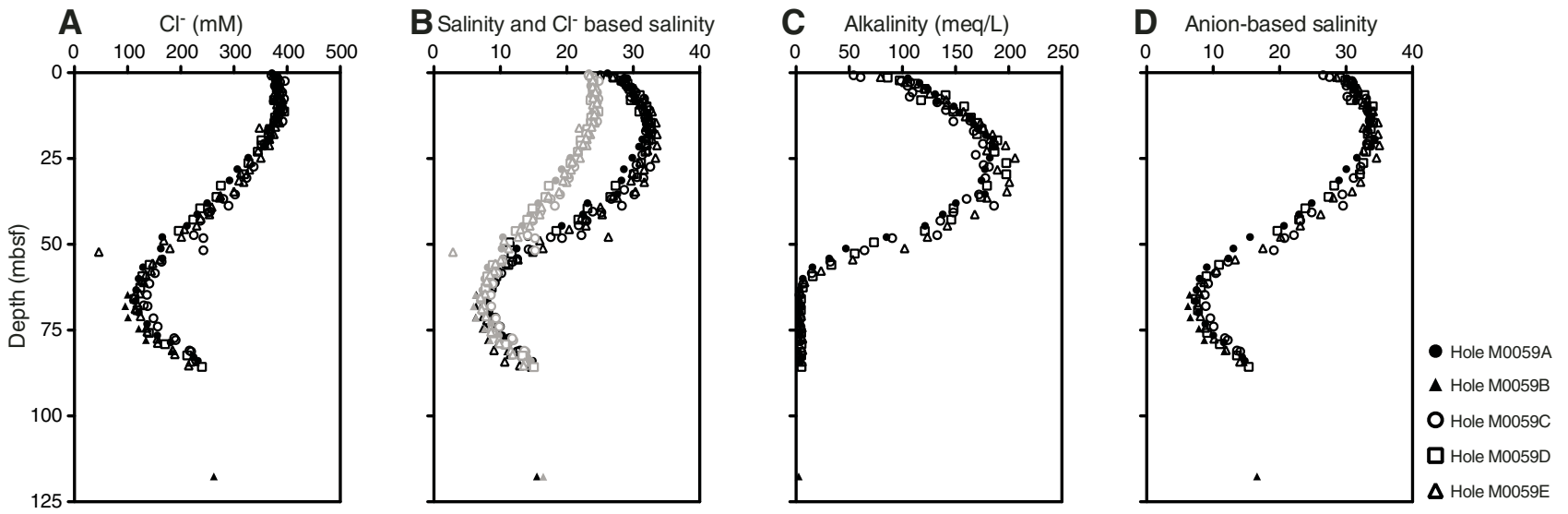

Figure F14. Concentrations of (**A**) methane, (**B**) sulfate, (**C**) hydrogen sulfide, (**D**) ammonium, (**E**) phosphate, (**F**) iron, (**G**) manganese, and (**H**) pH from interstitial water samples, Site M0059.

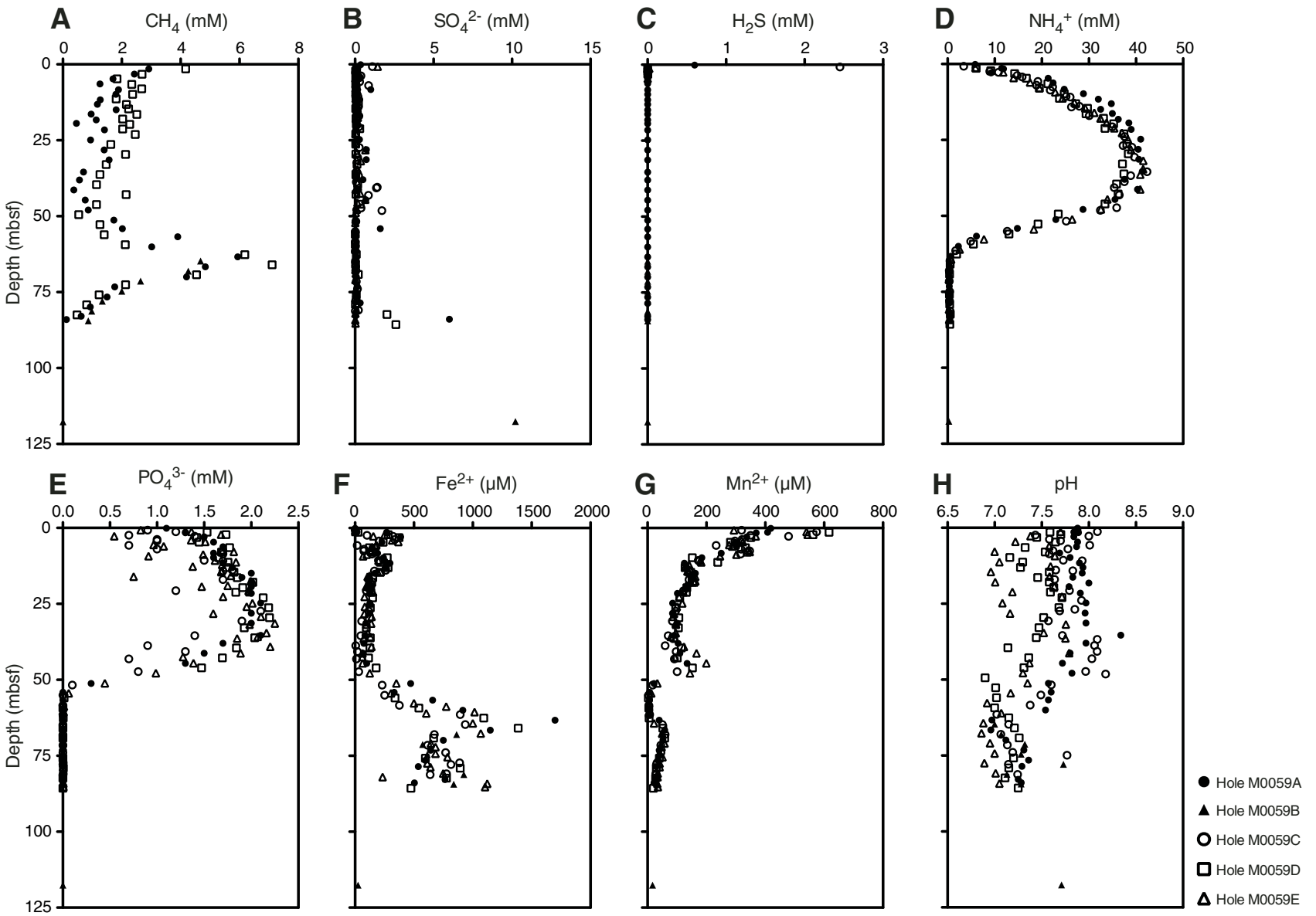

Figure F15. Concentrations of (**A**) bromide, (**B**) bromide/chloride, (**C**) boron, and (**D**) boron/chloride from interstitial water samples, Site M0059. Dashed lines = seawater ratio.

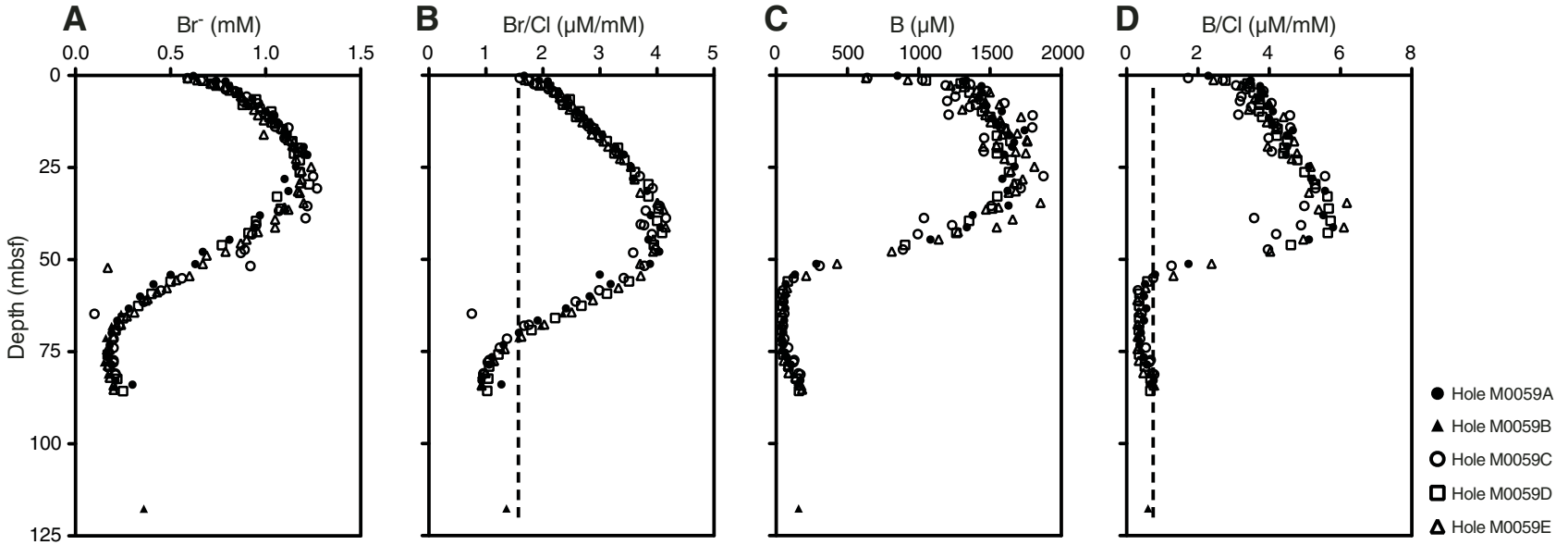

Figure F16. Concentrations of (**A**) sodium, (**B**) potassium, (**C**) magnesium, (**D**) calcium, (**E**) sodium/chloride, (**F**) potassium/chloride, (**G**) magnesium/chloride, and (**H**) calcium/chloride from interstitial water samples, Site M0059. Dashed lines = seawater ratio.

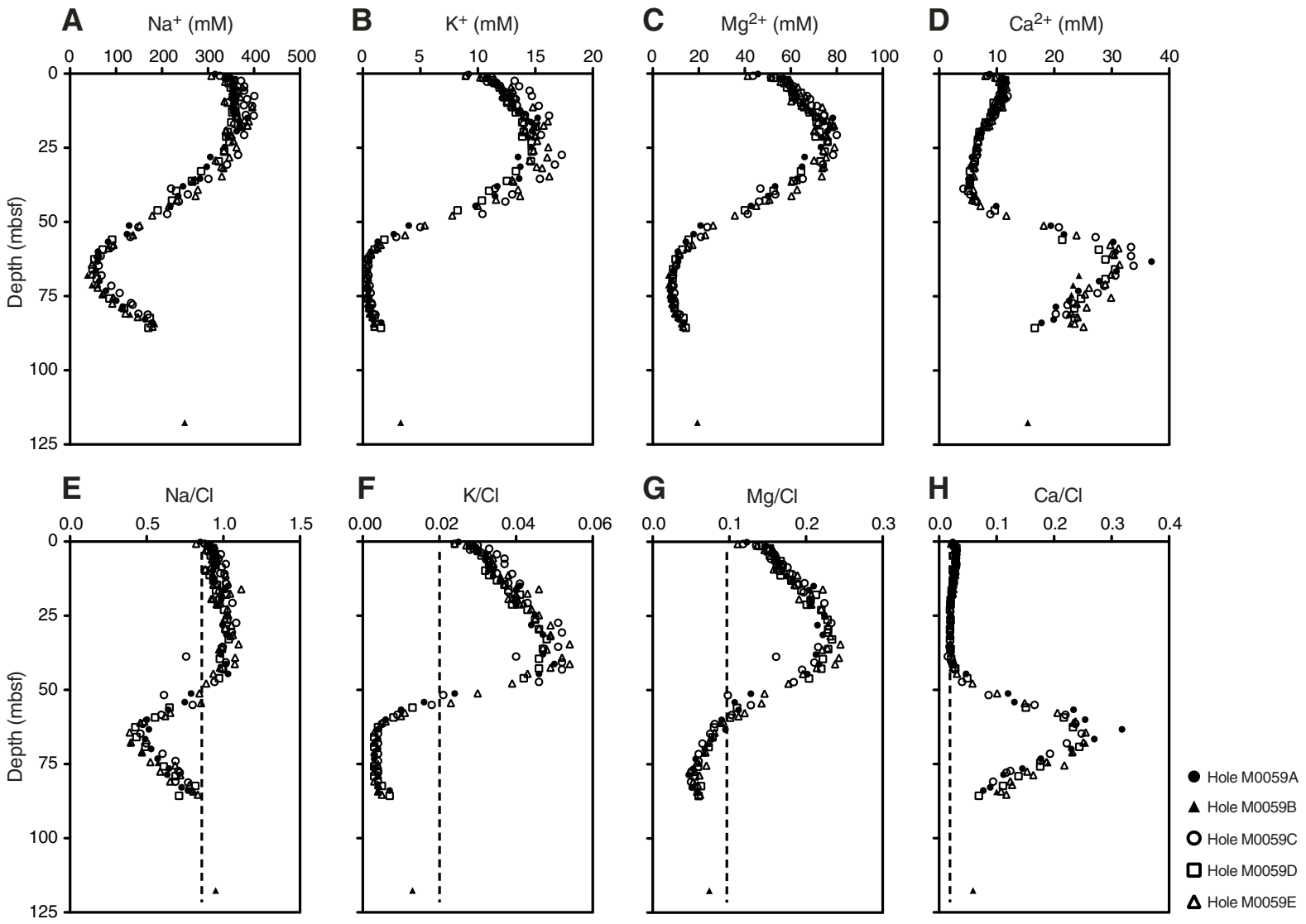

Figure F17. Concentrations of (**A**) dissolved silica, (**B**) lithium, (**C**) barium, and (**D**) strontium in interstitial water samples, Site M0059.

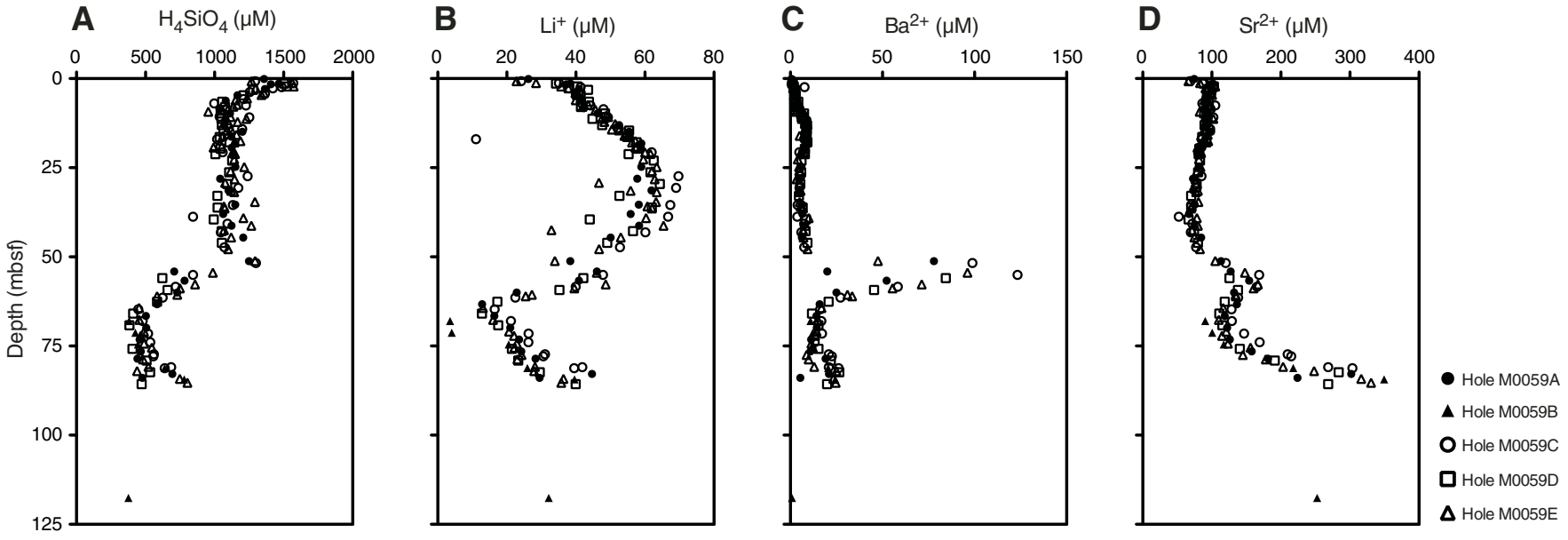

Figure F18. Contents of (**A**) total carbon (TC), (**B**) total organic carbon (TOC), (**C**) total inorganic carbon (TIC), and (**D**) total sulfur (TS) in sediment samples, Site M0059.

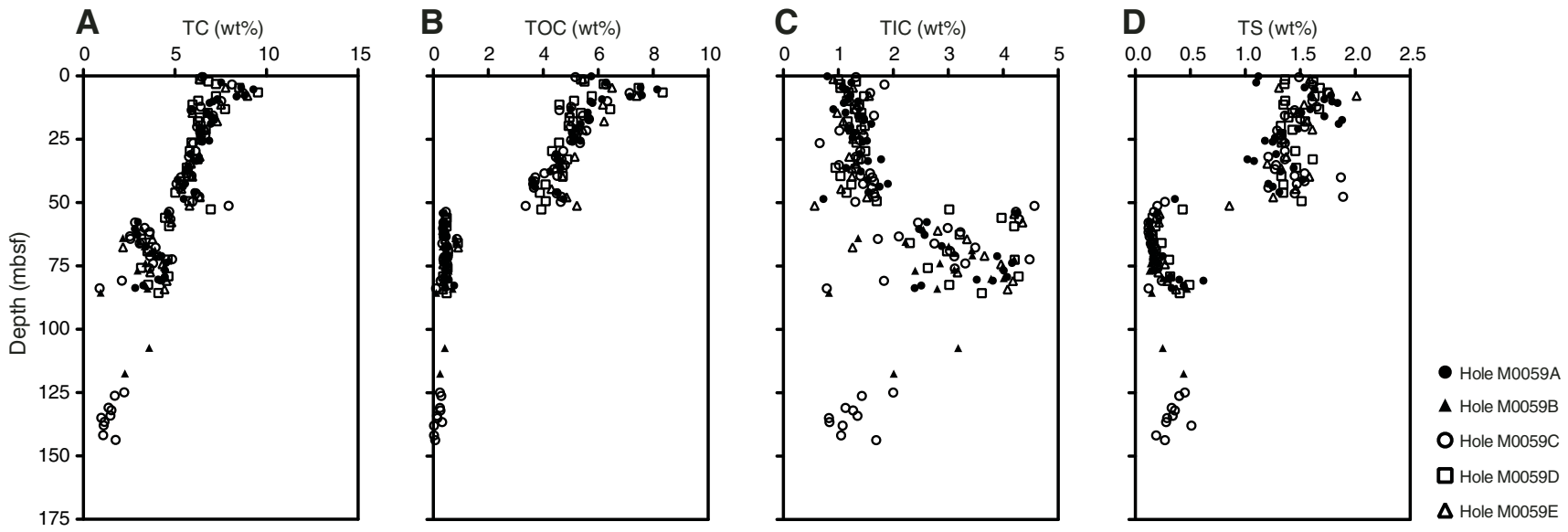

Figure F19. Natural gamma radiation (NGR) (cps), dry density (g/cm^3), and porosity (void fraction) exhibit a stepwise change at ~55 mbsf, Hole M0059D.

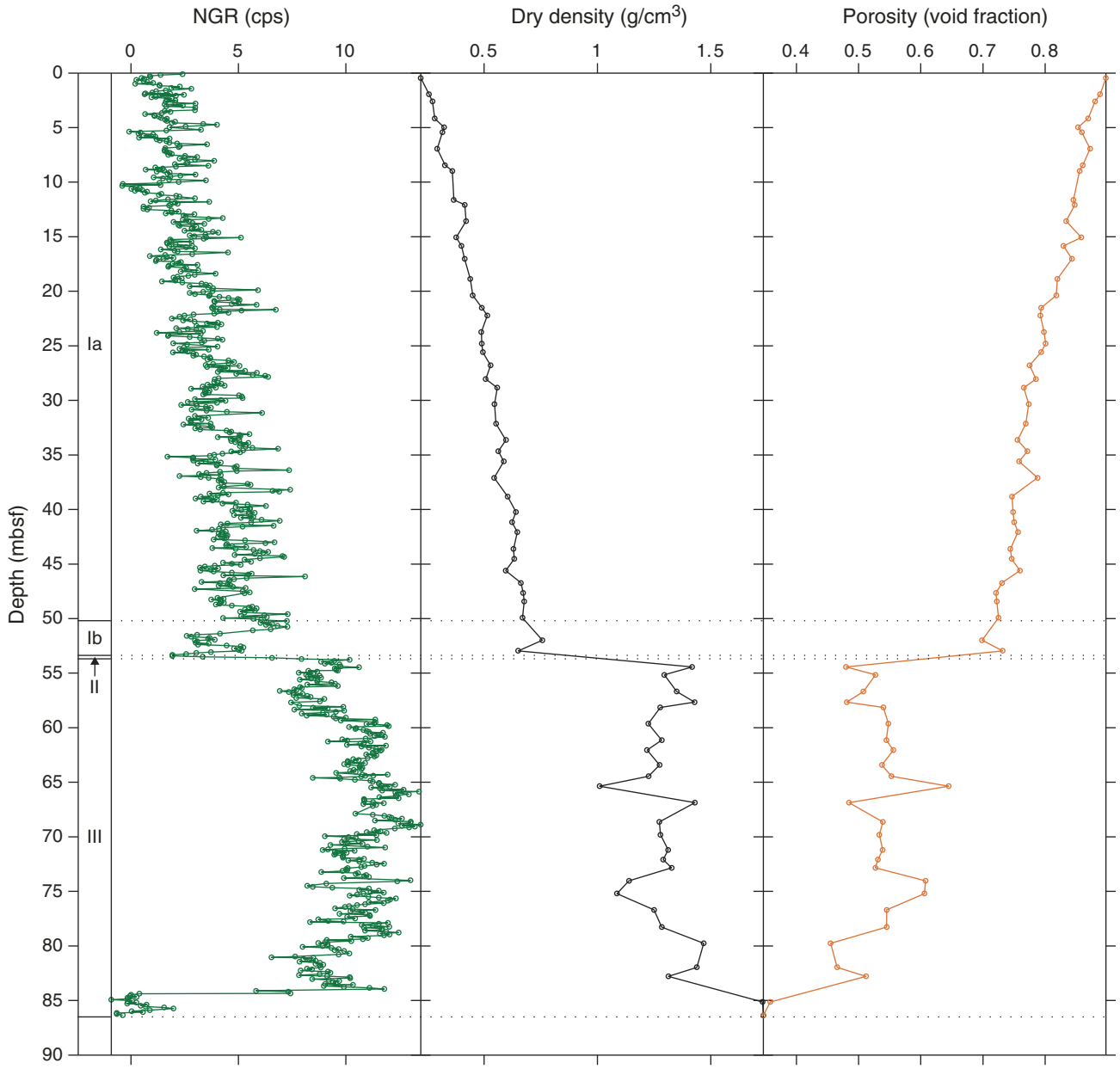

Figure F20. Gamma density (g/cm^3) and discrete bulk density (g/cm^3) measurements derived from pycnometer moisture and density analyses, Hole M0059D.

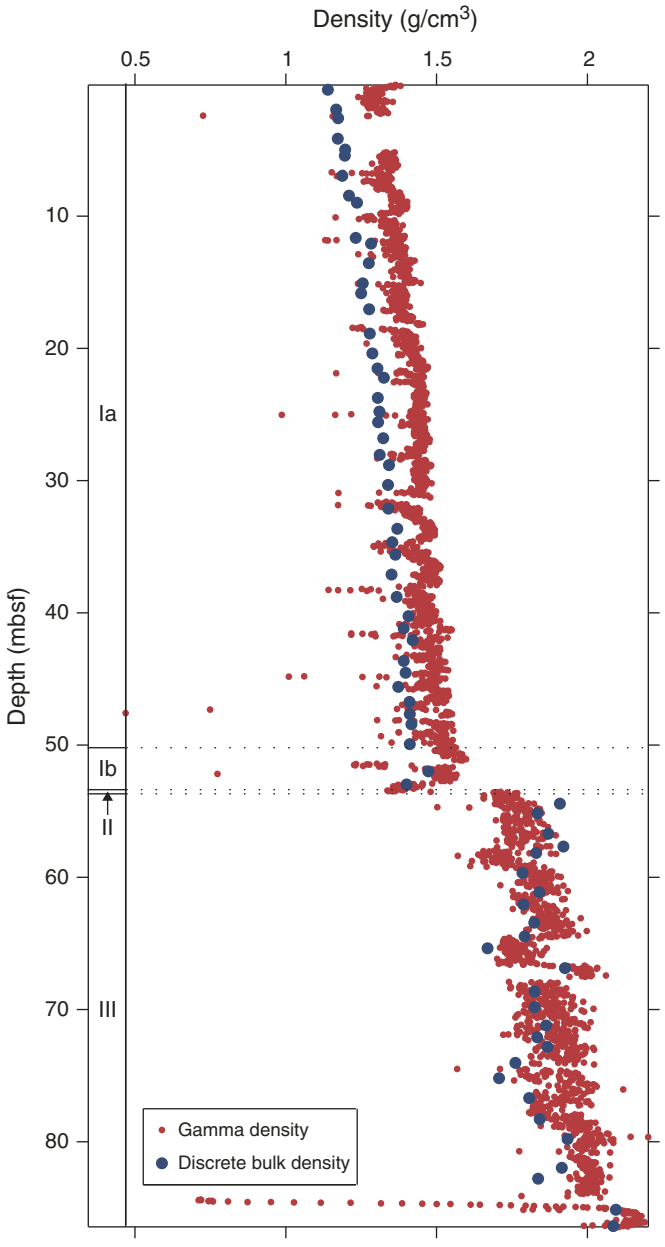

Figure F21. Gamma density (g/cm^3) and discrete bulk density (g/cm^3) measurements are highly correlated in Hole M0059D.

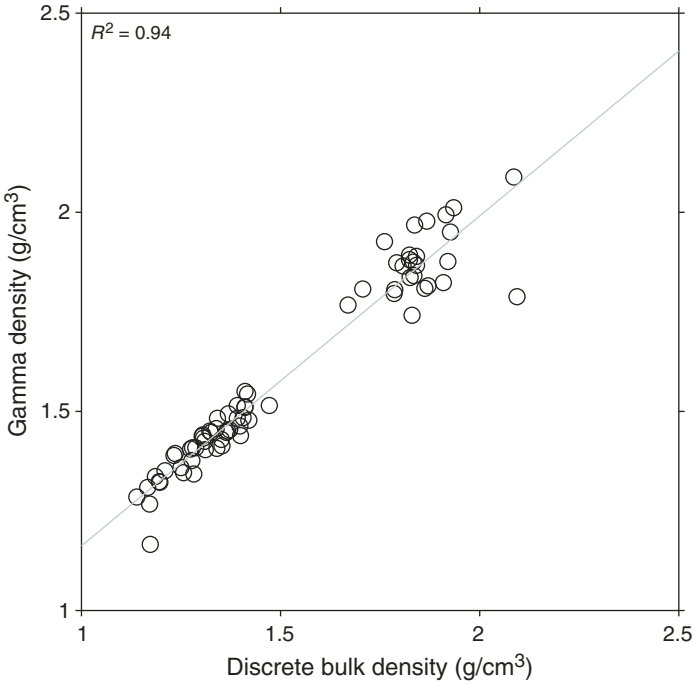

Figure F22. Plots and biplots of magnetic susceptibility (χ), natural remanent magnetization (NRM) intensity, and NRM inclination of discrete paleomagnetic samples, Holes M0059A–M0059E. Dashed line in inclination = geocentric axial dipole (GAD) prediction of inclination for the site latitude.

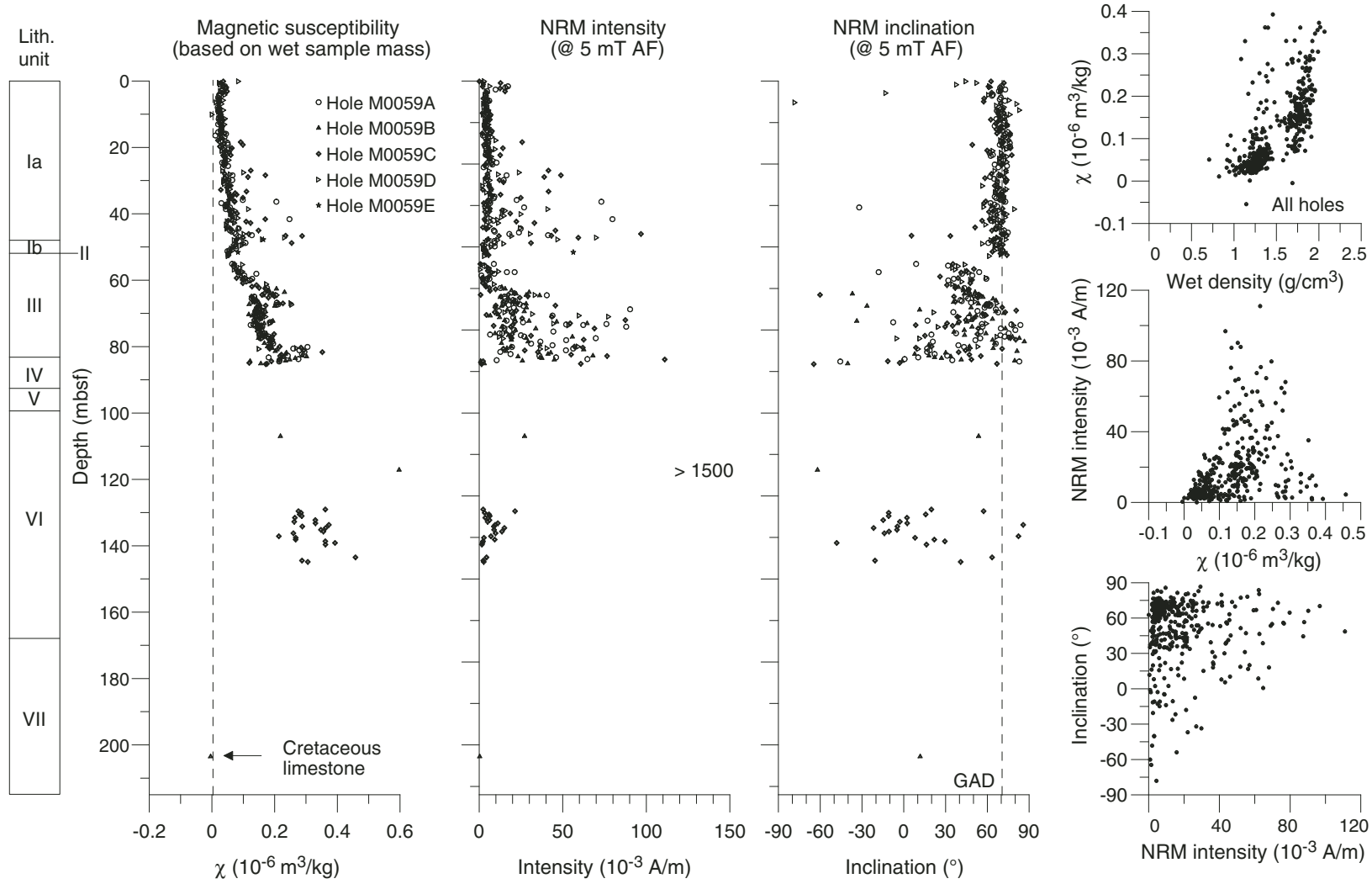

Figure F23. Plots of natural remanent magnetization (NRM) after alternating field (AF) demagnetization to 80 mT **A.** Sample 347-M0059A-15H-2, 17 cm; 49.82 mbsf. **B.** Sample 347-M0059A-5H-1, 123 cm; 15.41 mbsf. **C.** Sample 347-M0059A-18H-2, 69 cm; 59.56 mbsf. Category 1 and 2 vectors trend toward the origin, whereas Category 3 vectors veer into a plane perpendicular to the last demagnetization axis, which is a sign of gyroremanent magnetization acquisition. Open squares = vertical, solid squares = horizontal.

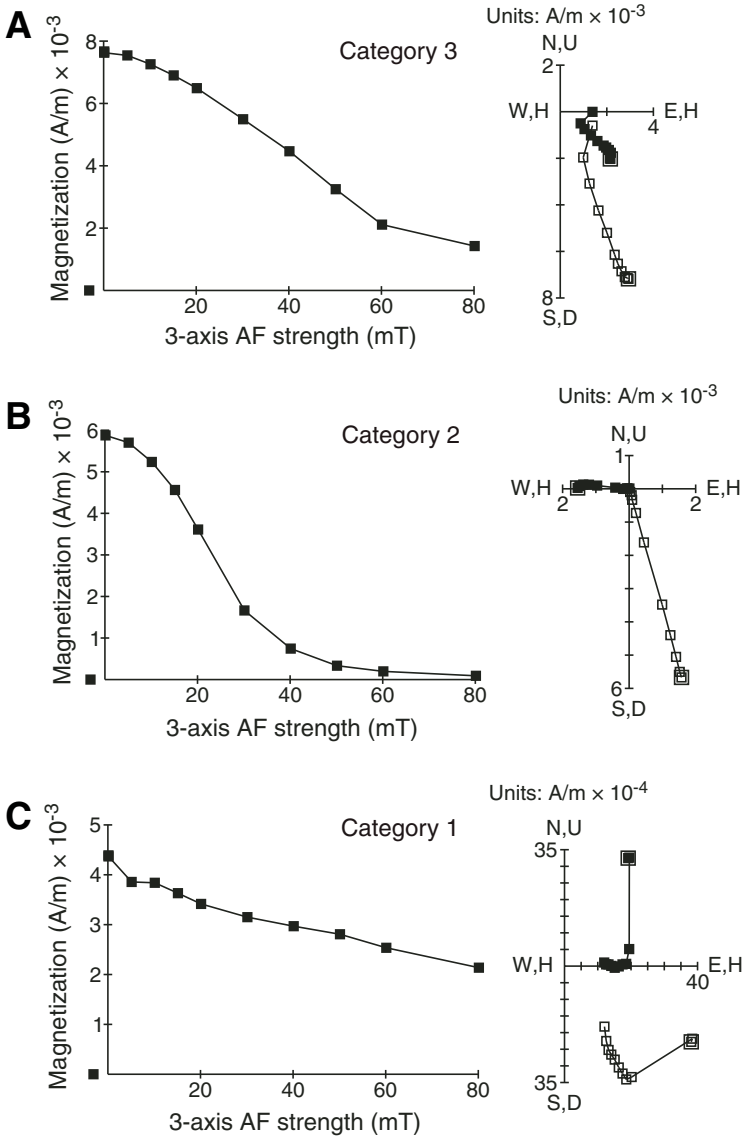

Figure F24. Plot of microbial cell abundances compared to chemical zonation and lithostratigraphy, Hole M0059C. **A.** Interstitial water alkalinity (blue dashed line) and salinity (red line). **B.** Cell numbers obtained by flow cytometry (blue circles) and acridine orange direct count (red diamonds). Solid black line = global regression line of prokaryote cell numbers with depth, dashed lines = upper and lower 95% prediction limits for regression line (Roussel et al., 2008). **C.** Lithology.

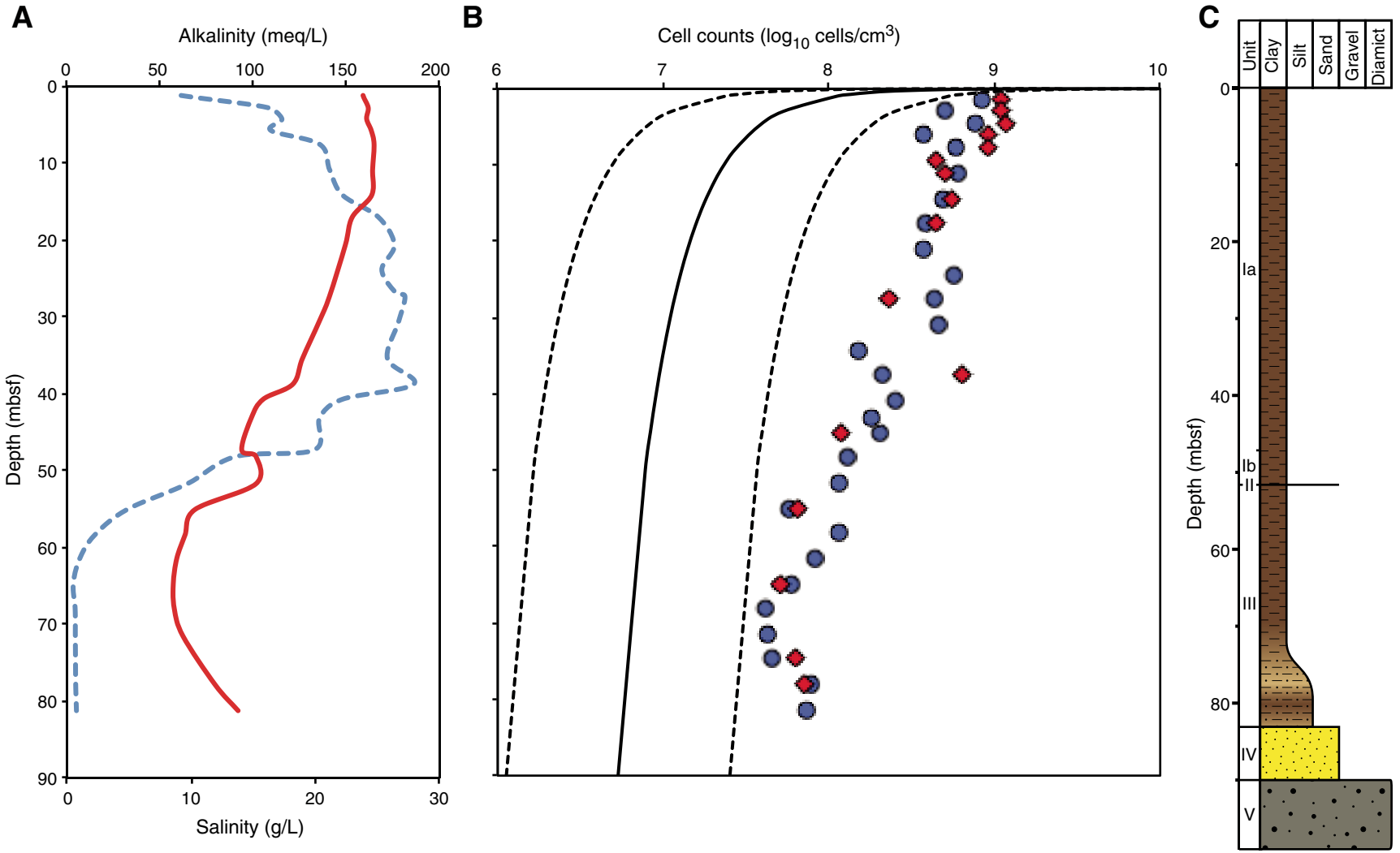

Figure F25. Plot of microbial cell abundances compared to chemical zonation and lithostratigraphy, Hole M0059E. **A.** Interstitial water alkalinity (blue dashed line) and salinity (red line). **B.** Cell numbers obtained by flow cytometry (blue circles) and acridine orange direct count (red diamonds). Solid black line = global regression line of prokaryote cell numbers with depth, dashed lines = upper and lower 95% prediction limits for regression line (Roussel et al., 2008). **C.** Lithology.

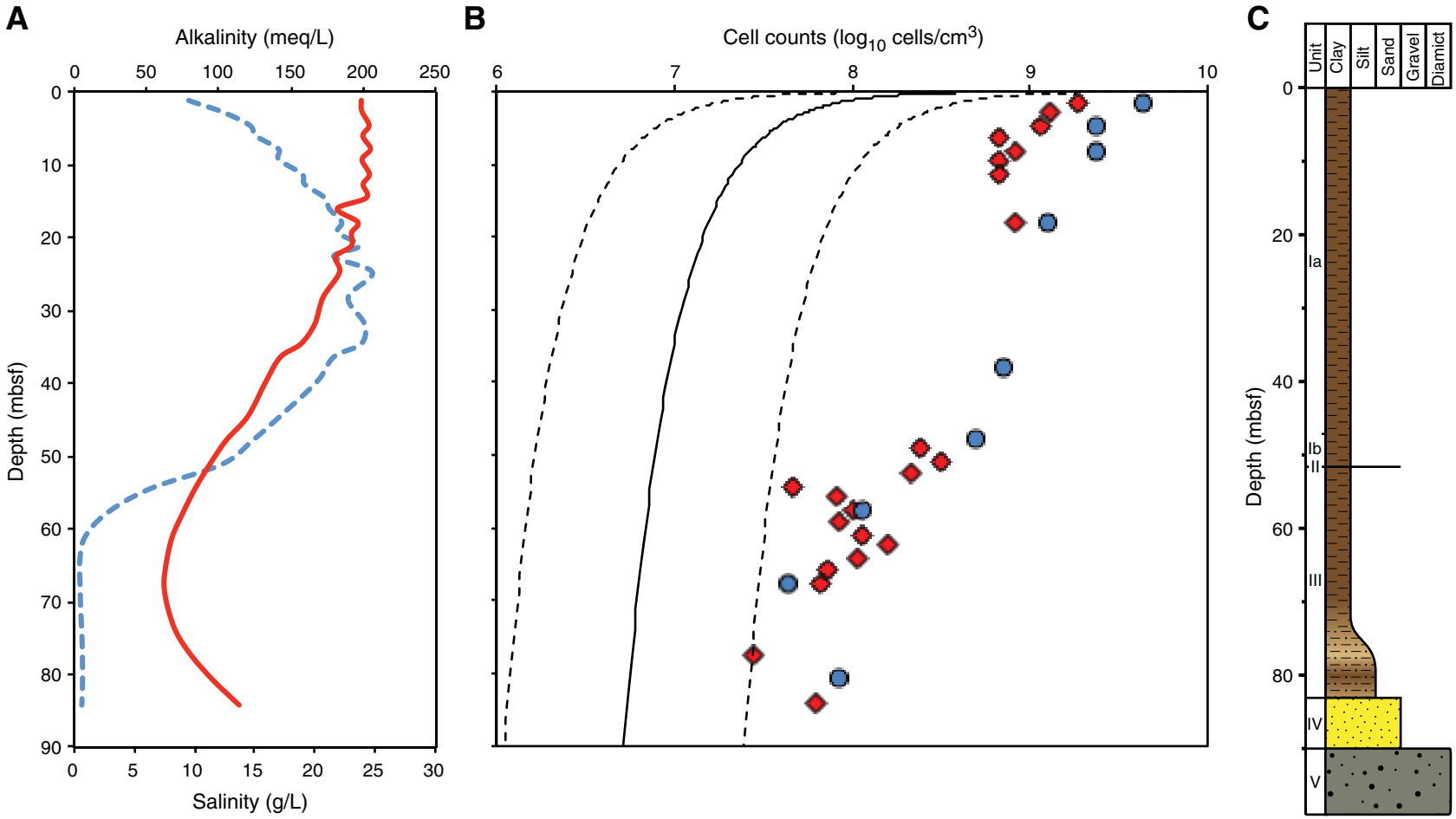

Figure F26. Comparison of paired counts between two methods of cell enumeration, Hole M0059E. Red line = linear regression between the two data sets, black dashed line = line of unity. FCM = flow cytometry, AODC = acridine orange direct counts.

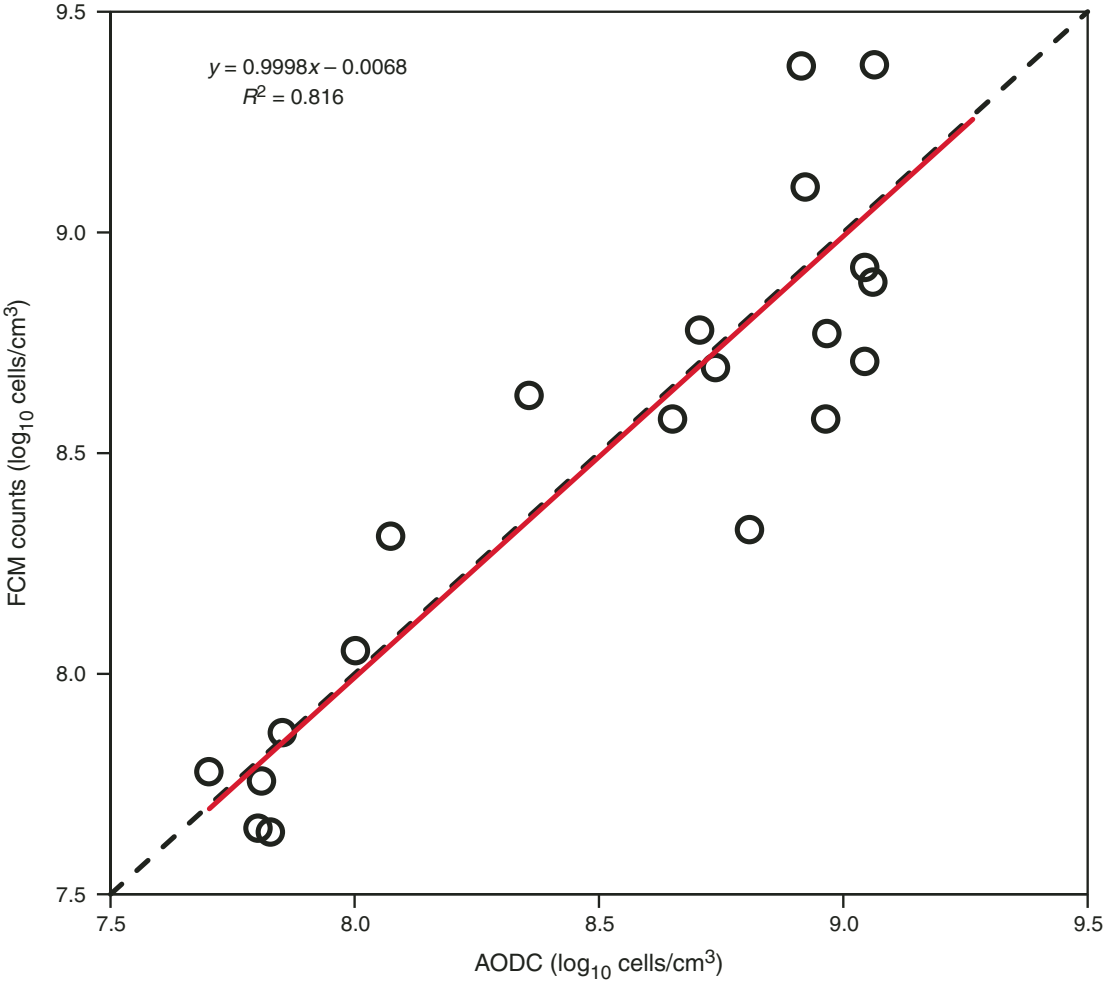

Figure F27. Fluorescence photomicrographs of sediment from 1.53 mbsf, Hole M0059C. **A.** Stained with SYBR green I without pretreatment. **B.** Stained with SYBR green I and sonicated. **C.** Stained with SYBR green I, sonicated, and treated with hydrofluoric acid. Red arrows = example cells.

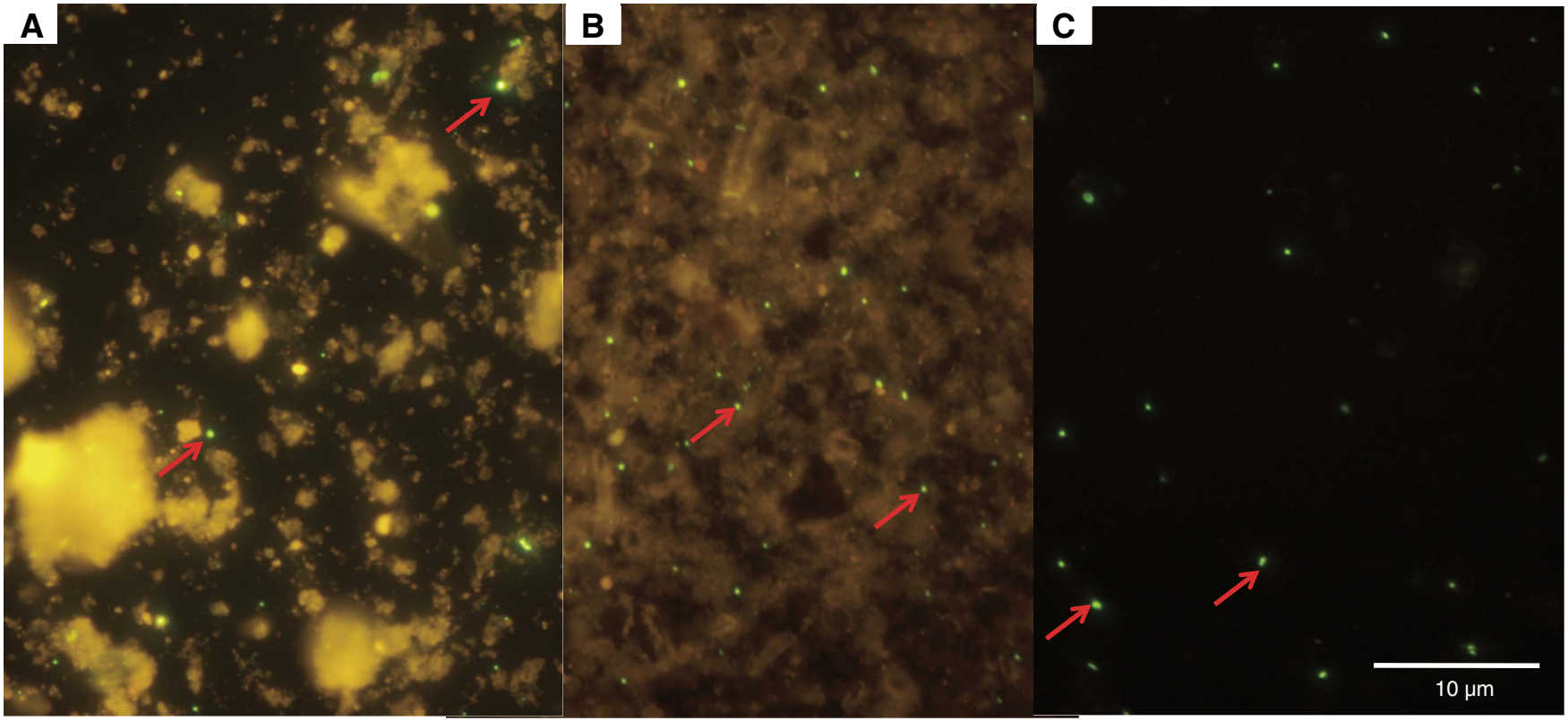

Figure F28. Plots of perfluorocarbon (PFC) tracer concentrations, Hole M0059E. **A.** Core liner fluid. **B.** Sediment core samples. (Continued on next page.)

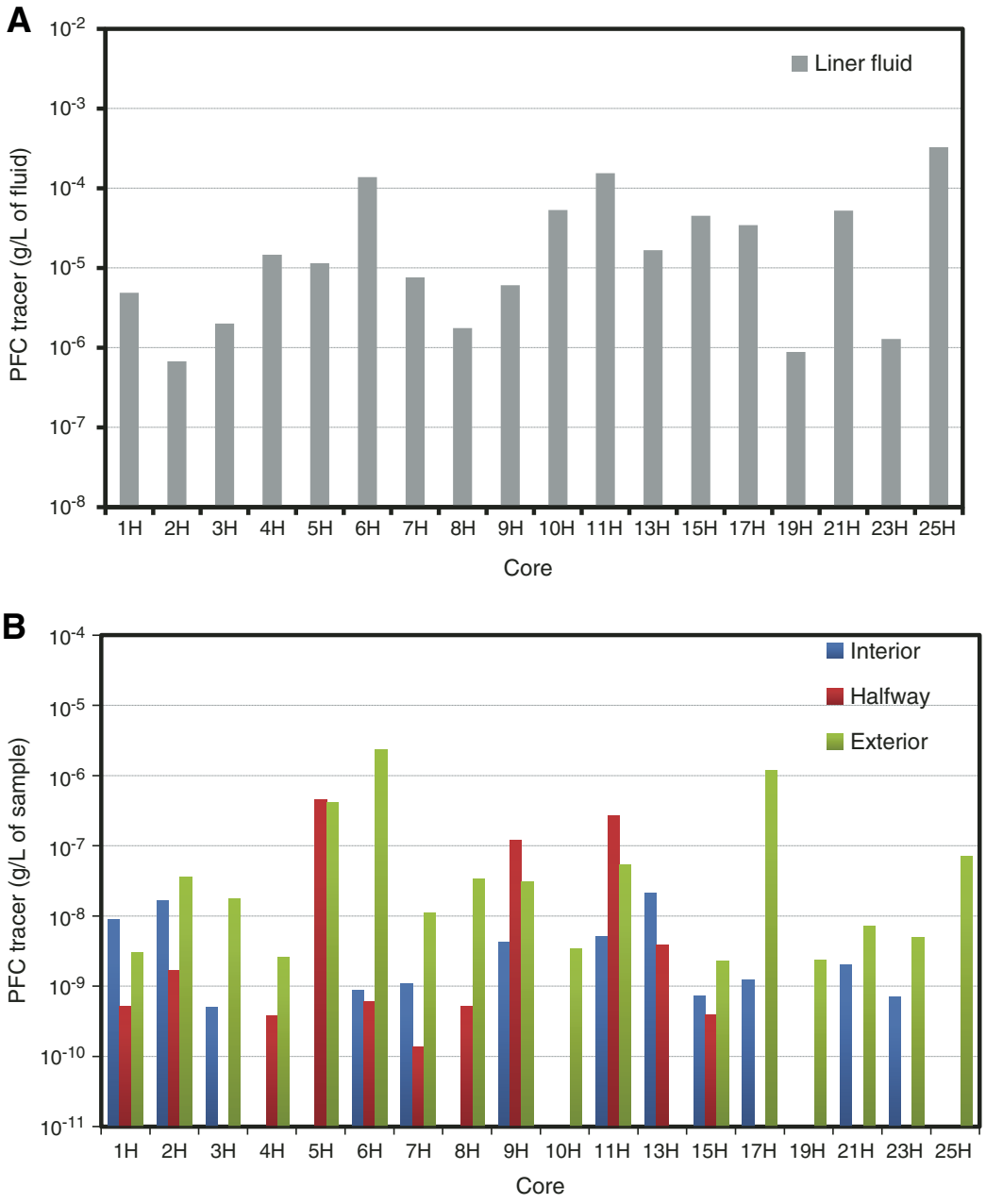

Figure F28 (continued). **C.** Estimated volume of liner fluid introduced into sediment cores shown as percentage of sediment core volume. **D.** Estimated potential number of contaminant cells per volume of sediment.

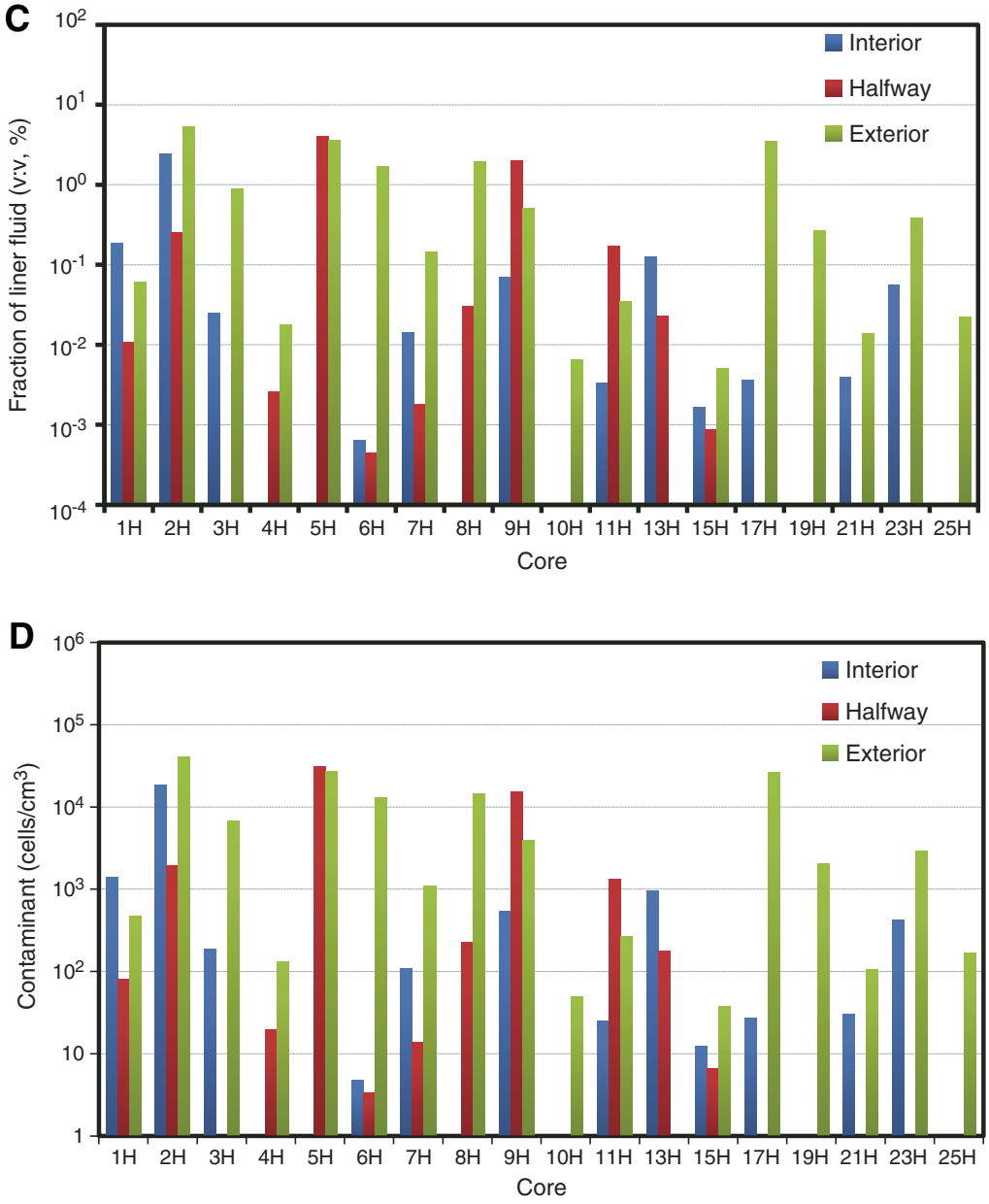

Figure F29. Plot of magnetic susceptibility (10^{-5} SI) data, Site M0059.

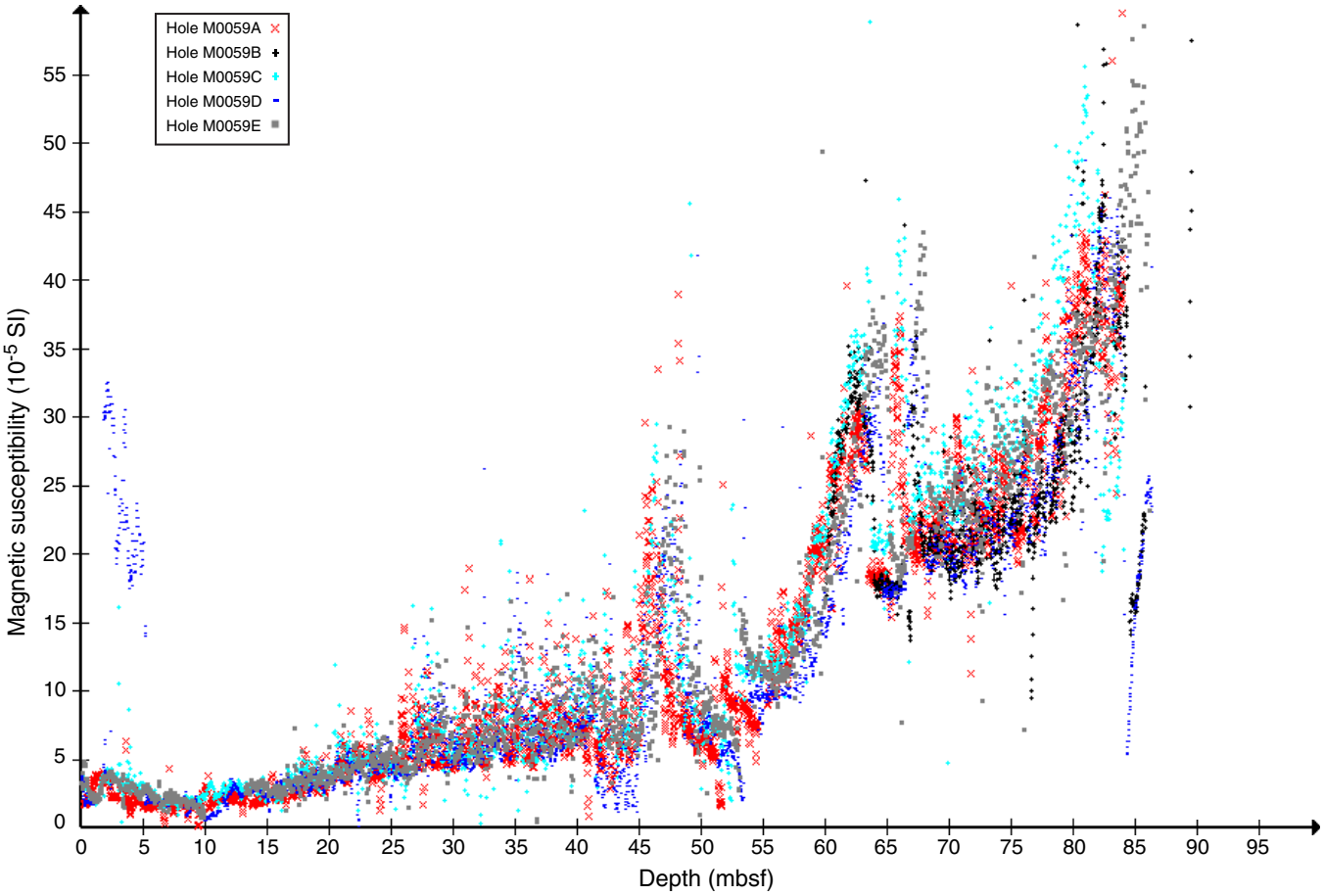

Figure F30. Plot of natural gamma ray (NGR) (cps) data, Site M0059.

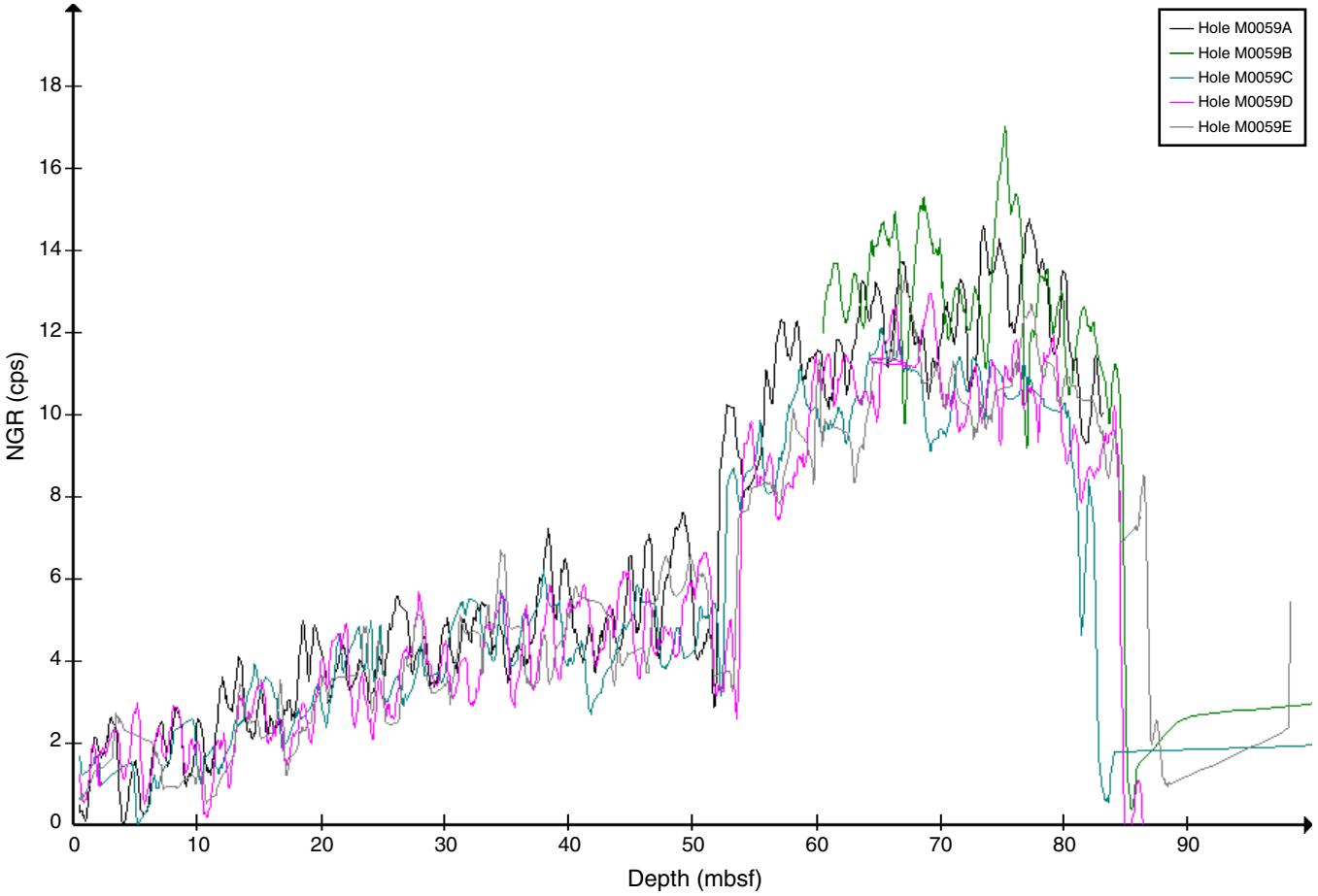

Figure F31. Comparison of downhole logging and core gamma measurements, Site M0059. NGR = natural gamma ray, HSGR = total spectral gamma ray.

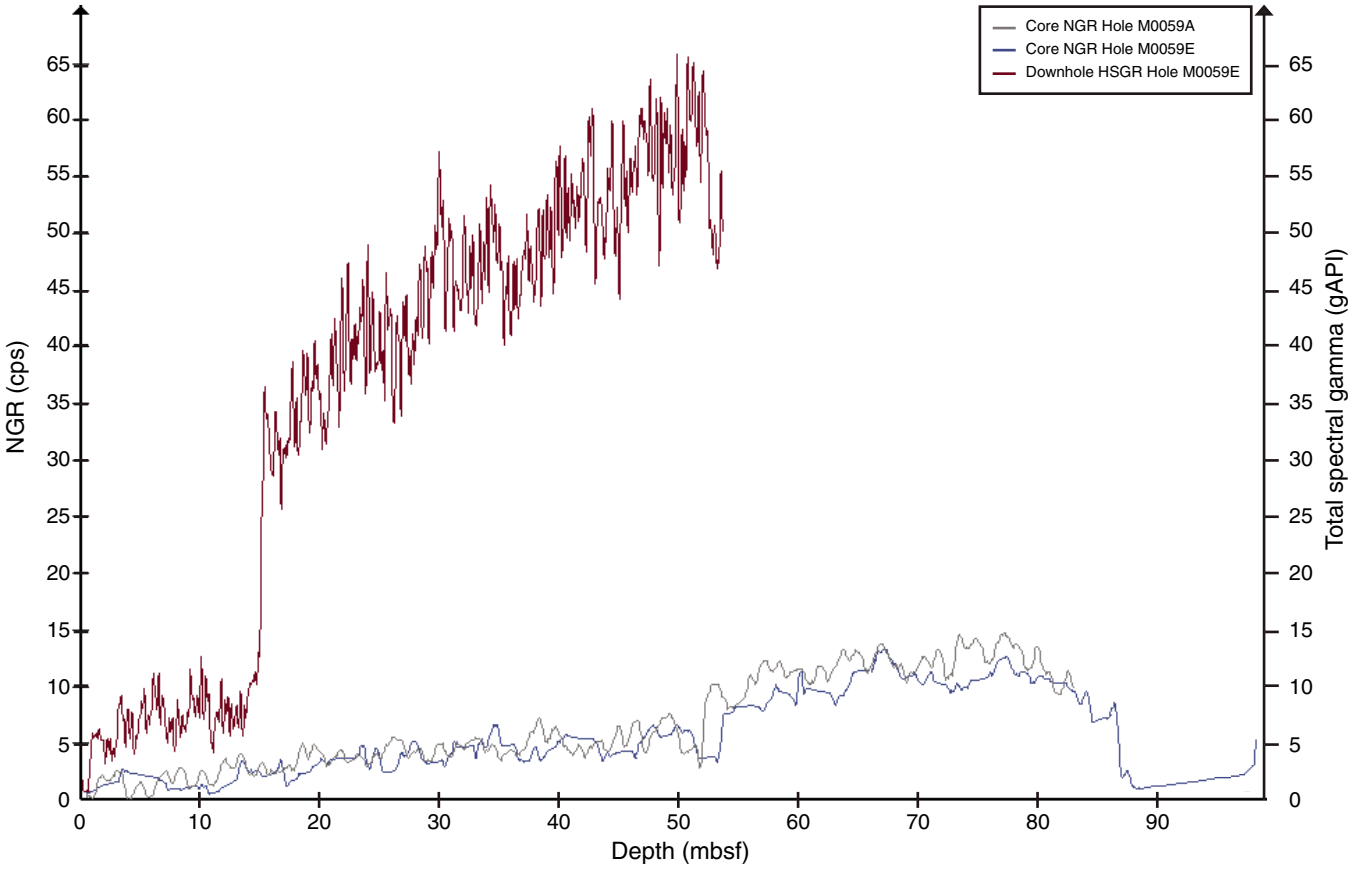

Figure F32. Correlation of seismic profile with lithostratigraphic units/boundaries, Site M0059. Dashed yellow line = bedrock surface calculated by velocities from core data. Precruise interpretation of seismic data is also shown: SF = seafloor, LG2 = lower boundary of late-glacial clays, BWT = bottom of Weichselian till, BR = bedrock. Seismic profile source: V. Spiess, 2013 (unpubl. data).

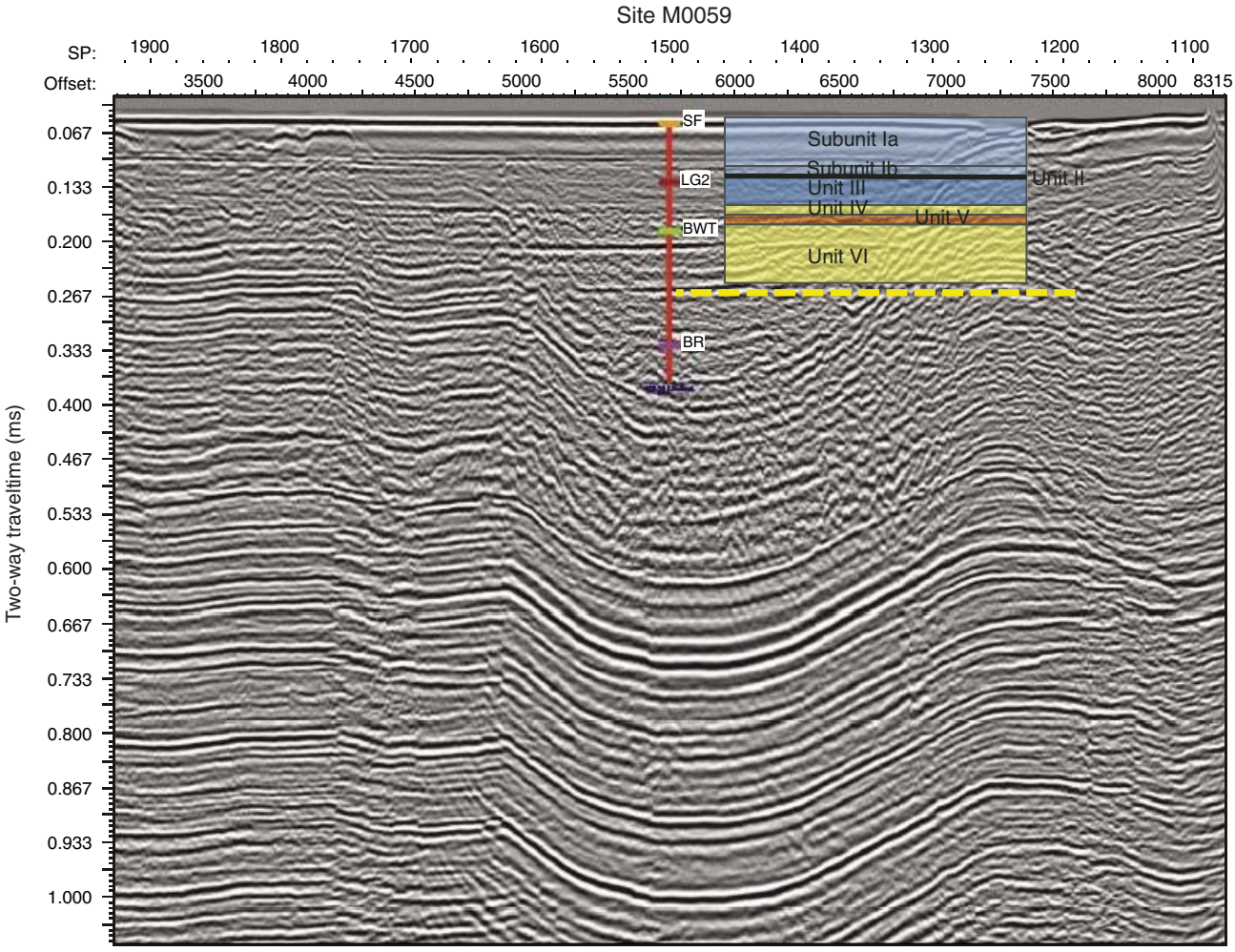

Figure F33. Gamma ray log, spectral gamma ray log, resistivity log (red = deep induction, blue = medium, black = shallow), and sonic log, Hole M0059B. Drill Pipe 1 is the pipe set at 20 m WSF and drill Pipe 2 is the pipe set at 87 m WSF.

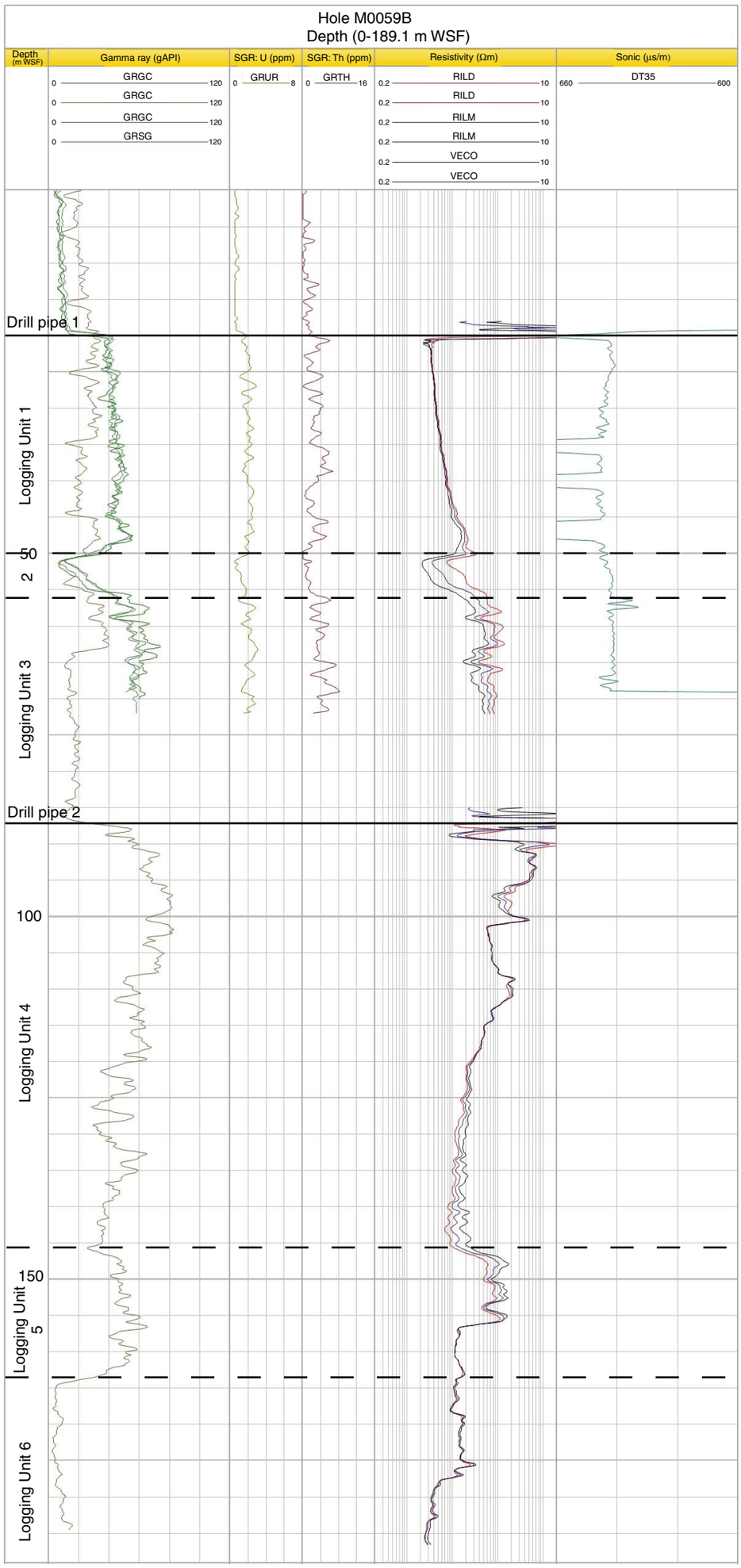

Figure F34. Caliper log, gamma ray log, spectral gamma ray log, resistivity log (red = deep induction, blue = medium, black = shallow), and sonic log, Hole M0059E. The drill pipe is set at 15 m WSF.

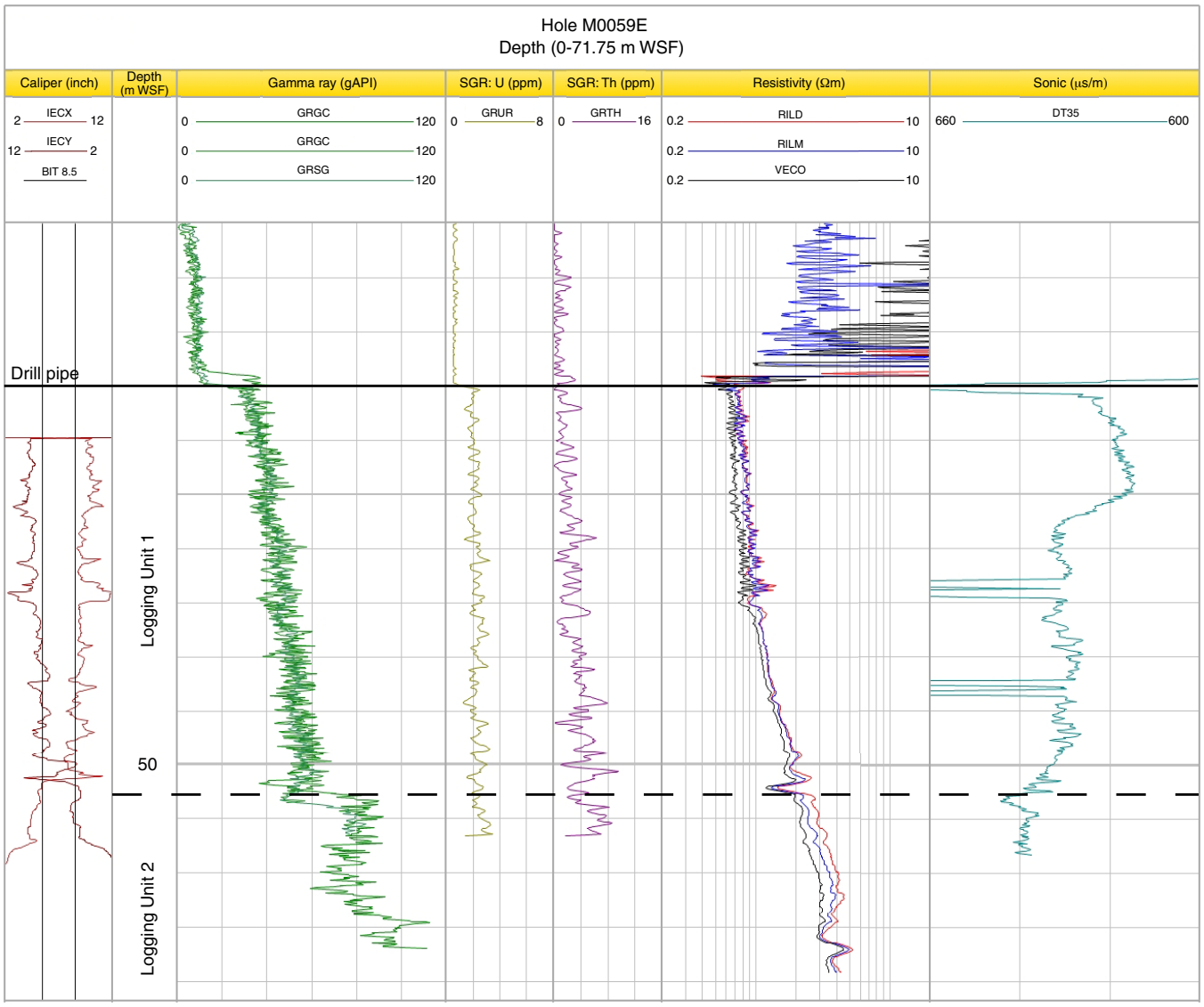

Table T1. Operations, Site M0059. (Continued on next six pages.)

Core	Coring method	Date (2013)	Time (UTC)	Depth (mbsf) Top	Depth (mbsf) Bottom	Recovered (m)	Recovery (%)	Mud type	Comments
347-M0059A-									
		13 Sep	1530						BHA in slips/running pipe; permit to work received and signed in Dog Shack; seabed template on seabed
1H	PCS	13 Sep	1920	0.00	3.33	3.33	100	Water	
2H	PCS	13 Sep	2020	3.33	6.90	3.30	92.44	Water	Advanced 3.59 m in error; additional core due to expanding mud
3H	PCS	13 Sep	2235	6.90	10.20	3.30	100	Water	
4H	PCS	13 Sep	2250	10.20	13.50	3.30	100	Water	
5H	PCS	14 Sep	0010	13.50	16.80	3.30	100	Water	
6H	PCS	14 Sep	0205	16.80	20.10	3.30	100	Water	
7H	PCS	14 Sep	0240	20.10	23.40	3.30	100	Water	
8H	PCS	14 Sep	0320	23.40	26.70	3.30	100	Water	
9H	PCS	14 Sep	0410	26.70	30.00	3.30	100	Water	
10H	PCS	14 Sep	0520	30.00	33.30	3.30	100	Water	Seal lost
11H	PCS	14 Sep	0617	33.30	36.60	3.50	106.06	Water	Pump refused to break shear pins, problems with pumps; retrieved PCS
		14 Sep	0730						Repaired mud pump
12H	PCS	14 Sep	1235	36.60	39.90	3.41	103.33	Water	Good fire: instant release of pressure
13H	PCS	14 Sep	1300	39.90	43.20	3.30	100	Water	
14H	PCS	14 Sep	1345	43.20	46.50	3.49	105.76	Water	Fired at 3–5 bar, seals damaged
15H	PCS	14 Sep	1440	46.50	49.80	3.52	106.67	Water	60 bar, damaged seals
16H	PCS	14 Sep	1515	49.80	53.10	3.25	98.48	Water	65 bar, damaged seals
17H	PCS	14 Sep	1635	53.10	55.30	1.55	70.45	Water	50 bar
18H	PCS	14 Sep	1750	55.30	58.60	3.22	97.58	Water	50 bar, damaged seals
19H	PCS	14 Sep	1915	58.60	61.90	3.23	97.88	Water	60 bar, damaged seals
20H	PCS	14 Sep	2015	61.90	65.20	3.38	102.42	Water	60 bar, damaged seals
21H	PCS	14 Sep	2115	65.20	68.50	3.47	105.15	Water	1 seal damaged
22H	PCS	14 Sep	2230	68.50	71.80	3.61	109.39	Water	
23H	PCS	14 Sep	2315	71.80	75.10	3.30	100	Water	1 seal missing
24H	PCS	15 Sep	0015	75.10	78.40	3.33	100.91	Water	
25H	PCS	15 Sep	0100	78.40	81.70	3.28	99.39	Water	
26H	PCS	15 Sep	0145	81.70	83.20	1.47	98	Water	Appeared to not fire at 80 bar but partial recovery
27H	PCS	15 Sep	0255	83.20	83.20	Washing	0	Water	Piston fired at 80 bar (single steel pin) collected washings of sand; lifted the string to release pressure
28X	ECS	15 Sep	0550	83.20	86.70	1.00	28.57	GS550	
29X	ECS	15 Sep	0650	86.70	90.20	0.00	0	GS550	No penetration below 3.1 mbsf; pulled barrel, returned top section; lower section lost from sheared spring spline
		15 Sep	0736						
		15 Sep	0800						2 attempts to recover lower section with magnet fishing tool without success
		15 Sep	0830						Considered overdrilling to hold barrel in BHA but unable to get back over the sheared pipe
		15 Sep	0900						Cleared deck to make room for pulling pipe
									End of hole
347-M0059B-									
		15 Sep	1330						Lowered template and running pipe; 1 metric ton weight of the template on the seabed
	NCA	15 Sep	1500	0.00	60.00	0.00	0	Water	Open hole to 60 mbsf
1H	PCS	15 Sep	1705	60.00	63.30	3.35	101.52	Water	Piston fired at 70 bar, 2 seals lost
		15 Sep	1745					Water	Corer hung in drill string; recovered to deck to find top seal stretched over sub, lower seal damaged; removed 4 pipes from string, as potential cause of seal damage; damage manifested in Hole M0059A at ~30 mbsf
		15 Sep	1820					Water	Tripping 4 API; one pipe was two welded together with internal joint not welded correctly, forming a lip
		15 Sep	1910					Water	Running pipe
		15 Sep	1955					Water	Attempted piston core but could not pressurize
		15 Sep	2050					Water	Piston core attempt became stuck in string close/at swivel
		15 Sep	2130					Water	Tested piston core through mud valve adjacent and tested mud valve
2H	PCS	15 Sep	2320	63.30	66.60	3.31	100.3	Water	Replaced piston head seals
3H	PCS	16 Sep	0025	66.60	69.90	3.58	108.48	Water	

Table T1 (continued). (Continued on next page.)

Core	Coring method	Date (2013)	Time (UTC)	Depth (mbsf) Top	Depth (mbsf) Bottom	Recovered (m)	Recovery (%)	Mud type	Comments
4H	PCS	16 Sep	0125	69.90	73.20	3.55	107.58	Water	
5H	PCS	16 Sep	0210	73.20	76.50	3.54	107.27	Water	Seal missing, other broken
6H	PCS	16 Sep	0320	76.50	79.80	3.57	108.18	Water	High pressure to fire but full stroke
		16 Sep	0512						Unable to run corer into pipe; pipe, mud valve, and saver sub all OK; suspect template wires rubbing on moonpool
		16 Sep	0600						Diagnosed problem as mud valve not opening again
7H	PCS	16 Sep	0620	79.80	83.10	3.07	93.03	Water	High firing pressure >50 bar but full stroke achieved
8H	PCS	16 Sep	0735	83.10	85.80	2.79	103.33	Guar	Fired but did not fully bleed off, unlikely to have achieved full stroke
		16 Sep	0815						Unable to lower ECS through mud valve
9X	ECS	16 Sep	0830	85.80	89.30	0.00	0	Guar	No recovery: sand and silt in inverted catcher
10X	ECS	16 Sep	0900	89.30	90.40	0.39	35.45	Guar	Cobble jammed in the throat of the bit
	ECS	16 Sep	1050						No penetration; failed in attempt to recover core tube and overshot rope snapped
		16 Sep	1115						Round trip
		16 Sep	1200						BHA in slips; removed locking sub and ECS, found bit damaged and bottom extension tube compressed onto core tube; lifted BHA to view damage to the bit, very little
		16 Sep	1200						Prepared NRCB
		16 Sep	1509						Lowered BHA, run pipe
		16 Sep	1700						Mudline, reentered Hole M0059B; NCA dropped in and washed down to bottom of hole
		16 Sep	1830						Swapped out NCA for NRCB
11N	NRCB	16 Sep	1840	90.40	91.40	0.00	0	Guar	No recovery; no hard layer; added pipe
12N	NRCB	16 Sep	1920	91.40	92.90	0.10	6.67	Guar	Attempted to core 2 m with NRCB before assessing the next option
13H	PCS	16 Sep	1955	92.90	93.00	0.12	120	Guar	Several attempts to shear pins at high pressure without success; appears they sheared but no release because of high-strength material; sand jamming several PC sections causing difficulty in breaking tool down; still in till, so reverted to ECS with shoe to attempt penetration with recovery
14X	ECS	16 Sep	2325	93.00	94.16	0.00	0	Guar	Penetration stopped
15O	NCA	17 Sep	0015	94.16	100.00	0.00	0	Guar	Drilled down with insert bit
16O	NCA	17 Sep	0155	100.00	101.37	0.00	0	Guar	Drilled until became blocked off
		17 Sep	0300						Drilled down with insert bit (NCA)
		17 Sep	0310						Leak in mud swivel connection: removed drill pipe and lower rooster box; locking welds on pipe thread may have broken loose
17X	ECS	17 Sep	0415	101.37	104.97	0.00	0	Guar	Pulled NCA and replaced with PCD bit—NOT shoe
18X	ECS	17 Sep	0523	104.97	107.28	0.00	0	Guar	
		17 Sep	0545					Guar	Prepared and lowered PCS; wireline cable lays had bitten in from last pull and would not free from drum winch
		17 Sep	0620					Guar	Freed wire lays from winch
19H	PCS	17 Sep	0700	107.28	107.43	0.15	100	Guar	PCS fired but no stroke; pulled string back to release pressure
20X	ECS	17 Sep	0720	107.43	109.63	0.00	0	Guar	Reasonable penetration, then stopped with no further downward movement
21X	ECS	17 Sep	0800	109.63	111.03	0.00	0	Guar	
22P	PCA	17 Sep	1050	111.03	111.03	0.00	0	Guar	Attempted push sample; 1 metric ton weight with no penetration; shoe end was bent as if in contact with stone
23S	HS	17 Sep	1120	111.03	111.05	0.02	100	Guar	Attempted HS with limited success; 10 blows produced a very small sample
		17 Sep	1230						Following discussions with drillers, tripped pipe to replace main PCD bit with six-cone RR; continue to open hole with addition of a tricone insert RR bit
									BHA in the slips
		17 Sep	1400						Removed PCD bit and replaced with six- cone RR; check length of tricone RR insert bit
24O	NCA	17 Sep	1722	111.05	117.30	0.00	0	Guar	Open hole; stopped when driller noted lithology change to softer material with small amount of mud pressure; swapped out NCA for push sampler
25P	PCA	17 Sep	1900	117.30	117.92	0.62	100	Guar	Recovered 62 cm of clay with small amount of worked material at the top
26O	NCA	17 Sep	2000	117.92	169.03	0.00	0	Guar	Returned NCA and continued to open hole
		17 Sep	2100	121.00				Guar	No sample attempted, comment only: drilling as if still in clay at 121 mbsf, switching between clay and sands
		18 Sep	0250	158.00					Addition of pipe showed infill, so reaming to clear hole
		18 Sep	0630	163.00					Same material; switch to water to drill
		18 Sep	0650	165.00	167.00			Water	Sudden, instant increase in drilling rate despite pulling back on WOB; stopped at 167 mbsf and conditioned hole
		18 Sep	0725	167.00					Added pipe and prepared ECS
27X	ECS	18 Sep	0800	169.03	172.50	0.02	0.58	Guar	Very soft, some torquing and harder bits in core run

Table T1 (continued). (Continued on next page.)

Core	Coring method	Date (2013)	Time (UTC)	Depth (mbsf) Top	Depth (mbsf) Bottom	Recovered (m)	Recovery (%)	Mud type	Comments
28O	NCA	18 Sep	0850	172.50	203.53	0.00	0	Guar	Hard and torquing, possibly still in the till
		18 Sep	0905	177.50					Soft to hard, very "torquey," like boulders in soft matrix (possibly chalk with flints)
		18 Sep	1130	181.55					Drillers comments: still in same material; pulled NCA and prepared to run HS but chalk and flints on tricone, so do not take a different sample type; prepared to run NCA again
29P	PCA	18 Sep	1245	203.53	204.03	0.40	80	Guar	Driller identified a change in parameters, loss of mud pressure, etc.; pulled NCA and prepared PCA
		18 Sep	1335						Overshot sleeve not correctly adjusted, caught in hoist rope; recovered and corrected to allow sample to be taken
30P	PCA	18 Sep	1335	204.03	204.03	0.00	0	Guar	Attempt made for push sample, but barrel may not have latched and string lowered to bottom of borehole but no penetration achieved; small scraping of chalk in shoe; Co-Chief called TD at 204.03 mbsf
		18 Sep	1355						Prepared drill floor for logging
		18 Sep	1925						Tripped pipe to 20 m from top of hole, but could not deploy logging tools below 70 mbsf; pulled tools out of hole and ran back in for a wiper trip before tripping pipe to 90 mbsf to log in two stages
		18 Sep	2100						Cleaned hole, tight at ~70 mbsf; ran pipe to 175 mbsf and flushed hole; pulled back to 90 mbsf, flushed in readiness for logging
		18 Sep	2210						Prepared drill floor for logging
		18 Sep	2300						Ran gamma and resistivity logging tool 185–90 mbsf
		19 Sep	0050						Lifted pipe back up 90–20 mbsf
		19 Sep	0200						Completed logging 73–20 mbsf
		19 Sep	0310						Pulled string
		19 Sep	0330						Lifted template
347-M0059C-									
		19 Sep	0611						Template sank far into the seabed; checked transponder, rechecked and fitted, clamps checked: operational
		19 Sep	0620						Moonpool floor closed; lowered the seabed template to seabed
		19 Sep	0730						Discovered bend in first pipe above collars on attempting to enter the template clamps with the bit; tripped out pipes to remove this one from the string
		19 Sep	0818						Repositioned ship 5 m with the template off the seabed; attempted again to pass through clamps
1H	PCS	19 Sep	0850	0.00	3.00	3.43	114.33	Seawater	
2H	PCS	19 Sep	1018	3.00	6.30	3.50	106.06	Seawater	
3H	PCS	19 Sep	1122	6.30	9.60	3.37	102.12	Seawater	Failed to build pressure; pins sheared, presumably on the way down, but full recovery achieved in soft sediment
4H	PCS	19 Sep	1210	9.60	12.90	3.59	108.79	Seawater	60 bar
5H	PCS	19 Sep	1210	12.90	16.20	3.51	106.36	Seawater	60 bar
6H	PCS	19 Sep	1403	16.20	19.50	3.39	102.73	Seawater	10 bar
7H	PCS	19 Sep	1513	19.50	22.80	3.41	103.33	Seawater	10 bar
8H	PCS	19 Sep	1613	22.80	26.10	3.44	104.24	Seawater	25 bar
9H	PCS	19 Sep	1715	26.10	29.40	3.40	103.03	Seawater	35 bar
10H	PCS	19 Sep	1818	29.40	32.70	3.48	105.45	Seawater	35 bar; apparent double fire; pressure rose to 35 bar, fell to ~25 bar, rose again to 35 bar, and fell back to zero
11H	PCS	19 Sep	1909	32.70	36.00	3.47	105.15	Seawater	65 bar
12H	PCS	19 Sep	1944	36.00	39.30	3.68	111.52	Seawater	75 bar
13H	PCS	19 Sep	2039	39.30	42.60	3.45	104.55	Seawater	35 bar; pressure did not drop immediately after firing
14H	PCS	19 Sep	2148	42.60	45.90	0.92	27.88	Seawater	20 bar
15H	PCS	19 Sep	2258	43.50	46.80	3.31	100.3	Seawater	
16H	PCS	20 Sep	0150	46.80	50.10	3.37	102.12	Seawater	50 bar; apparent double fire
17H	PCS	20 Sep	0238	50.10	53.40	3.48	105.45	Seawater	Into gray clay
18H	PCS	20 Sep	0310	53.40	56.70	3.51	106.36	Seawater	Apparent double fire (two 50 bar spikes)
19H	PCS	20 Sep	0503	56.72	60.02	3.59	108.79	Seawater	
20H	PCS	20 Sep	0545	60.02	63.32	3.50	106.06	Seawater	One each steel and brass pin inserted to piston
		20 Sep	0635						Did not fire on 3 attempts; pulled back to remove steel pin but unable to do so; replaced entire inner rod assembly
		20 Sep	0730						Steel and brass pins: thought it fired but pressure did not release, so pulled back to bleed off but when recovered to the deck it was intact
21H	PCS	20 Sep	0810	63.32	66.62	3.65	110.61	Seawater	Set with two brass pins; fired and recovered a good core
22H	PCS	20 Sep	0855	66.62	69.92	3.48	105.45	Seawater	
23H	PCS	20 Sep	0940	69.92	73.22	3.42	103.64	Seawater	Good recovery; seals broken

Table T1 (continued). (Continued on next page.)

Core	Coring method	Date (2013)	Time (UTC)	Depth (mbsf) Top	Depth (mbsf) Bottom	Recovered (m)	Recovery (%)	Mud type	Comments
24H	PCS	20 Sep	1038	73.22	76.52	3.66	110.91	Seawater	75 bar
25H	PCS	20 Sep	1124	76.52	79.82	3.40	103.03	Seawater	90 bar
26H	PCS	20 Sep	1155	79.92	82.32	2.40	100	Seawater	Steel and brass pins fired at 100 bar; slightly sandy in shoe
27H	PCS	20 Sep	1255	82.23	84.11	1.88	100	Seawater	Sand
28S	HS	20 Sep	1425	84.12	84.62	0.50	100		Ran NCA in alternative coring strategy of advancing 3 m before taking a hammer sample
29O	NCA	20 Sep	1450	84.62	87.12	0.00	0	Guar	All stop for 20 min to switch out hydraulic hose
30S	HS	20 Sep	1535	87.12	87.62	0.50	100		HS: 50 blows
31O	NCA	20 Sep	1610	87.62	90.12	0.00	0	Guar	Washed down to 90.12 mbsf
32S	HS	20 Sep	1710	90.12	90.13	0.01	100		HS: 50 blows; granite stone recovered
33O	NCA	20 Sep	1730	90.62	93.12	0.00	0	Guar	Washed down to 93.12 mbsf
34S	HS	20 Sep	1930	93.12	93.52	0.40	100		HS: 50 blows; till recovered, gray clay with rare chalk pebbles
35O	NCA	20 Sep	1945	93.12	96.12	0.00	0	Guar	Washed down to 96.12 mbsf
36S	HS	20 Sep	2045	96.12	96.32	0.20	100		HS: 50 blows; hard slightly clayey sand recovered
37O	NCA	20 Sep	2130	96.12	99.12	0.00	0	Guar	Washed down to 99.12 mbsf
38S	HS	20 Sep	2250	99.12	99.62	0.50	100		HS: only needed 8 blows; soft gritty clay
39O	NCA	20 Sep	2320	99.12	102.12	0.00	0	Guar	Washed down to 102.12 mbsf
40S	HS	21 Sep	0115	102.12	102.62	0.50	100		HS: needed just 15 blows for full penetration
41O	NCA	21 Sep	0140	102.12	105.12	0.00	0	Guar	Washed down to 105.12 mbsf
42S	HS	21 Sep	0245	105.12	105.52	0.40	100		HS: needed 20 blows
43O	NCA	21 Sep	0305	105.12	108.12	0.00	0	Guar	Washed down to 108.12 mbsf
44S	HS	21 Sep	0344	108.12	108.32	0.20	100		
45O	NCA	21 Sep	0420	108.12	111.12	0.00	0	Guar	
46S	HS	21 Sep	0512	111.12	111.22	0.10	100		
47O	NCA	21 Sep	0535	111.12	114.12	0.00	0	Guar	
48S	HS	21 Sep	0610	114.12	114.62	0.50	100		
49O	NCA	21 Sep	0610	114.12	117.12	0.00	0	Guar	
50S	HS	21 Sep	0730	117.12	117.22	0.10	100		
51O	NCA	21 Sep	0900	117.12	120.12	0.00	0	Guar	
52S	HS	21 Sep	0917	120.12	120.22	0.10	100		
53O	NCA	21 Sep	0935	120.12	123.12	0.00	0	Guar	
54S	HS	21 Sep	1035	123.12	123.15	0.03	100		
55O	NCA	21 Sep	1055	123.12	124.62	0.00	0	Guar	
56S	HS	21 Sep	1110	124.62	125.12	0.50	100		
57O	NCA	21 Sep	1120	124.62	126.12	0.00	0	Guar	
58S	HS	21 Sep	1210	126.12	126.47	0.35	100		
59O	NCA	21 Sep	1230	126.12	127.62	0.00	0	Guar	
60S	HS	21 Sep	1300	127.62	128.22	0.60	100		
61H	PCS	21 Sep	1325	127.62	130.62	3.00	100	Guar	100 bar; no pressure drop, left for a minute before raising rooster box; sand; no advance between Runs 60 and 61
62H	PCS	21 Sep	1400	130.62	131.72	0.95	86.36	Guar	60 bar
63H	PCS	21 Sep	1520	131.72	134.72	3.02	100.67	Guar	80 bar; pump stalled
64H	PCS	21 Sep	1630	134.72	135.20	0.24	50	Guar	90 bar; pressure did not fall off, so left for a minute before raising rooster box; sand
65O	NCA	21 Sep	1740	134.96	135.72	0.00	0	Guar	
66H	PCS	21 Sep	1745	135.72	138.72	2.81	93.67	Guar	90 bar; pressure did not fall off, so left for a minute before raising rooster box; sand
67H	PCS	21 Sep	1835	138.72	138.97	0.20	80	Guar	90 bar; pressure did not fall off, so left until pressure released; suggestion is piston acting like a vibrocorer with the combined pressure and movement from the ship allowing penetration over time
68X	ECS	21 Sep	1900	138.72	139.72	0.00	0	Guar	Open hole using flush without insert bit
69H	PCS	21 Sep	1920	139.72	141.70	2.00	101.01	Guar	100 bar; pressure did not release and was left for 3 min before lifting rooster box
70H	PCS	21 Sep	2020	141.70	144.00	2.30	100	Guar	100 bar; pressure did not release and was left for 60 s before lifting rooster box
71H	PCS	21 Sep	2132	144.00	144.50	0.05	10	Guar	
72S	HS	21 Sep	2224	144.50	144.55	0.05	100	Guar	
73O	NCA	21 Sep	2235	144.55	145.00	0.00	0		Open hole using flush without insert bit

Table T1 (continued). (Continued on next page.)

Core	Coring method	Date (2013)	Time (UTC)	Depth (mbsf) Top	Depth (mbsf) Bottom	Recovered (m)	Recovery (%)	Mud type	Comments
74S	HS	21 Sep	2245	145.00	145.20	0.20	100	Guar	
75O	NCA	21 Sep	2315	145.20	146.00	0.00	0		Open hole with insert bit
76S	HS	21 Sep	2355	146.00	146.10	0.10	100	Guar	HS: 25 blows
77O	NCA	22 Sep	0016	146.10	148.00	0.00	0		Open hole with insert bit
78S	HS	22 Sep	0050	148.00	148.15	0.15	100	Guar	HS: 15 blows
79O	NCA	22 Sep	0145	148.15	153.00	0.00	0		Open hole with insert bit
80S	HS	22 Sep	0220	153.00	153.10	0.10	100	Guar	
81O	NCA	22 Sep	0240	153.10	154.00	0.00	0		Open hole with insert bit
82S	HS	22 Sep	0313	154.00	154.05	0.05	100	Guar	
83O	NCA	22 Sep	0340	154.00	158.00	0.00	0		Open hole with insert bit; last meter very hard, took 0.5 h to drill out
		22 Sep	0450						Flushing and reaming hole; bit had some hard dark gray clay on it
84S	HS	22 Sep	0517	158.00	158.10	0.10	100	Guar	Very stiff clay with stones recovered
		22 Sep	0535						End of hole
		22 Sep	0545						Prepared drill floor to pull string; pulled pipes; first collar in slips
		22 Sep	0728						BHA in slips
		22 Sep	0832						Template on the deck but still in guide
		22 Sep	0835						Removed transponder
347-M0059D-									
		29 Oct	0340						Bridge stated we were on location
		29 Oct	0350						Lowered seabed frame
		29 Oct	0405						Started to add drill pipe to BHA and two drill collars
1H	PCS	29 Oct	0435	0.00	1.80	2.54	141.11	Seawater	Fired from 1.5 m above seabed
2H	PCS	29 Oct	0455	1.80	5.10	3.5	106.06	Seawater	
3H	PCS	29 Oct	0600	5.10	8.40	3.56	107.88	Seawater	
4H	PCS	29 Oct	0635	8.40	11.70	3.56	107.88	Seawater	
5H	PCS	29 Oct	0715	11.70	15.00	3.62	109.7	Seawater	
6H	PCS	29 Oct	0745	15.00	18.30	3.5	106.06	Seawater	
7H	PCS	29 Oct	0815	18.30	21.60	3.62	109.7	Seawater	
8H	PCS	29 Oct	0855	21.60	24.90	3.55	107.58	Seawater	
9H	PCS	29 Oct	0945	24.90	28.20	3.51	106.36	Seawater	
10H	PCS	29 Oct	1020	28.20	31.50	3.33	100.91	Seawater	
11H	PCS	29 Oct	1115	31.50	34.80	3.51	106.36	Seawater	
12H	PCS	29 Oct	1155	34.80	38.10	3.47	105.15	Seawater	
13H	PCS	29 Oct	1225	38.10	41.40	3.54	107.27	Seawater	
14H	PCS	29 Oct	1310	41.40	44.70	3.52	106.67	Seawater	
15H	PCS	29 Oct	1355	44.70	48.00	3.32	100.61	Seawater	
16H	PCS	29 Oct	1430	48.00	51.30	3.40	103.03	Seawater	Color changed in shoe from black/gray to light brown
17H	PCS	29 Oct	1500	51.30	54.60	3.78	114.55	Seawater	
18H	PCS	29 Oct	1545	54.60	57.90	3.45	104.55	Seawater	
19H	PCS	29 Oct	1654	57.90	61.20	3.80	115.15	Seawater	
20H	PCS	29 Oct	1739	61.20	64.50	3.67	111.21	Seawater	
21H	PCS	29 Oct	1820	64.50	67.80	3.26	98.79	Seawater	
22H	PCS	29 Oct	1900	67.80	71.10	3.70	112.12	Seawater	
23H	PCS	29 Oct	1940	71.10	74.40	3.33	100.91	Seawater	
24H	PCS	29 Oct	2025	74.40	77.70	3.47	105.15	Seawater	
25H	PCS	29 Oct	2115	77.70	81.00	3.39	102.73	Seawater	
26H	PCS	29 Oct	2150	81.00	84.30	3.42	103.64	Seawater	
27H	PCS	29 Oct	2245	84.30	86.50	2.17	98.64	Seawater	
28S	HS	29 Oct	2315	86.50	86.60	0.05	50	Seawater	
		29 Oct	2335						Started to trip string
		30 Oct	0010						Seabed frame lifted

Table T1 (continued). (Continued on next page.)

Core	Coring method	Date (2013)	Time (UTC)	Depth (mbsf) Top	Depth (mbsf) Bottom	Recovered (m)	Recovery (%)	Mud type	Comments
347-M0059E-									
		30 Oct	0020						On site
		30 Oct	0028						Lowered seabed frame
1H	PCS	30 Oct	0050	0.00	3.30	3.5	106.06	Seawater	60 bar
2H	PCS	30 Oct	0145	3.30	6.60	3.5	106.06	Seawater	40 bar
3H	PCS	30 Oct	0232	6.60	9.90	3.49	105.76	Seawater	50 bar
4H	PCS	30 Oct	0315	9.90	13.20	3.49	105.76	Seawater	50 bar
5H	PCS	30 Oct	0400	13.20	16.50	3.45	104.55	Seawater	60 bar
6H	PCS	30 Oct	0445	16.50	19.80	3.48	105.45	Seawater	50 bar
7H	PCS	30 Oct	0605	19.80	23.10	3.34	101.21	Seawater	
8H	PCS	30 Oct	0650	23.10	26.40	3.39	102.73	Seawater	
9H	PCS	30 Oct	0735	26.40	29.70	3.37	102.12	Seawater	
10H	PCS	30 Oct	0820	29.70	33.00	3.51	106.36	Seawater	
11H	PCS	30 Oct	0915	33.00	36.30	3.45	104.55	Seawater	
12H	PCS	30 Oct	1005	36.30	39.60	3.32	100.61	Seawater	
13H	PCS	30 Oct	1055	39.60	42.90	3.47	105.15	Seawater	
14H	PCS	30 Oct	1200	42.90	46.20	3.61	109.39	Seawater	
15H	PCS	30 Oct	1250	46.20	49.50	3.66	110.91	Seawater	
16H	PCS	30 Oct	1339	49.50	52.80	3.51	106.36	Seawater	Core on deck 4.5 h after being collected because of broken seal (see below)
		30 Oct	1350						Wireline rope parted on retrieving PCS; first fishing attempt failed but overshot was clear; extended fishing tool fabricated to pick up at emergency overshot slot; second attempt picked up overshot and barrel; barrel assembly firmly jammed in BHA; back-hammering attempted to free it; after considerable time the assembly was dropped by the fishing tool and the string was tripped
		30 Oct	1630						Tripping pipe
		30 Oct	1700						First collar in slips
		30 Oct	1800						PCS in slips: still jammed; unscrewed core barrel from bottom and removed core
		30 Oct	1805						Core on deck
		30 Oct	1810						Backed off stabilizer sub to access PCS head and remove damaged seal (partially split and moved from bed, causing the jam)
		30 Oct	1820						Removed piston rod from BHA
		30 Oct	1830						Rebuilt BHA and ran pipe
17H	PCS	30 Oct	1930	52.80	56.10	3.42	103.64	Seawater	
18H	PCS	30 Oct	2020	56.10	59.40	3.62	109.7	Seawater	
19H	PCS	30 Oct	2109	59.40	62.70	3.36	101.82	Seawater	
20H	PCS	30 Oct	2205	62.70	66.00	3.54	107.27	Seawater	
21H	PCS	30 Oct	2315	66.00	69.30	3.46	104.85	Seawater	50 bar
22H	PCS	31 Oct	0005	69.30	72.60	3.45	104.55	Seawater	50 bar
23H	PCS	31 Oct	0048	72.60	75.90	3.36	101.82	Seawater	50 bar
24H	PCS	31 Oct	0136	75.90	79.20	3.57	108.18	Seawater	60 bar
25H	PCS	31 Oct	0230	79.20	82.50	3.41	103.33	Seawater	
26H	PCS	31 Oct	0325	82.50	85.80	3.62	109.7	Seawater	60 bar
27H	PCS	31 Oct	0415	85.80	88.80	2.97	99	GS550	150 bar and no full stroke, as pressure remained high
28X	ECS	31 Oct	0545	88.80	91.80	0.00	0	GS550	
29S	HS	31 Oct	0710	91.80	92.80	0.10	10	GS550	
30X	ECS	31 Oct	0745	92.80	93.80	0.17	17	GS550	
31S	HS	31 Oct	0815	93.80	94.80	0.18	18	GS550	
32S	HS	31 Oct	0900	94.80	95.80	0.15	15	GS550	
33X	ECS	31 Oct	0930	95.80	96.80	0.3	30	GS550	
34X	ECS	31 Oct	0958	96.80	97.80	0.03	3	GS550	
35X	ECS	31 Oct	1035	97.80	98.80	0.64	64	GS550	Uncut “stub” of diamicton on end of bit; tool unlatched; checked bit was clear before sending next one down
36X	ECS	31 Oct	1135	98.80	99.60	0.20	25	GS550	Cleaned ECS head, which had a lot of sand in the movable parts

Table T1 (continued).

Core	Coring method	Date (2013)	Time (UTC)	Depth (mbsf) Top	Depth (mbsf) Bottom	Recovered (m)	Recovery (%)	Mud type	Comments
37X	ECS	31 Oct	1220	99.60	100.80	0.20	16.67	GS550	Sand in head again
		31 Oct	1305						Tool did not latch in; pressure in string up to 55 bar, indicating bit blocked; pulled tool to flush and clear
		31 Oct	1320						Flushing cleared bit, but when pumping stopped to RIH the hole collapsed; pulled back, thickened mud, tried to stabilize hole
		31 Oct	1340						Used some heavy mud (saturated brine) to stabilize the clay in the upper sections; pulled back a few pipes to clear clay bridge, stopping cuttings moving up the hole
		31 Oct	1410						Pumped back to 65 mbsf; still experiencing hole collapse through pipe (mud rising out of mud valve to 50 cm when pumping stops)
		31 Oct	1435						Allowed hole to settle and sand to stabilize; drilled back down to attempt to get to 100.8 mbsf
		31 Oct	1605						Unable to satisfactorily stabilize hole; end of hole called
		31 Oct	1700						Cleaned hole preparing to log
		31 Oct	1800						Set up logging
		31 Oct	1910						Completed first run to 70 mbsf
		31 Oct	2000						Completed second run to 60 mbsf
		31 Oct	2040						Completed third run to 60 mbsf
		31 Oct	2100						Logging derigged
		31 Oct	2110						Started lifting pipe
		31 Oct	2130						Lifted template

ECS = extended coring system, HS = hammer sampler, NCA = noncoring assembly, NRCB = nonrotating core barrel, PCA = push coring assembly, PCS = piston coring system. BHA = bottom-hole assembly, API = American Petroleum Institute size drill pipe, PC = piston core, PCD = polycrystalline diamond, RR = Rock Roller, WOB = weight on bit, TD = total depth, RIH = run in hole.

Table T2. Diatom species, Site M0059. (Continued on next page.)

Taxonomic list

Marine taxa
- *Actinoptychus senarius* (Ehrenberg) Ehrenberg
- *Ardissonea fulgens* (Greville) Grunow
- *Auliscus caelatus* Bailey
- *Caloneis elongata* (Grunow) Boyer
- *Dimeregramma minor* (Gregory) Ralfs
- *Diploneis coffaeiformis* (Schmidt) Cleve
- *Diploneis decipiens* var. *parallela* A. Cleve
- *Diploneis subcincta* (A. Schmidt) Cleve
- *Eucampia zodiacus* Ehrenberg
- *Fallacia litoricola* (Hustedt) D.G. Mann
- *Fragilaria capensis* Grunow
- *Fragilariopsis oceanica* (Cleve) Hasle
- *Hyalodiscus scoticus* (Kützing) Grunow
- *Lyrella* cf. *spectabilis* (Gregory) D.G. Mann
- *Mastogloia* cf. *grunowii* A. Schmidt
- *Navicula arenaria* Donkin
- *Navicula kariana* var. *frigida* (Grunow) Cleve
- *Navicula ramosissima* (C. Agardh) Cleve
- *Nitzschia grossestriata* Hustedt
- *Nitzschia marginulata* Grunow
- *Nitzschia rorida* M.H. Giffen
- *Nitzschia scabra* Cleve
- *Odontella aurita* (Lyngbye) C. Agardh
- *Opephora marina* (Gregory) Petit
- *Opephora minuta* (Cleve-Euler) Witkowski
- *Opephora pacifica* (Grunow) Petit
- *Pinnularia quadratarea* (A. Schmidt) Cleve
- *Plagiogramma staurophorum* (W. Gregory) Heiberg
- *Pleurosigma angulatum* (Queckett) W. Smith
- *Porosira glacialis* (Grunow) Jorgensen
- *Psammodiscus nitidus* (W. Gregory) Round and D.G. Mann
- *Pseudosolenia calcar-avis* (Schultze) B.G. Sundström
- *Rhizosolenia antennata* fo. *semispina* Sundström
- *Rhizosolenia pungens* Cleve-Euler
- *Thalassiosira* cf. *angulata* (W. Gregory) Hasle
- *Thalassiosira eccentrica* (Ehrenberg) Cleve
- *Thalassiosira oestrupii* (Ostenfeld) Hasle
- *Thalassiosira* spp.
- *Toxarium undulatum* Bailey
- *Trachyneis aspera* (Ehrenberg) Cleve

Brackish-marine taxa
- *Actinocyclus octonarius* Ehrenberg
- *Bacillaria socialis* (Gregory) Ralfs
- *Chaetoceros* spp. resting spores
- *Chaetoceros* spp. vegetative cells
- *Cocconeis peltoides* Hustedt
- *Fallacia pseudony* (Hustedt) D.G. Mann
- *Fallacia* spp.
- *Grammatophora macilenta* W. Smith
- *Grammatophora oceanica* Ehrenberg
- *Mastogloia exigua* F.W. Lewis
- *Rhabdonema arcuatum* (Lyngbye) Küzing
- *Rhizosolenia hebetata* fo. *semispina* (Hensen) Gran
- *Rhopalodia acuminata* Krammer
- *Tabularia fasciculata* (C. Agardh) D.M. Williams and Round
- *Tabularia* spp.
- *Thalassionema nitzschioides* (Grunow) Mereschkowsky
- *Tryblionella coarctata* (Grunow) D.G. Mann

Brackish taxa
- *Achnanthes lemmermannii* Hustedt
- *Amphora robusta* Gregory
- *Amphora subholstatica* Krammer
- *Caloneis aemula* (A. Schmidt) Cleve
- *Cocconeis neothumensis* Krammer
- *Cocconeis scutellum* Ehrenberg
- *Coscinodiscus astermophalus* Ehrenberg
- *Coscinodiscus granii* Gough
- *Cyclotella choctawhatcheeana* Prasad

Taxonomic list

- *Cyclotella striata* (Kützing) Grunow
- *Diploneis didyma* (Ehrenberg) Ehrenberg
- *Diploneis stroemii* Hustedt
- *Entomoneis pseudoduplex* Osada and Kobayasi
- *Epithemia adnata* (Kützing) Brébisson
- *Fragilaria amicorum* Witkowski and Lange-Bertalot
- *Fragilaria gedanensis* Witkowski
- *Mastogloia lanceolata* Thwaites ex W. Smith
- *Mastogloia pusilla* Grunow
- *Mastogloia smithii* var. *amphicephala* Grunow
- *Mastogloia* sp.
- *Navicula digitoradiata* (Gregory) Ralfs
- *Navicula palpebralis* Brébisson ex W. Smith
- *Navicula peregrina* (Ehrenberg) Küzing
- *Navicula phyllepta* Küzing
- *Nitzschia lorenziana* Grunow
- *Opephora mutabilis* (Grunow) Sabbe and Wyverman
- *Paralia sulcata* (Ehrenberg) Cleve
- *Petroneis humerosa* (Brébisson ex W. Smith) A.J. Stickle and D.G. Mann
- *Placoneis clementis* (Grunow) E.J. Cox
- *Planothidium quarnerensis* (Grunow) Witkowski, Lange-Bertalot, and Metzelin
- *Psuedostaurosira perminuta* (Grunow) K. Sabbe and W. Wyverman
- *Pseudopododira westii* (W. Smith) Sheshukova-Poretzskaya and Glezer
- *Rhoicosphenia curvata* (Kützing) Grunow
- *Skeletonema costatum* (Greville) Cleve
- *Staurosira* cf. *elliptica* (Schumann) Williams and Round
- *Tabularia* cf. *laevis* Küzing
- *Thalassiosira levanderi* Van Goor
- *Thalassiosira proschkinae* Makarova

Brackish-freswater taxa
- *Actinocyclus octonarius* var. *tenellus* (Brébisson) Hendey
- *Amphora ovalis* (Kützing) Küzing
- *Amphora pediculus* (Kützing) Grunow ex A. Schmidt
- *Campylodiscus bicostatus* W. Smith
- *Cocconeis placentula* Ehrenberg
- *Cymatopleura solea* var. *apiculata* (W. Smith) Ralfs
- *Diploneis smithii* (Brébisson) Cleve
- *Epithemia sorex* Küzing
- *Epithemia turgida* (Ehrenberg) Küzing
- *Epithemia turgida* var. *westermannii* (Ehrenberg) Grunow
- *Mastogloia elliptica* (C. Agardh) Cleve
- *Mastogloia smithii* Thwaites ex W. Smith
- *Navicula cincta* (Ehrenberg) Ralfs
- *Navicula rhynocephala* Küzing
- *Pseudostaurosira brevistriata* (Grunow) D.M. Williams and Round
- *Rhopalodia gibba* (Ehrenberg) O. Müller
- *Thalassiosira baltica* (Grunow) Ostenfeld
- *Tryblionella plana* (W. Smith) Pelletan

Freshwater taxa
- *Actinocyclus normanii* fo. *subsalsa* (Juhlin-Dannfelt) Hustedt
- *Amphora copulata* (Kützing) Schoeman and Archibald
- *Aulacoseira ambigua* (Grunow) Simonsen
- *Aulacoseira granulata* (Ehrenberg) Simonsen
- *Auloacoseira islandica* (O. Müller) Simonsen
- *Caloneis schumanniana* (Grunow) Cleve
- *Cocconeis disculus* (Schumann) Cleve
- *Cyclotella ocellata* Pantocsek
- *Cyclotella radiosa* (Grunow) Lemmermann
- *Denticula tenuis* var. *crassula* (Nägeli) Hustedt
- *Diatoma tenuis* C.A. Agardh
- *Diploneis mauleri* (Brun) Cleve
- *Ellerbeckia arenaria* (Moore) Crawford
- *Epithemia frickei* Krammer
- *Fragilaria heidenii* Østrup
- *Fragilaria inflata* var. *istvanffyi* (Pantocsek) Hustedt
- *Fragilaria tenera* (W. Smith) Lange-Bertalot
- *Ulnaria delicatissima* (W. Smith) M. Aboal and P.C. Silva
- *Karayevia clevei* (Grunow) Bukhtiyarova
- *Martyana martyii* (Héribaud-Joseph) Round

Table T2 (continued).

Taxonomic list
Navicula radiosa Küzing
Navicula scutelloides W. Smith
Staurophora salina (W. Smith) Mereschkowsky
Staurosirella lapponica (Grunow) D.M. Williams and Round
Stephanodiscus cf. *alpinus* Hustedt
Stephanodiscus minutulus (Kützing) Cleve and Müller
Stephanodiscus neoastraea Håkansson and Hickel
Stephanodiscus parvus Stoermer and Håkansson
Synedra acus Küzing
Synedra ulna (Nitzsch) Ehrenberg
Tabelaria flocculosa (Roth) Küzing

Salinity affinities follow Snoeijs et al. (1993–1998). Diatom authorities according to AlgaeBase (www.algaebase.org).

Table T3. Diatoms, Hole M0059A. This table is available in **oversized format.**

Table T4. Foraminifers, Site M0059. (Continued on next three pages.)

Hole, core, section, interval (cm)	Depth (mbsf) Top	Depth (mbsf) Bottom	Abundance	Pre-Quaternary redeposited tests	Number of species	*Ammonia beccarii*	*Bucella frigida*	*Elphidium albiumbilicatum*	*Elphidium excavatum clavatum*	*Elphidium excavatum selseyensis*	*Elphidium incertum*	*Elphidium williamsoni*	Other *Elphidium* and *Haynesina* spp.	*Hyalinea balthica*	*Nonionella labradorica*	*Quinqueloculina* sp.	Agglutinated (all species)	Other species, total
347-																		
M0059A-1H-1, 15–17	0.15	0.17	C		3				x	x							x	
M0059A-1H-1, 75–77	0.75	0.77	R		3				x	x					x			
M0059A-1H-2, 11–13	1.62	1.64	V		1				x									
M0059D-1H-2, 15–17	1.63	1.65	A		3				x	x							x	
M0059D-1H-CC	2.51	2.54	C		3				x				x			x		
M0059E-2H-CC	2.75	2.80	C		3			x	x							x		
M0059A-1H-CC	3.23	3.23	A		1				x									
M0059D-2H-2, 15–17	3.43	3.45	A		2				x							x		
M0059A-2H-2, 13.5–15	4.94	4.95	A		3			x	x			x						
M0059D-3H-1, 15–17	5.23	5.25	A		2				x	x								
M0059D-2H-CC	5.28	5.30	A		3				x				x			x		
M0059D-3H-2, 15–17	6.73	6.75	A		2				x	x								
M0059A-2H-CC	6.80	6.90	A		4	x			x									
M0059A-3H-2, 13–15	8.52	8.54	C		2				x				x					
M0059D-3H-CC	8.51	8.66	A		3				x				x			x		
M0059D-4H-1, 44–46	8.82	8.84	A		2				x	x								
M0059C-3H-bottom		9.47	C		4			x	x		x					x		
M0059D-4H-2, 19–21	10.07	10.09	A		2				x	x								
M0059A-3H-CC	10.26	10.36	A		1				x									
M0059A-4H-2, 12–14	11.84	11.86	F		2				x				x					
M0059D-4H-CC	11.94	11.96	A		3				x				x			x		
M0059C-4H-bottom		12.97	A		3				x		x		x					
M0059D-5H-2, 16–18	13.36	13.38	A		3				x	x						x		
M0059A-4H-CC	13.55	13.60	A		2	x			x									
M0059A-5H-2, 23–25	15.22	15.24	C		2				x				x					
M0059C-5H-bottom		16.21	C		1				x									
M0059E-5H-CC	16.53	16.66	C		4			x	x				x			x		
M0059D-6H-2, 15–17	16.65	16.67	A		2				x	x								
M0059A-5H-CC	16.71	16.73	C		1				x									
M0059A-6H-2, 15–17	18.45	18.47	C		1				x				x					
M0059C-6H-bottom		19.49	C		2				x		x							
M0059D-7H-2, 15–17	19.95	19.97	C		2				x	x								
M0059A-6H-CC	19.95	19.97	R		1				x									
M0059A-7H-2, 14–15.5	21.73	21.75	C		1				x									
M0059C-7H-bottom		22.71	F		2				x		x							
M0059D-8H-2, 15–17	23.25	23.27	A		2				x				x					
M0059A-7H-CC	23.56	23.59	R		1				x									
M0059A-8H-2, 16–18	25.06	25.08	C		1				x									
M0059C-8H-bottom		26.04	V		1				x									
M0059D-9H-2, 15–17	26.55	26.57	F		2				x				x					
M0059A-8H-CC	26.75	26.80	F		1				x									
M0059A-9H-2, 15–18	28.35	28.37	C		1				x									
M0059C-9H-bottom		29.30	V		1				x									
M0059D-10H-2, 15–17	29.84	29.86	V		1				x									
M0059A-9H-CC	29.95	30.00	V		1				x									
M0059A-10H-2, 15–17	31.65	31.67	F		1				x									
M0059C-10H-bottom		32.68	F		1				x									
M0059D-11H-2, 15–17	33.15	33.17	C		2				x	x								
M0059E-10H-CC	33.18	33.21	F		2				x				x					
M0059A-10H-CC	33.40	33.45	F		1				x									
M0059A-11H-2, 15–17	34.15	34.17	B															
M0059D-11H-CC	35.00	35.01	R		1				x									
M0059C-11H-bottom		35.97	F		2	x			x									
M0059D-12H-2, 15–17	36.45	36.47	R		2			x		x								
M0059A-11H-CC	36.76	36.80	R		1				x									
M0059E-12H-2, 26–28	38.04	38.06	B															
M0059A-12H-2, 15–17	38.25	38.27	V		2				x				x					

Table T4 (continued). (Continued on next page.)

Hole, core, section, interval (cm)	Depth (mbsf) Top	Depth (mbsf) Bottom	Abundance	Pre-Quaternary redeposited tests	Number of species	*Ammonia beccarii*	*Bucella frigida*	*Elphidium albiumbilicatum*	*Elphidium excavatum clavatum*	*Elphidium excavatum selseyensis*	*Elphidium incertum*	*Elphidium williamsoni*	Other *Elphidium* and *Haynesina* spp.	*Hyalinea balthica*	*Nonionella labradorica*	*Quinqueloculina* sp.	Agglutinated (all species)	Other species, total
M0059C-12H-bottom		39.48	R		1				x									
M0059D-13H-2, 15–17	39.75	39.75	R		2				x	x								
M0059A-12H-CC	39.99	40.02	R		1				x									
M0059A-13H-2, 12–14	41.52	41.54	R		3	x			x				x					
M0059A-13H-2, 15–17	41.55	41.57	R		3			x	x							x		
M0059C-13H-bottom		42.65	A		4				x		x					x		x
M0059D-14H-2, 15–17	43.05	43.07	V		1				x									
M0059A-13H-CC	43.13	43.20	V		1				x									
M0059C-14H-bottom		43.29	C		5	x			x		x					x		x
M0059A-14H-2, 14–16	44.84	44.86	V		1				x									
M0059D-14H-CC	44.92	44.93	R		1				x									
M0059D-15H-2, 15–17	46.35	46.37	F		3	x			x	x								
M0059A-14H-CC	46.67	46.69	R		1				x									
M0059C-15H-bottom		47.42	F		1				x									
M0059D-15H-CC	47.97	48.02	V		1				x									
M0059A-15H-2, 15–17	48.15	48.17	B															
M0059D-16H-2, 15–17	49.65	49.67	B															
M0059C-16H-bottom		49.97	B															
M0059A-15H-CC	50.00	50.02	B															
M0059A-16H-1, 140–142	51.20	51.22	B															
M0059D-16H-CC	51.35	51.40	B															
M0059E-16H-2, 104–106	52.02	52.04	F		1				x									
M0059D-17H-1, 139–141	52.69	52.71	B															
M0059A-16H-CC	53.01	53.05	B															
M0059C-17H-bottom		53.38	B															
M0059A-17H-2, 11–13	54.32	54.34	B															
M0059A-17H-CC	54.61	54.65	B															
M0059C-18H-2, 53–55	55.45	55.47	B															
M0059D-18H-2, 15–17	56.25	56.27	B															
M0059C-18H-bottom		56.71	B	x														
M0059D-18H-CC	58.03	58.05	B	x														
M0059A-18H-CC	58.86	58.88	B															
M0059D-19H-2, 10–12	59.50	59.52	B															
M0059C-19H-bottom		60.11	B	x														
M0059A-19H-2, 14–16	60.22	60.24	B															
M0059A-18H-2, 11–13	60.24	60.26	B	x														
M0059B-1H-2, 15–17	61.63	61.65	V		1				x									
M0059D-19H-CC	61.67	61.70	B	x														
M0059A-19H-CC	61.80	61.83	B															
M0059D-20H-2, 15–17	62.85	62.87	B	x														
M0059C-20H-bottom		63.32	B	x														
M0059B-1H-CC	63.30	63.35	B															
M0059D-20H-CC	64.84	64.87	B	x														
M0059B-2H-2, 15–17	64.95	64.97	B	x														
M0059A-20H-CC	65.26	65.28	B															
M0059D-21H-2, 15–17	66.15	66.17	B	x														
M0059B-2H-CC	66.59	66.61	V		1				x									
M0059C-21H-bottom		66.77	B	x														
M0059A-21H-2, 15–17	66.83	66.85	R		3		x	x	x									
M0059D-21H-CC	67.74	67.76	B	x														
M0059B-3H-2, 15–17	68.25	68.25	B															
M0059A-21H-CC	68.65	68.67	V		1				x									
M0059D-22H-2, 15–17	69.45	69.47	B	x														
M0059C-22H-bottom		69.90	R		1				x									
M0059B-3H-CC	70.16	70.18	B															
M0059D-22H-CC		71.50	B															
M0059B-4H-2, 15–17	71.54	71.56	B															
M0059A-22H-CC	72.08	72.11	B															
M0059D-23H-2, 15–17	72.74	72.76	B	x														

Table T4 (continued). (Continued on next page.)

Hole, core, section, interval (cm)	Depth (mbsf)		Abundance	Pre-Quaternary redeposited tests	Number of species	*Ammonia beccarii*	*Bucella frigida*	*Elphidium albiumbilicatum*	*Elphidium excavatum clavatum*	*Elphidium excavatum selseyensis*	*Elphidium incertum*	*Elphidium williamsoni*	Other *Elphidium* and *Haynesina* spp.	*Hyalinea balthica*	*Nonionella labradorica*	*Quinqueloculina* sp.	Agglutinated (all species)	Other species, total
	Top	Bottom																
M0059C-23H-bottom		73.14	B															
M0059A-23H-2, 15–17	73.45	73.47	B															
M0059B-4H-CC	73.48	73.50	B															
M0059D-23H-CC	74.38	74.43	B	x														
M0059A-23H-CC	75.07	75.10	B															
M0059D-24H-2, 15–17	76.05	76.07	B	x														
M0059C-24H-bottom		76.68	B															
M0059B-5H-CC	76.72	76.74	B															
M0059D-24H-CC	77.85	77.87	B	x														
M0059B-6H-2, 15–17	78.13	78.15	B															
M0059A-24H-CC	78.41	78.43	B															
M0059A-25H-1, 15–17	78.55	78.57	B															
M0059C-25H-bottom		79.72	V		1				x									
M0059B-6H-CC	80.05	80.07	B															
M0059A-25H-2, 20–22	80.10	80.12	B															
M0059D-25H-CC	81.07	81.09	B	x														
M0059B-7H-2, 15–17	81.45	81.47	B	x														
M0059A-25H-CC	81.66	81.68	A		8	x	x	x	x		x							x
M0059A-26H-1, 15–17	81.85	81.87	C	x	3		x	x	x									
M0059B-7H-2, 64–66	81.94	81.96	B															
M0059C-26H-bottom		82.23	F		1			x										
M0059B-7H-2, 117–119	82.47	82.49	R	x	3		x	x	x									
M0059B-7H-CC	82.85	82.87	A		4				x		x				x			x
M0059A-26H-CC	83.15	83.17	V		1				x									
M0059B-8H-1, 10–12	83.18	83.20	C		3		x		x				x					
M0059A-27H-CC	83.20	83.30	V		1				x									x
M0059A-28X-1, 30–32	83.50	83.52	B	x														
M0059C-27H-bottom		84.11	R	x	1				x									
M0059A-28H-CC	84.10	84.14	B															
M0059D-26H-CC	84.41	84.42	V	x	1				x									
M0059B-8H-2, 3–5	84.50	84.52	R	x	4		x	x	x							x		
M0059C-28S-bottom		84.61	B															
M0059B-8H-CC	85.84	85.89	F		1				x									
M0059D-27H-CC	86.46	86.47	V	x	1				x									
M0059C-30S-bottom		87.62	B															
M0059B-10H-CC	89.64	89.69	B															
M0059C-32S-bottom		90.13	B															
M0059B-12H-CC	91.40	91.50	B															
M0059B-13X-CC	92.90	93.02	B															
M0059C-34S-bottom		93.52	R		1				x									
M0059C-36S-bottom		96.32	R	x	1				x									
M0059C-38S-bottom		99.62	B															
M0059C-40S-bottom		102.62	R															
M0059C-42S-bottom		105.52	B															
M0059B-19H-CC	107.28	107.43	B															
M0059C-44S-bottom		108.32	B															
M0059B-23X-CC	111.03	111.05	B															
M0059C-48S-bottom		114.62	B															
M0059C-50S-bottom		117.22	B															
M0059B-25P-1, 15–17	117.43	117.45	B	x														
M0059B-25M-CC	117.90	117.92	F		2	x												x
M0059C-52S-bottom		120.22	B	x														
M0059C-54S-bottom		123.15	B	x														
M0059C-56S-1, 3–5	124.65	124.67	B	x														
M0059C-56S-bottom silt		125.12	R		2		x							x				
M0059C-56S-bottom clay		125.12	B	x														
M0059C-58S-bottom		126.47	B	x														
M0059C-60S-1, 5–7	127.67	127.69	B															
M0059C-60S-bottom		128.22	B															

Table T4 (continued).

Hole, core, section, interval (cm)	Depth (mbsf) Top	Depth (mbsf) Bottom	Abundance	Pre-Quaternary redeposited tests	Number of species	*Ammonia beccarii*	*Bucella frigida*	*Elphidium albiumbilicatum*	*Elphidium excavatum clavatum*	*Elphidium excavatum selseyensis*	*Elphidium incertum*	*Elphidium williamsoni*	Other *Elphidium* and *Haynesina* spp.	*Hyalinea balthica*	*Nonionella labradorica*	*Quinqueloculina* sp.	Agglutinated (all species)	Other species, total
M0059C-61H-1, 78–80	128.40	128.42	B	x														
M0059C-61H-2, 18–20	129.30	129.30	B															
M0059C-61H-bottom		130.62	B	x														
M0059C-62H-1, 2.5–4.5	130.65	130.67	B	x														
M0059C-62H-bottom		131.57	B															
M0059C-63H-1, 15–17	131.87	131.89	V	x	1								x					
M0059C-64H-1, 0–3	134.72	134.74	B	x														
M0059C-63H-bottom		134.74	B	x														
M0059C-64H-bottom		134.96	B															
M0059C-66H-1, 15–17	135.85	135.87	B	x														
M0059C-66H-bottom		138.51	B	x														
M0059C-67H-bottom		138.90	B	x														
M0059C-70H-bottom		144.00	B	x														
M0059C-72S-bottom		144.51	B															
M0059C-74S-bottom		145.10	B															
M0059C-76S-bottom		146.10	B															
M0059C-80S-bottom		153.10	R	x	1				x									
M0059C-82S-bottom		154.10																
M0059C-84S-bottom		158.08	R	x	1				x									
M0059B-27X-CC	169.03	169.05	F		1				x									
M0059B-29M-CC	203.90	203.93	C		1				x									

Abundance: A = abundant, C = common, F = few, R = rare, B = barren, V = very high.

Table T5. Distribution and abundance of ostracods, Site M0059. (Continued on next three pages.)

Core, section, interval (cm)	Depth (mbsf)	Abundance (offshore samples, 5–30 cm^3)	Overall abundance/20 cm^3	*Acanthocythereideis dunelmensis*	*Candona* spp.	*Cyprideis torosa*	*Cythere lutea*	*Cytherissa lacustris*	*Cytherois* sp.	*Cytheropteron latissimum*	*Cytherura* spp.	*Elofsonella concinna*	*Finmarchinella* sp.	*Hirschmania viridis*	*Jonesia acuminata*	*Leptocythere* spp.	*Paracyprideis* sp.	*Palmoconcha* spp.	*Robertsonites tuberculatus*	*Sarsicytheridea bradii*	*Sclerochilus* sp.	*Xestoleberis* sp.	Undetermined	Redeposited
347-M0059A-																								
1H-1, 15–17	0.16		B																					
1H-1, 75–77	0.76		B																					
1H-2, 11–13	1.61		R															R						
1H-CC, 0–8	3.23	R																R						
2H-2, 13.5–15	4.93		B																					
2H-CC, 32–42	6.80	B																						
3H-2, 13–15	8.51		B																					
3H-CC, 5–10	10.31	R														R		R						
4H-2, 12–14	11.82		R	R																R			R	
4H-CC, 13–15	13.58	B																						
5H-2, 23–25	15.23		F							R						R		R		R				
5H-CC, 11–13	16.71	B																						
6H-2, 15–17	18.46		B																					
6H-CC, 10–12	19.95	B																						
7H-2, 14–15.5	21.74		R																R					
7H-CC, 12–15	23.46	B																						
8H-2, 16–18	25.07		B																					
8H-CC, 17–22	26.75	R																R		R				
9H-2, 15–18	28.36		F						R									R		R			R	
9H-CC, 0–5	29.95	R																		R			R	R
10H-2, 15–17	31.66		R																				R	
10H-CC, 10–15	33.40	B																						
11H-2, 15–17	34.16		F	R						R								R	R				R	
11H-CC, 10–14	36.76	B																						
12H-2, 15–17	38.26		F							R				R				F		R	R			
12H-CC, 10–13	39.99	R																R						
13H-2, 12–14	41.53		C						R	R	R							C	R	R	R		F	
13H-2, 15–17	41.56		F						R									R		R			R	
13H-CC, 0–7	43.13	R																R						
14H-2, 14–16	44.85		B																				R	
14H-CC, 13–15	46.67	B																						
15H-2, 15–17	48.16		B																					
15H-CC, 13–15	50.00	B																						
16H-1, 140–142	51.21		F		R																		F	
16H-CC, 23–25	53.03	B																						
17H-2, 11–13	54.33		B																					
17H-CC, 0–4	54.61	B																						
18H-CC, 16–18	58.86	B																						
19H-2, 14–16	60.23		R					R																
19H-CC, 20–23	61.80	B																						
20H-CC, 18–20	65.26	B																						
21H-2, 15–17	66.84		B																					
21H-CC, 29–31	68.65	B																						
22H-CC, 13–15	72.09	B																						
23H-2, 15–17	73.46		B																					
23H-CC, 27–30	75.07	B																						
24H-CC, 10–12	78.41	B																						
25H-1, 15–17	78.56		B																					
25H-2, 20–22	80.11		B																					
25H-CC, 13–15	81.66	B																						
26H-1, 15–17	81.86		C		R			R											R				F	
26H-CC, 19–21	83.15	B																						
27H-CC	83.25	R				R																		
28X-1, 30–32	83.51		R			R																		
28H-CC, 7–11	84.10	B																						

Table T5 (continued). (Continued on next page.)

Core, section, interval (cm)	Depth (mbsf)	Abundance (offshore samples, 5–30 cm³)	Overall abundance/20 cm³	*Acanthocythereideis dunelmensis*	*Candona* spp.	*Cyprideis torosa*	*Cythere lutea*	*Cytherissa lacustris*	*Cytherois* sp.	*Cytheropteron latissimum*	*Cytherura* spp.	*Elofsonella concinna*	*Finmarchinella* sp.	*Hirschmania viridis*	*Jonesia acuminata*	*Leptocythere* spp.	*Paracyprideis* sp.	*Palmoconcha* spp.	*Robertsonites tuberculatus*	*Sarsicytheridea bradii*	*Sclerochilus* sp.	*Xestoleberis* sp.	Undetermined	Redeposited
347-M0059B-																								
1H-2, 15–17	61.64		B																					
1H-CC, 0–5	63.30	B																						
2H-2, 15–17	64.96		B																					
2H-CC, 13–15	66.59	B																						
3H-2, 15–17	68.25		B																					
3H-CC, 20–22	70.16	B																						
4H-2, 15–17	71.55		B																					
4H-CC, 14–16	73.48	B																						
5H-CC, 10–13	76.71	B																						
6H-2, 15–17	78.14		B																					
6H-CC, 9–11	80.05	B																						
7H-2, 15–17	81.46		B																					R
7H-2, 64–66	81.95		B																					
7H-2, 117–119	82.48		R																				R	
7H-CC, 15–17	82.85	B																						
8H-1, 10–12	83.19		F			R																	R	
8H-2, 3–5	84.51		R			R																		
8H-CC, 0–5	85.84	R				R																		
10X-CC, 0–5	89.64	B																						
12H-CC, 0–10	91.40	B																						
13X-CC, 0–12	92.90	B																						
19H-CC, 13–15	107.41	B																						
23X-CC, 0–2	111.03	B																						
25P-1, 15–17	117.44		B																					
25M-CC, 17–19	117.90	B																						
27X-CC, 0–2	169.03	B																						
29M-CC, 38–40	203.91	R																						R
347-M0059C-																								
3H-bottom, 15–17	9.45	B																						
4H-bottom, 35–37	12.95	B																						
5H-bottom, 29–31	16.19	B																						
6H-bottom, 26–28	19.47	B																						
7H-bottom, 19–21	22.69	B																						
8H-bottom, 22–24	26.02	B																						
9H-bottom, 18–20	29.28	B																						
10H-bottom, 26–28	32.66	R																						
11H-bottom, 25–27	35.95	B																						
12H-bottom, 46–48	39.46	R																R						
13H-bottom, 33–35	42.63	R																R						
14H-bottom, 67–69	43.27	R																R						
15H-bottom, 88–90	47.40	B																						
16H-bottom, 13–15	49.95	F			F																			
17H-bottom, 24–26	53.36	R						R																
18H-2, 53–55	55.46		B																					
18H-bottom, 27–29	56.69	B																						
19H-bottom, 37–39	60.09	B																						
20H-bottom, 28–30	63.30	B																						
21H-bottom, 43–45	66.75	B																						
22H-bottom, 26–28	69.88	B																						
23H-bottom, 21–23	73.12	B																						
24H-bottom, 44–46	76.66	B																						
25H-bottom, 18–20	79.70	B																						
26H-bottom, 89–91	82.21	B																						
27H-bottom, 36–38	84.09	B																						
28S-bottom	84.61	B																						
30S-bottom	87.62	B																						

Table T5 (continued). (Continued on next page.)

Core, section, interval (cm)	Depth (mbsf)	Abundance (offshore samples, 5–30 cm³)	Overall abundance/20 cm³	*Acanthocythereis dunelmensis*	*Candona* spp.	*Cyprideis torosa*	*Cythere lutea*	*Cytherissa lacustris*	*Cytheroi*s sp.	*Cytheropteron latissimum*	*Cytherura* spp.	*Elofsonella concinna*	*Finmarchinella* sp.	*Hirschmania viridis*	*Jonesia acuminata*	*Leptocythere* spp.	*Paracyprideis* sp.	*Palmoconcha* spp.	*Robertsonites tuberculatus*	*Sarsicytheridea bradii*	*Sclerochilus* sp.	*Xestoleberis* sp.	Undetermined	Redeposited
32S-bottom	90.13	B																						
34S-bottom, 38–40	102.60	B																						
40S-bottom, 48–50	102.60	B																						
36S-bottom, 18–20	105.50	B																						
42S-bottom, 38–40	105.52	B																						
38S-bottom, 48–50	108.30	B																						
44S-bottom, 18–20	108.32	B																						
48S-bottom, 48–50	114.62	B																						
50S-bottom, 8–10	117.20	B																						
52S-bottom, 8–10	120.20	B																						
54S-bottom, 0–3	123.12	B																						
56S-1, 3–5	124.66		B																					
56S-bottom silt, 48–50	125.10	B																						
58S-bottom, 33–35	126.45	B																						
60S-1, 5–7	127.68		B																					
60S-bottom, 58–60	128.20	B																						
61H-1, 78–80	128.41		B																					
61H-2, 18–20	129.30		B																					
61H-bottom	130.62	B																						
62H-1, 2.5–4.5	130.66		B																					
62H-bottom, 93–95	131.55	B																						
63H-1, 15–17	131.88		B																					
63H-bottom, 149–151	134.72	B																						
64H-bottom, 22–24	134.94	B																						
66H-1, 15–17	135.86		B																					
66H-bottom, 129–131	138.49	B																						
67H-bottom, 18–20	138.88	B																						
70H-bottom, 78–80	143.98	B																						
72S-bottom, 0–1	144.50	B																						
74S-bottom, 8–10	145.08	B																						
76S-bottom, 8–10	146.08	B																						
80S-bottom, 0–10	153.00	B																						
82S-bottom, 0–5	154.00	B																						
84S-bottom, 0–8	158.00	B																						
347-M0059D-																								
1H-2, 15–17	1.64		R	R																				
1H-CC, 20–23	2.51	B																						
2H-2, 15–17	3.44		R																	R				
3H-1, 15–17	5.24		F							R				R				R					R	
2H-CC, 17–19	5.28	R														R								
3H-2, 15–17	6.74		R																				R	
3H-CC, 0–15	8.51	B																						
4H-1, 44–46	8.83		F				R				R		R			F		R		R	R	R		
4H-2, 19–21	10.08		R										R										R	
4H-CC, 13–15	11.94	B																						
5H-2, 16–18	13.37		R													R							R	
6H-2, 15–17	16.66		F											R		R								
7H-2, 15–17	19.96		C							F		R				R		R		R			R	
8H-2, 15–17	23.26		C							R					R	R	F		R				R	
9H-2, 15–17	26.56		R								R	R		R										
10H-2, 15–17	29.85		R																				R	
11H-2, 15–17	33.16		F	R						R	R					R				R			R	
11H-CC, 14–15	35.00	R																		R				
12H-2, 15–17	36.46		R																		R			
13H-2, 15–17	39.75		F	R										R				F					F	
14H-2, 15–17	43.06		F							R	R							R		R	R		R	
14H-CC	44.93	B																						

Table T5 (continued).

Core, section, interval (cm)	Depth (mbsf)	Abundance (offshore samples, 5–30 cm^3)	Overall abundance/20 cm^3	*Acanthocythereideis dunelmensis*	*Candona* spp.	*Cyprideis torosa*	*Cythere lutea*	*Cytherissa lacustris*	*Cytheroïs* sp.	*Cytheropteron latissimum*	*Cytherura* spp.	*Elofsonella concinna*	*Finmarchinella* sp.	*Hirschmania viridis*	*Jonesia acuminata*	*Leptocythere* spp.	*Paracyprideis* sp.	*Palmoconcha* spp.	*Robertsonites tuberculatus*	*Sarsicytheridea bradii*	*Sclerochilus* sp.	*Xestoleberis* sp.	Undetermined	Redeposited
15H-2, 15–17	46.36		R											R										
15H-CC, 16–21	47.97	B																						
16H-2, 15–17	49.64		C		C																			
16H-CC, 15–20	51.35	F			F																			
17H-1, 139–141	52.70		R					R																
18H-2, 15–17	56.24		B																					
18H-CC, 22–24	58.03	B																						
19H-2, 10–12	59.49		R																				R	
19H-CC, 30–33	61.67	B																						
20H-2, 15–17	62.86		B																					
20H-CC, 20–23	64.84	B																						
21H-2, 15–17	66.16		B																					
21H-CC, 17–19	67.74	B																						
22H-2, 15–17	69.46		B																					
22H-CC	71.50	B																						
23H-2, 15–17	72.75		B																					
23H-CC, 18–23	74.38	B																						
24H-2, 15–17	76.06		B																					R
26H-2, 15–17	76.06		F		R	R		R															F	
24H-CC, 21–23	77.85	B																						
25H-CC, 18–20	81.07	B																						
26H-CC, 14–15	84.41	B																						
27H-2, 15–17	85.96		R			R																		R
27H-CC, 0–1	86.46	B																						
347-M0059E-																								
2H-CC, 11–16	6.75	R														R		R						
5H-CC, 0–13	16.53	R												R										
10H-CC, 14–17	33.18	B																						
12H-2, 26–28	38.05		F		R					R											R		R	
16H-2, 104–106	52.03		C		C																			

Abundance: C = common, F = few, R = rare, B = barren.

Table T6. Palynomorphs and freshwater algae counts, Hole M0059C.

Depth (mbsf)	Tree pollen		Herb pollen and spores		Freshwater green algae		Organic-walled dinoflagellate cysts (partly reworked)		Tertiary reworked pollen	
	Type	Count	Type	Count	Type	Count	Type	Count	Type	Count
124.85	*Pinus sylvestris* type	6	*Typha latifolia* type	1	*Pediastrum*	10	Dinoflagellate	38	Taxodiacceae/Cupressaceae	1
	Picea	2	*Sphagnum*	1						
	Corylus avellana	2								
	Ulmas	1								
126.24	*P. sylvestris* type	7	Poaceae	1	*Pediastrum*	10	Dinoflagellate	23	Taxodiacceae/Cupressaceae	1
	Betula alba type	2	Cyperaceae	1	*Botryococcus*	2				
	Quercus	1								
	Tilia cordata type	1								
127.69	*P. sylvestris* type	10	Poaceae	1	*Pediastrum*	7	Dinoflagellate	32	*Pinus haploxylon* Rudolph type	2
	Picea	4	Cyperaceae	1	*P. kawraiskyi*	2			*Castanea/Castanopsis*	1
	Juniperus	3	*Artemisia*	2	*Botryococcus*	6			*Engelhardia*	1
	B. alba type	1	Chenopodiaceae	2					Taxodiacceae/Cupressaceae	1
	Quercus	2								
	Corylus avellana	4								
131.89	*P. sylvestris* type	2	—		*Pediastrum*	1	Dinoflagellate	23	*P. haploxylon* Rudolph type	1
	Picea	2			*Botryococcus*	1			Taxodiacceae/Cupressaceae	1
									Indeterminable corroded	5
141.72	*P. sylvestris* type	1	*Artemisia*	1	*Pediastrum*	1	Dinoflagellate	8	*P. haploxylon* Rudolph type	1
	Quercus	2							Varia	1

Table T7. Calculated salinities and elemental ratios of interstitial water, Site M0059. (Continued on next two pages.)

Core, section, interval (cm)	Type	Depth (mbsf)	Cl^- based salinity	Anion-based salinity	Na/Cl (mM/mM)	Ca/Cl (mM/mM)	Mg/Cl (mM/mM)	K/Cl (mM/mM)	Br/Cl (μM/mM)	B/Cl (μM/mM)
347-M0059A-										
1H-1, 10	Rh	0.10	23.31	—	0.85	0.02	0.12	0.02	1.672	2.293
1H-1, 141	Rh	1.41	24.02	—	0.90	0.03	0.15	0.03	1.932	3.483
1H-2, 10	Rh	1.61	23.69	30.11	0.89	0.03	0.15	0.03	2.086	3.467
1H-2, 140	Rh	2.91	24.12	31.20	0.92	0.03	0.16	0.03	2.110	3.745
2H-1, 140	Rh	4.70	23.74	31.30	0.94	0.03	0.16	0.03	2.278	3.820
2H-2, 140	Rh	6.20	23.96	31.94	0.93	0.03	0.16	0.03	2.431	3.732
3H-1, 139	Rh	8.29	23.40	31.47	0.94	0.03	0.16	0.03	2.433	3.955
3H-2, 140	Rh	9.79	24.20	33.25	0.93	0.03	0.17	0.03	2.598	4.102
4H-1, 139	Rh	11.59	23.85	33.22	0.93	0.02	0.18	0.03	2.724	3.989
4H-2, 139	Rh	13.08	23.73	33.77	0.94	0.02	0.18	0.04	2.827	4.090
5H-1, 139	Rh	14.89	23.43	33.62	1.03	0.02	0.21	0.04	2.941	4.664
5H-2, 132	Rh	16.31	22.83	33.26	1.01	0.02	0.20	0.04	3.043	4.492
6H-1, 140	Rh	18.20	—	—	—	—	—	—	—	—
6H-1, 106	Rh	19.36	23.02	34.34	0.99	0.02	0.21	0.04	3.271	4.506
7H-1, 140	Rh	21.50	22.45	33.79	0.96	0.02	0.20	0.04	3.421	4.470
8H-1, 135–140	Rh	24.78	20.52	31.63	1.03	0.02	0.22	0.04	3.539	5.113
9H-1, 135–140	Rh	28.08	19.21	30.05	0.99	0.02	0.22	0.04	3.579	5.179
10H-1, 135–140	Rh	31.38	18.30	28.93	1.02	0.02	0.22	0.05	3.827	5.566
11H-2, 135–140	Rh	35.38	—	—	—	—	—	—	—	—
12H-1, 135–140	Rh	37.98	15.67	24.84	0.98	0.02	0.21	0.05	3.889	5.517
13H-1, 135–140	Rh	41.28	14.48	22.91	1.02	0.03	0.22	0.05	4.058	5.792
14H-2, 135–140	Rh	44.58	13.27	20.67	1.03	0.05	0.20	0.05	3.852	5.116
15H-1, 135–140	Rh	47.88	10.37	15.56	—	—	—	—	—	—
16H-1, 135–140	Rh	51.18	10.19	13.05	0.79	0.12	0.13	0.02	3.879	1.734
17H-1, 96–101	Rh	54.09	10.38	12.29	0.75	0.13	0.11	0.02	2.997	0.798
18H-1, 135–140	Rh	56.68	8.10	9.04	0.64	0.23	0.11	0.01	3.189	0.516
19H-1, 135–140	Rh	59.98	7.58	7.97	0.50	0.25	0.09	0.01	2.818	0.491
20H-1, 135–140	Rh	63.28	7.29	7.49	0.51	0.32	0.10	0.00	2.406	0.551
21H-1, 135–140	Rh	66.58	7.16	7.34	0.49	0.27	0.08	0.00	1.909	0.490
22H-1, 135–140	Rh	69.88	7.57	7.79	0.53	0.23	0.07	0.00	1.580	0.400
23H-1, 135–140	Rh	73.18	8.58	8.83	0.57	0.18	0.06	0.00	1.308	0.360
24H-1, 135–140	Rh	76.50	9.77	10.02	0.64	0.14	0.05	0.00	1.111	0.480
25H-1, 10–15	Rh	78.53	11.36	11.61	0.63	0.11	0.05	0.00	1.058	0.567
26H-1, 111–116	Rh	82.84	14.06	14.38	0.73	0.09	0.05	0.00	0.921	0.761
28X-1, 63–78	Rh	83.91	14.57	14.77	0.77	0.08	0.06	0.01	1.271	0.653
347-M0059B-										
2H-1, 135–140	Rh	64.68	6.28	6.48	—	—	—	—	—	—
3H-1, 135–140	Rh	67.98	5.99	6.23	0.39	0.26	0.07	0.00	1.966	0.347
4H-1, 135–140	Rh	71.28	6.33	6.57	0.47	0.23	0.07	0.00	1.569	0.343
5H-1, 135–140	Rh	74.58	7.60	7.86	0.57	0.19	0.06	0.00	1.291	0.383
6H-1, 135–140	Rh	77.88	8.44	8.68	—	—	—	—	1.128	—
7H-1, 125–130	Rh	81.18	11.48	11.71	—	—	—	—	0.917	0.633
8H-1, 121–126	Rh	84.34	14.36	14.63	0.81	0.10	0.06	0.00	0.926	0.806
25P-1, 28–33	Rh	117.61	16.45	16.60	0.95	0.06	0.07	0.01	1.362	0.603
347-M0059C-										
1H-1, 120–130	Sq	1.25	23.80	27.51	0.91	0.03	0.14	0.03	1.741	2.699
1H-2, 120–130	Sq	2.75	24.26	30.82	0.92	0.03	0.15	0.03	1.970	3.073
2H-1, 120–130	Sq	4.25	24.14	31.18	0.98	0.03	0.16	0.04	2.175	3.836
2H-2, 120–130	Sq	5.75	24.51	31.19	0.97	0.03	0.15	0.04	2.295	3.217
3H-1, 120–130	Sq	7.55	24.74	33.02	1.02	0.03	0.17	0.04	2.443	4.062
4H-2, 120–130	Sq	10.85	24.62	33.22	1.01	0.03	0.18	0.04	2.656	4.584
5H-1, 120–130	Sq	14.15	24.55	33.58	1.02	0.02	0.19	0.04	2.869	4.592
9H-1, 120–130	Sq	27.35	21.14	32.21	1.08	0.02	0.23	0.05	3.700	5.566
10H-1, 120–130	Sq	30.65	20.30	31.16	1.06	0.02	0.23	0.05	3.924	5.301
11H-2, 120–130	Sq	35.45	18.96	29.45	1.00	0.02	0.22	0.05	4.046	4.989
12H-2, 120–130	Sq	38.75	18.19	29.55	0.76	0.01	0.16	0.04	4.158	3.576
13H-1, 135–145	Sq	40.70	15.81	24.84	1.02	0.02	0.21	0.05	3.773	4.896
14H-2, 45–55	Sq	43.10	14.85	23.13	1.00	0.03	0.20	0.05	3.912	4.195
15H-1, 135–145	Sq	47.30	14.07	22.17	0.94	0.04	0.18	0.05	3.972	3.964
16H-1, 130–140	Sq	48.17	15.22	20.74	—	—	—	—	3.585	—
17H-2, 5–15	Sq	51.72	15.21	19.14	0.61	0.09	0.10	0.02	3.779	1.259
18H-2, 10–20	Sq	55.07	10.29	12.25	0.80	0.17	0.13	0.02	3.418	0.743
19H-2, 10–20	Sq	58.37	9.50	10.41	0.59	0.22	0.10	0.01	2.989	0.316
20H-1, 135–145	Sq	61.42	8.84	9.25	0.47	0.24	0.08	0.00	2.574	0.353
21H-1, 135–145	Sq	64.72	8.55	8.76	0.46	0.25	0.07	0.00	0.754	0.421

Table T7 (continued). (Continued on next page.)

Core, section, interval (cm)	Type	Depth (mbsf)	Cl^- based salinity	Anion-based salinity	Na/Cl (mM/mM)	Ca/Cl (mM/mM)	Mg/Cl (mM/mM)	K/Cl (mM/mM)	Br/Cl (μM/mM)	B/Cl (μM/mM)
22H-1, 130–140	Sq	67.97	8.64	8.90	0.50	0.22	0.06	0.00	1.671	0.349
23H-2, 5–15	Sq	71.52	9.33	9.60	0.60	0.19	0.06	0.00	1.371	0.381
24H-2, 10–20	Sq	74.87	—	—	—	—	—	—	—	—
25H-1, 130–140	Sq	77.87	11.94	12.22	0.72	0.12	0.05	0.00	1.032	0.643
26H-1, 135–145	Sq	81.22	13.78	14.08	0.77	—	—	—	0.955	0.774
347-M0059C-										
1H-1, 69–74	Rh	0.72	23.25	26.55	0.88	0.02	0.12	0.02	1.596	1.724
1H-2, 89–94	Rh	2.42	24.82	30.87	0.94	0.03	0.15	0.03	1.843	3.438
2H-1, 73–78	Rh	3.76	23.65	30.06	0.94	0.03	0.16	0.03	2.097	3.351
3H-1, 64–69	Rh	6.97	23.68	30.20	0.96	0.03	0.16	0.03	2.325	3.180
3H-2, 75–80	Rh	8.58	24.38	32.48	0.99	0.03	0.18	0.03	2.488	3.496
4H-1, 106–111	Rh	10.69	24.19	33.18	0.98	0.03	0.18	0.03	2.605	3.138
5H-1, 100–105	Rh	13.93	23.59	33.58	1.02	0.03	0.20	0.04	2.794	4.190
6H-1, 79–84	Rh	17.02	22.98	33.18	0.97	0.02	0.20	0.04	2.991	3.984
7H-1, 112–117	Rh	20.65	22.42	33.15	1.06	0.02	0.22	0.04	3.282	4.075
8H-1, 105–110	Rh	23.88	—	—	—	—	—	—	—	—
9H-1, 71–76	Rh	26.84	—	—	—	—	—	—	—	—
10H-1, 100–105	Rh	30.43	—	—	—	—	—	—	—	—
11H-1, 135–140	Rh	34.08	—	—	—	—	—	—	—	—
12H-1, 71–76	Rh	36.74	17.57	—	—	—	—	—	3.805	—
13H-1, 110–115	Rh	40.43	16.01	—	—	—	—	—	3.717	—
14H-1, 21–26	Rh	42.84	—	—	—	—	—	—	—	—
15H-1, 91–96	Rh	44.46	—	—	—	—	—	—	—	—
16H-1, 103–108	Rh	47.88	—	—	—	—	—	—	—	—
17H-1, 130–135	Rh	51.45	—	—	—	—	—	—	—	—
18H-1, 78–83	Rh	54.23	—	—	—	—	—	—	—	—
19H-1, 110–115	Rh	57.85	—	—	—	—	—	—	—	—
20H-1, 110–115	Rh	61.15	—	—	—	—	—	—	—	—
21H-1, 110–115	Rh	64.24	—	—	—	—	—	—	—	—
22H-1, 110–115	Rh	67.75	—	—	—	—	—	—	1.753	
23H-1, 135–140	Rh	71.30	—	—	—	—	—	—	—	—
24H-1, 68–73	Rh	73.93	9.83	10.09	0.69	0.18	0.06	0.00	1.246	0.537
25H-1, 75–80	Rh	77.30	11.78	11.78	0.71	0.12	0.05	0.00	1.061	0.675
26H-1, 110–115	Rh	80.95	13.59	13.59	0.69	0.09	0.05	0.00	0.960	0.720
347-M0059D-										
1H-1, 135–140	Rh	1.38	23.79	29.05	0.90	0.03	0.14	0.03	1.755	2.770
1H-2, 66–71	Rh	2.19	23.95	29.91	0.93	0.03	0.15	0.03	1.895	3.391
2H-1, 135–140	Rh	3.18	23.96	30.79	0.90	0.03	0.15	0.03	2.106	3.460
2H-2, 135–140	Rh	4.68	23.88	31.26	0.92	0.03	0.15	0.03	2.228	3.562
3H-1, 135–140	Rh	6.48	24.18	32.76	0.94	0.03	0.17	0.03	2.469	3.731
3H-2, 135–140	Rh	7.98	23.55	30.73	0.95	0.03	0.16	0.03	2.354	3.737
4H-1, 135–140	Rh	9.78	24.37	34.01	0.88	0.02	0.17	0.03	2.645	3.717
4H-2, 135–140	Rh	11.28	24.75	33.78	0.91	0.03	0.17	0.03	2.582	3.802
5H-1, 135–140	Rh	13.08	23.67	33.71	0.93	0.02	0.18	0.04	2.779	4.117
5H-2, 135–140	Rh	14.58	23.67	34.06	0.96	0.02	0.19	0.04	2.883	4.235
6H-1, 135–140	Rh	16.38	23.08	33.72	0.95	0.02	0.19	0.04	3.003	4.209
6H-2, 135–140	Rh	17.88	22.90	33.29	1.02	0.02	0.21	0.04	3.120	4.499
7H-1, 135–140	Rh	19.68	22.07	33.62	0.97	0.02	0.21	0.04	3.317	4.428
7H-2, 135–140	Rh	21.18	22.10	33.43	0.96	0.02	0.20	0.04	3.255	4.396
8H-1, 135–140	Rh	22.98	21.64	33.02	1.00	0.02	0.22	0.04	3.430	4.786
9H-1, 135–140	Rh	26.28	20.53	32.59	1.02	0.02	0.23	0.04	3.615	4.992
10H-1, 134–139	Rh	29.57	20.01	32.08	1.01	0.02	0.23	0.05	3.852	5.293
11H-1, 135–140	Rh	32.88	17.27	28.23	1.03	0.02	0.23	0.05	3.850	5.634
12H-1, 135–140	Rh	36.18	16.76	27.37	0.99	0.02	0.23	0.05	4.028	5.670
13H-1, 135–140	Rh	39.48	14.83	23.87	0.98	0.02	0.22	0.05	4.005	5.722
14H-1, 135–140	Rh	42.78	14.03	22.94	0.99	0.03	0.22	0.05	4.089	5.647
15H-1, 135–140	Rh	46.08	12.30	19.69	0.97	0.05	0.20	0.04	3.945	4.611
16H-1, 135–140	Rh	49.38	—	—	—	—	—	—	—	—
17H-1, 134–139	Rh	52.67	—	—	—	—	—	—	—	—
18H-1, 135–140	Rh	55.98	8.86	10.89	0.65	0.15	0.11	0.01	3.509	0.581
19H-1, 135–140	Rh	59.28	8.02	8.99	0.55	0.22	0.10	0.01	3.123	0.362
20H-1, 135–140	Rh	62.58	7.77	8.16	0.43	0.23	0.08	0.00	2.676	0.349
21H-1, 135–140	Rh	65.88	7.10	7.38	0.43	—	0.08	0.00	2.216	0.352
22H-1, 135–140	Rh	69.18	7.44	7.72	0.49	0.24	0.07	0.00	1.800	0.340
23H-1, 135–140	Rh	72.48	—	—	—	—	—	—	—	—
24H-1, 135–140	Rh	75.78	8.79	9.09	0.61	0.18	0.06	0.00	1.220	0.351
25H-1, 135–140	Rh	79.08	10.70	11.02	0.69	0.14	0.06	0.00	1.056	0.511
26H-1, 135–140	Rh	82.38	13.31	13.60	0.82	0.11	0.06	0.00	1.043	0.670
27H-1, 135–140	Rh	85.68	15.05	15.36	0.71	0.07	0.06	0.01	1.025	0.667

Table T7 (continued).

Core, section, interval (cm)	Type	Depth (mbsf)	Cl^- based salinity	Anion-based salinity	Na/Cl (mM/mM)	Ca/Cl (mM/mM)	Mg/Cl (mM/mM)	K/Cl (mM/mM)	Br/Cl (μM/mM)	B/Cl (μM/mM)
347-M0059E-										
1H-1, 120–130	Sq	1.25	23.75	28.60	0.90	0.03	0.14	0.03	1.685	2.439
1H-2, 125	Sq	2.75	23.88	30.13	0.89	0.03	0.15	0.03	1.935	3.214
2H-1, 125–135	Sq	4.60	24.46	31.87	0.96	0.03	0.16	0.03	2.189	3.843
2H-2, 125	Sq	6.05	23.95	31.61	0.93	0.03	0.16	0.03	2.295	3.608
3H-1, 120–130	Sq	7.85	24.57	33.19	0.95	0.03	0.17	0.03	2.405	4.004
3H-2, 120	Sq	9.30	23.88	32.52	0.88	0.03	0.16	0.03	2.468	3.431
4H-1, 135–145	Sq	11.30	24.48	34.10	1.02	0.03	0.19	0.04	2.640	4.401
4H-2, 130	Sq	12.70	23.97	33.69	0.95	0.03	0.18	0.04	2.693	3.936
5H-1, 130–140	Sq	14.55	24.23	34.80	0.94	0.02	0.19	0.04	2.858	4.183
5H-2, 135	Sq	16.05	21.83	32.59	1.12	0.03	0.22	0.05	2.857	4.556
6H-1, 135–145	Sq	17.90	23.53	34.81	0.99	0.02	0.21	0.04	3.063	4.703
6H-2, 135	Sq	19.35	23.01	34.13	0.92	0.02	0.19	0.04	3.146	3.959
7H-1, 130–140	Sq	21.15	22.99	35.02	0.96	0.02	0.21	0.04	3.314	4.779
7H-2, 135	Sq	22.65	21.69	32.64	1.03	0.02	0.22	0.04	3.352	4.632
8H-2, 15–25	Sq	24.80	22.00	34.58	1.03	0.02	0.23	0.05	3.544	5.165
9H-2, 30–40	Sq	28.25	20.64	32.19	1.05	0.02	0.23	0.05	3.609	5.253
10H-2, 60–70	Sq	31.85	19.97	32.21	1.05	0.02	0.23	0.05	3.709	5.122
11H-2, 5–15	Sq	34.60	18.83	30.93	1.10	0.02	0.24	0.05	4.008	6.179
12H-1, 5–15	Sq	36.40	17.13	28.08	0.97	0.02	0.22	0.05	4.115	5.392
13H-1, 10–20	Sq	39.75	15.92	26.18	1.07	0.02	0.24	0.05	4.155	6.095
14H-2, 10–20	Sq	44.55	14.42	23.11	0.94	0.03	0.20	0.04	3.935	4.960
15H-2, 10–20	Sq	47.85	12.63	20.17	0.89	0.06	0.18	0.04	3.932	4.028
16H-2, 10–20	Sq	51.15	11.27	17.50	0.84	0.10	0.15	0.03	3.705	2.384
17H-2, 10–20	Sq	54.45	10.06	13.32	0.86	0.15	0.14	0.02	3.715	1.312
18H-2, 10–20	Sq	57.74	9.06	10.50	0.65	0.21	0.12	0.01	3.325	0.531
19H-2, 10–20	Sq	61.05	8.17	8.66	0.46	0.23	0.09	0.01	2.879	0.300
20H-2, 10–20	Sq	64.35	7.70	7.96	0.39	0.26	0.08	0.00	2.502	0.340
21H-2, 10–20	Sq	67.65	7.48	7.75	0.40	0.25	0.07	0.00	2.023	0.306
22H-2, 10–20	Sq	70.94	7.81	8.10	0.47	0.23	0.07	0.00	1.621	0.311
23H-2, 15–25	Sq	74.30	8.52	8.86	0.52	0.19	0.06	0.00	1.330	0.308
24H-2, 5–15	Sq	77.50	9.79	10.15	0.59	0.15	0.05	0.00	1.143	0.342
25H-2, 10–20	Sq	80.85	11.58	11.95	0.65	0.12	0.05	0.00	0.996	0.471
26H-2, 15–25	Sq	84.20	13.69	14.03	0.80	0.11	0.06	0.00	0.924	0.759
347-M0059E-										
1H-1, 70–75	Rh	0.73	23.42	—	0.82	0.02	0.11	0.02	—	—
1H-2, 70–75	Rh	2.23	23.90	—	0.94	0.03	0.16	0.03	—	—
2H-1, 75–80	Rh	4.08	23.89	—	0.93	0.03	0.16	0.03	—	—
2H-2, 80	Rh	5.60	24.27	—	0.95	0.03	0.16	0.03	—	—
3H-1, 70–75	Rh	7.33	23.93	—	0.94	0.03	0.17	0.03	—	—
3H-2, 65–70	Rh	8.78	24.51	—	0.92	0.03	0.16	0.03	—	—
4H-1, 85–90	Rh	10.78	24.19	—	—	—	—	—	—	—
4H-2, 73–78	Rh	12.16	24.12	—	0.94	0.03	—	0.04	—	—
5H-1, 105–110	Rh	14.28	23.96	—	0.95	0.02	—	0.04	—	—
5H-2, 104–109	Rh	15.77	23.73	—	1.00	0.02	—	0.04	—	—
6H-1, 100–110	Rh	17.55	23.17	—	1.05	0.02	—	0.04	—	—
6H-2, 104–109	Rh	19.07	22.85	—	0.93	0.02	—	0.04	—	—
7H-1, 95–100	Rh	20.78	22.43	—	0.98	0.02	—	0.04	—	—
8H-2, 130–135	Rh	25.93	20.80	—	1.01	0.02	—	0.04	—	—
9H-2, 130–135	Rh	29.23	19.63	—	1.01	0.02	—	0.05	—	—
10H-2, 25–30	Rh	31.48	19.42	—	1.06	0.02	—	0.05	—	—
11H-2, 130–135	Rh	35.83	17.22	—	0.99	0.02	0.23	0.05	—	—
12H-2, 131–136	Rh	39.14	16.19	—	1.08	0.02	0.24	0.05	—	—
13H-2, 135–145	Rh	42.50	14.89	—	0.98	0.02	0.21	0.05	—	—
14H-2, 116–121	Rh	45.59	12.99	—	—	—	—	—	—	—
15H-2, 115–120	Rh	48.88	10.54	—	—	—	—	—	—	—
16H-2, 117–122	Rh	52.20	2.87	—	—	—	—	—	—	—
17H-2, 119–124	Rh	55.52	9.24	—	—	—	—	—	—	—
18H-2, 117–122	Rh	58.79	8.43	—	0.62		0.11	0.01	—	—
19H-1, 117–122	Rh	60.60	7.95	—	0.48	0.24	0.09	0.01	—	—
20H-2, 115–120	Rh	65.38	7.00	—	—	—	—	—	—	—
21H-2, 130–135	Rh	68.83	7.19	—	—	—	—	—	—	—
22H-2, 130–135	Rh	72.12	—	—	—	—	—	—	—	—
23H-2, 135–140	Rh	75.48	8.59	—	0.69	0.22	0.07	0.00	—	—
24H-2, 135–140	Rh	78.73	9.83	—	0.72	0.16	0.06	0.00	—	—
25H-2, 130–135	Rh	82.03	11.85	—	0.78	0.13	0.06	0.00	—	—
26H-2, 130–135	Rh	85.33	13.49	—	0.83	0.12	0.06	0.00	—	—

Rh = Rhizon sample, Sq = squeezed sample. — = no data are reported for samples with insufficient pore water volumes.

Table T8. Concentration of methane in interstitial water, Site M0059.

Core, section, interval (cm)	Depth (mbsf)	CH_4 (mM)
347-M0059A-		
1H-1, 146–151	0.10	2.92
1H-3, 17–22	1.41	2.43
2H-1, 145–150	1.61	1.70
2H-3, 13–18	2.91	1.26
3H-1, 144–149	4.70	1.89
3H-2, 145–150	6.20	1.80
4H-1, 144–149	8.29	1.27
4H-2, 144–149	9.79	1.17
5H-1, 144–149	11.59	1.81
5H-2, 138–142	13.08	0.96
6H-1, 145–150	14.89	1.13
6H-2, 111–116	16.31	0.46
7H-1, 144–149	18.20	1.41
8H-1, 145–150	19.36	0.94
9H-1, 145–150	21.50	1.40
10H-1, 145–150	24.78	1.57
11H-2, 145–150	28.08	0.70
12H-1, 145–150	31.38	0.56
13H-1, 145–150	35.38	0.37
14H-1, 145–150	37.98	0.76
15H-1, 145–150	41.28	0.86
16H-1, 145–150	44.58	1.73
17H-1, 96–101	47.88	2.02
18H-1, 145–150	51.18	3.90
19H-1, 145–150	54.09	3.02
20H-1, 145–150	56.68	5.94
21H-1, 145–150	59.98	4.84
22H-1, 145–150	63.28	4.20
23H-1, 145–150	66.58	1.76
24H-1, 145–150	69.88	1.50
25H-1, 145–150	73.18	0.93
26H-1, 121–126	76.50	0.62
28X-1, 78–83	78.53	0.12
347-M0059B-		
2H-1, 145–150	64.78	0.06
3H-1, 145–150	68.08	0.07
4H-1, 145–150	71.38	0.07
5H-1, 145–150	74.68	0.07
6H-1, 145–150	77.98	0.08
7H-1, 145–150	81.28	0.08
8H-1, 132–137	84.45	0.08
25P-1, 38–43	117.71	0.12
347-M0059D-		
1H-1, 145–150	1.48	4.17
2H-1, 145–150	3.28	2.69
2H-2, 145–150	4.78	1.84
3H-1, 145–150	6.58	2.34
3H-2, 145–150	8.08	2.68
4H-1, 145–150	9.88	2.37
4H-2, 145–150	11.38	1.81
5H-1, 145–150	13.18	2.16
5H-2, 145–150	14.68	2.23
6H-1, 145–150	16.48	2.51
6H-2, 145–150	17.98	2.03
7H-1, 145–150	19.78	2.27
7H-2, 145–150	21.28	2.03
8H-1, 145–150	23.08	2.46
9H-1, 145–150	26.38	1.63
10H-1, 144–149	29.67	2.13
11H-1, 145–150	32.98	1.47
12H-1, 145–150	36.28	1.26
13H-1, 145–150	39.58	1.14
14H-1, 145–150	42.88	2.15
15H-1, 145–150	46.18	1.14
16H-1, 145–150	49.48	0.54
17H-1, 144–149	52.77	1.26
18H-1, 145–150	56.08	1.40
19H-1, 145–150	59.38	2.12
20H-1, 145–150	62.68	6.18
21H-1, 145–150	65.98	7.11
22H-1, 145–150	69.28	4.54
23S-1, 145–150	72.58	2.13
24H-1, 145–150	75.88	1.23
25H-1, 145–150	79.18	0.81
26H-1, 145–150	82.48	0.48

Table T9. Interstitial water geochemistry, Site M0059. This table is available in **oversized format.**

Table T10. Sedimentary total carbon (TC), total organic carbon (TOC), total inorganic carbon (TIC), and total sulfur (TS), Site M0059. (Continued on next two pages.)

Core, section, interval (cm)	Depth (mbsf)	TC (wt%)	TOC (wt%)	TIC (wt%)	TS (wt%)
347-M0059A-					
1H-1, 7–9	0.07	6.55	5.75	0.80	1.12
1H-2, 103–105	2.54	7.53	6.29	1.24	1.10
2H-1, 119–121	4.49	8.61	7.54	1.08	1.54
2H-2, 48–50	5.28	9.29	8.15	1.14	1.63
3H-1, 75–77	7.65	8.81	7.59	1.22	1.78
3H-1, 117–119	8.07	8.37	7.16	1.21	1.60
3H-2, 77–79	9.16	7.32	6.14	1.18	1.72
3H-3, 14–16	10.03	7.08	5.72	1.36	1.79
4H-1, 40–42	10.60	6.89	5.79	1.10	1.84
4H-2, 137–139	13.07	5.89	4.99	0.91	1.59
5H-1, 92–94	14.42	6.74	5.62	1.13	1.51
5H-2, 92–94	15.91	6.97	5.62	1.36	1.72
6H-1, 56–58	17.36	7.13	5.66	1.47	1.88
6H-2, 56–58	18.86	6.96	5.36	1.60	1.85
7H-1, 73–74	20.83	6.37	5.20	1.17	1.48
7H-2, 77–78	22.36	6.32	5.04	1.28	1.33
8H-1, 92.5–94	24.33	6.40	5.14	1.26	1.27
8H-2, 62–64	25.91	6.50	5.06	1.44	1.25
8H-2, 101–102.5	25.52	6.87	5.36	1.52	1.18
10H-1, 80–81.5	30.80	5.84	4.46	1.39	1.28
10H-2, 136–137.5	32.86	6.29	4.51	1.78	1.02
11H-1, 23–25.5	33.53	6.16	4.63	1.54	1.08
11H-3, 77–78.5	36.27	5.77	4.63	1.14	1.44
12H-1, 105–106	37.65	5.66	4.25	1.41	1.32
13H-1, 104–106	40.94	5.15	3.60	1.54	1.52
13H-2, 114–116	42.54	5.56	3.66	1.90	1.21
14H-1, 45–46	43.65	5.44	3.69	1.75	1.25
14H-2, 115–116	45.85	6.06	4.51	1.55	1.31
15H-2, 48–49	48.48	5.48	4.75	0.73	0.36
17H-1, 100–102	54.10	4.60	0.34	4.26	0.20
18H-2, 84–86	57.64	2.98	0.38	2.61	0.13
19H-2, 28–30	60.38	2.81	0.33	2.47	0.14
20H-1, 82–83.5	62.72	2.96	0.38	2.57	0.13
21H-2, 36–37	67.06	3.43	0.54	2.88	0.14
22H-2, 106.5–108	71.07	4.27	0.38	3.89	0.25
23H-2, 47.5–49	73.78	4.52	0.36	4.16	0.21
24H-2, 86–88	76.77	4.46	0.45	4.01	0.17
25H-1, 86–88	79.26	4.45	0.38	4.07	0.32
25H-2, 44–45	80.34	4.08	0.56	3.52	0.40
25H-2, 86–88	80.76	4.21	0.40	3.81	0.62
26H-1, 100–102	82.70	3.27	0.76	2.51	0.44
28H-1, 45–46	83.65	2.83	0.44	2.39	0.33
347-M0059B-					
1H-1, 63.5–65.5	60.64	2.90	0.35	2.55	0.13
2H-1, 65–66	63.95	2.16	0.80	1.36	0.15
2H-2, 65–66	65.45	3.08	0.86	2.22	0.18
3H-1, 65–66	67.25	3.35	0.34	3.01	0.16
3H-2, 65–66	68.75	3.91	0.48	3.43	0.16
3H-3, 25–26	69.85	3.63	0.52	3.11	0.16
4H-1, 84.5–86.5	70.75	3.92	0.48	3.44	0.17
4H-2, 85–87	72.24	4.66	0.47	4.20	0.16
5H-1, 65–66	73.85	3.39	0.54	2.85	0.14
5H-2, 65–66	75.35	4.40	0.41	3.99	0.20
5H-3, 18–20	76.38	3.65	0.54	3.11	0.15
6H-1, 34.5–35.5	76.85	2.96	0.56	2.40	0.13
6H-3, 27–28	79.77	4.41	0.40	4.01	0.25
7H-1, 20–21	80.00	4.27	0.49	3.78	0.30
8H-1, 85–86.5	83.95	3.50	0.70	2.80	0.47
8H-2, 105–106.5	85.52	0.94	0.11	0.83	0.15
19H-CC, 3–4.5	107.31	3.60	0.42	3.18	0.25
25P-1, 13–14	117.43	2.27	0.25	2.01	0.44
29P-1, 26–27	203.79	11.82	0.00	11.82	0.10
347-M0059C-					
1H-1, 45–46	0.45	6.49	5.17	1.32	1.49
2H-1, 35–36	3.35	8.12	6.28	1.84	1.61

Table T10 (continued). (Continued on next page.)

Core, section, interval (cm)	Depth (mbsf)	TC (wt%)	TOC (wt%)	TIC (wt%)	TS (wt%)
3H-1, 37–38	6.67	8.72	7.14	1.58	1.76
4H-1, 30–31	9.90	7.53	6.33	1.20	1.61
4H-2, 107–108	12.17	6.40	5.02	1.38	1.65
5H-1, 60–61	13.50	5.92	4.59	1.33	1.45
5H-2, 120–121	15.60	7.08	5.44	1.65	1.36
6H-1, 80–81	17.00	7.11	5.66	1.45	1.50
7H-1, 57–58	20.07	6.21	5.00	1.20	1.54
7H-2, 54–55	21.54	6.59	5.57	1.02	1.29
8H-1, 59–61	23.39	6.66	5.21	1.46	1.32
8H-2, 106–108	25.36	6.41	5.01	1.39	1.33
9H-1, 36–37	26.46	6.00	5.34	0.66	1.36
10H-1, 20–21	29.60	6.13	4.73	1.40	1.36
10H-2, 95–96	31.85	5.77	4.46	1.32	1.21
11H-1, 15–16	32.85	6.09	4.67	1.42	1.36
11H-2, 92–93	35.12	5.80	4.79	1.01	1.28
12H-1, 72–73	36.72	5.71	4.39	1.32	1.27
12H-2, 90.5–91.5	38.41	5.62	4.04	1.58	1.54
12H-3, 38–39	39.38	5.91	4.51	1.40	1.45
13H-1, 66–67	39.96	5.33	3.71	1.62	1.87
13H-2, 70–71	41.50	5.34	3.69	1.65	1.54
13H-3, 26–27	42.56	5.09	3.64	1.45	1.47
15H-1, 50–51	44.02	5.27	3.66	1.61	1.21
15H-2, 130–131	46.32	6.15	4.49	1.65	1.45
16H-1, 80–81	47.62	6.33	4.66	1.67	1.89
16H-2, 130–131	49.62	5.95	4.64	1.31	0.27
17H-1, 110–111	51.22	7.93	3.36	4.57	0.20
18H-1, 16–17	53.58	4.69	0.46	4.23	0.17
18H-3, 8–9	56.50	4.76	0.47	4.29	0.20
19H-1, 110–111	57.82	2.82	0.37	2.45	0.12
19H-3, 21.5–22.5	59.94	3.35	0.36	2.99	0.12
20H-2, 13–14	61.65	3.62	0.40	3.22	0.12
20H-3, 25–26	63.27	2.55	0.45	2.10	0.13
21H-1, 100–101	64.32	2.57	0.86	1.72	0.16
21H-2, 125–126	66.07	3.08	0.33	2.75	0.14
22H-1, 109–110.5	67.71	3.95	0.46	3.49	0.18
22H-2, 90–91.5	69.02	3.58	0.55	3.03	0.16
23H-1, 119.5–120.5	71.12	3.64	0.53	3.11	0.18
23H-2, 90–91	72.32	4.85	0.37	4.48	0.17
24H-1, 70–71.5	73.92	3.81	0.50	3.31	0.17
24H-2, 120–121.5	75.92	3.61	0.49	3.12	0.20
26H-1, 100–101.5	80.82	2.10	0.27	1.83	0.24
27H-2, 10–11	83.83	0.89	0.10	0.79	0.12
56S-1, 28–29	124.90	2.23	0.24	2.00	0.45
58S-1, 10–11	126.22	1.72	0.29	1.43	0.40
62H-1, 36–37	130.98	1.38	0.24	1.13	0.33
63H-1, 22–23.5	131.94	1.53	0.26	1.27	0.36
63H-2, 81.5–83	134.05	1.48	0.14	1.35	0.34
64H-1, 22–23	134.94	0.98	0.15	0.83	0.29
66H-1, 83–84	136.53	1.16	0.32	0.84	0.28
66H-2, 73–74	137.93	1.11	0.03	1.08	0.51
70H-1, 11–12	141.81	1.08	0.03	1.05	0.19
70H-2, 47–48	143.67	1.76	0.07	1.69	0.27
347-M0059D-					
1H-1, 24–25	0.24	6.38	5.37	1.00	1.36
1H-2, 47–48	1.97	6.83	5.50	1.32	1.62
2H-2, 73–74	4.03	7.25	6.20	1.04	1.36
3H-1, 115–116	6.25	8.52	7.47	1.04	1.68
3H-2, 130–131	7.90	9.54	8.34	1.19	1.75
4H-1, 49–50	8.89	7.24	5.77	1.47	1.63
5H-1, 82–83	12.52	6.28	5.12	1.16	1.36
5H-2, 82–83	14.02	5.96	4.59	1.38	1.35
6H-1, 73–74	15.73	7.74	6.44	1.30	1.67
7H-1, 81–82	19.11	6.79	5.37	1.42	1.43
8H-1, 47–48	22.07	6.36	4.96	1.40	1.39
8H-3, 25–26	24.85	6.26	5.08	1.17	1.54
9H-1, 57–58	25.47	6.40	4.93	1.48	1.32
9H-2, 33–34	26.73	6.68	5.26	1.42	1.43
10H-1, 58.5–60	28.79	6.42	5.12	1.30	1.33
11H-1, 25–26	31.75	5.91	4.57	1.33	1.33

Table T10 (continued).

Core, section, interval (cm)	Depth (mbsf)	TC (wt%)	TOC (wt%)	TIC (wt%)	TS (wt%)
11H-2, 120–121	34.20	5.81	4.33	1.49	1.45
12H-1, 126–127	36.06	6.24	4.87	1.36	1.61
12H-2, 99–100	37.29	5.65	4.70	0.95	1.46
13H-1, 38–39	38.48	5.75	4.71	1.04	1.33
13H-2, 42–43	40.02	5.32	4.08	1.24	1.35
14H-1, 13–14	41.53	5.03	3.88	1.15	1.35
15H-1, 84–85	45.54	5.79	4.09	1.70	1.51
17H-1, 9.5–10.5	51.40	6.95	3.93	3.02	0.43
18H-1, 40–41	55.00	4.46	0.49	3.97	0.16
19H-1, 72–73	58.62	4.69	0.48	4.20	0.18
20H-1, 50–51	61.70	3.59	0.39	3.21	0.16
21H-1, 46–47	64.96	3.19	0.89	2.30	0.24
22H-1, 50–51	68.30	3.51	0.53	2.98	0.19
23H-1, 49–50	71.59	4.60	0.39	4.21	0.31
24H-1, 64–65	75.04	3.15	0.52	2.63	0.19
25H-1, 90–91	78.60	4.64	0.36	4.28	0.32
26H-1, 59–60	81.59	3.54	0.52	3.02	0.49
26H-2, 45–46	82.95	4.10	0.49	3.61	0.40
347-M0059E-					
1H-1, 10–11.5	0.10	6.35	5.44	0.91	1.59
2H-1, 45–46	3.75	7.77	6.50	1.27	1.31
3H-1, 50–51	7.10	8.96	7.40	1.56	2.01
4H-1, 50–51	10.40	7.52	6.17	1.34	1.54
5H-1, 50–51	13.70	5.95	4.97	0.98	1.47
6H-1, 28–29.5	16.78	7.31	6.21	1.09	1.56
7H-1, 34–35.5	20.14	6.67	5.44	1.23	1.61
8H-1, 67–68	23.77	6.35	5.08	1.27	1.35
9H-1, 40–41	26.80	6.35	5.15	1.20	1.37
10H-1, 65–66	30.35	5.87	4.55	1.32	1.20
11H-1, 53–54	33.53	5.70	4.45	1.25	1.33
12H-1, 58–59	36.88	5.95	4.71	1.25	1.58
13H-1, 42–43	40.02	5.35	4.30	1.05	1.46
15H-1, 54–55	46.74	6.37	4.85	1.52	1.26
16H-1, 47–48	49.97	5.80	5.23	0.57	0.86
17H-1, 98–99	53.78	4.64	0.45	4.20	0.22
18H-1, 75–76	56.85	4.81	0.46	4.35	0.22
19H-1, 65–66	60.05	3.17	0.35	2.81	0.16
20H-1, 78–79	63.48	3.77	0.43	3.34	0.15
21H-1, 76–77	66.76	2.17	0.91	1.26	0.16
22H-1, 74–75	70.04	4.17	0.51	3.66	0.21
23H-1, 50–51	73.10	4.32	0.36	3.96	0.27
24H-1, 50–51	76.40	3.65	0.48	3.17	0.21
25H-1, 44–45	79.64	4.55	0.37	4.18	0.29
26H-1, 50–51	83.00	4.44	0.36	4.08	0.37
27H-1, 49–50	86.29	3.76	0.71	3.05	0.41
35H-1, 24.5–26	98.05	2.78	0.16	2.62	—

Table T11. Samples taken for cell counts by flow cytometry and acridine orange direct count (AODC), Hole M0059C.

Core, section, interval (cm)	Top depth (mbsf)	Cytometer counts (log cells/cm^3)	AODC (log cells/cm^3)
347-M0059C-			
1H-2, 3	1.53	8.92	9.04
1H-2, 146	2.96	8.71	9.05
2H-2, 3	4.53	8.89	9.06
2H-2, 146	5.96	8.58	8.97
3H-2, 3	7.83	8.77	8.97
3H-2, 146	9.26		8.65
4H-2, 3	11.13	8.78	8.71
5H-2, 3	14.43	8.69	8.74
6H-2, 3	17.73	8.58	8.65
7H-2, 3	21.03	8.57	
8H-2, 3	24.33	8.76	
9H-2, 3	27.63	8.63	8.36
10H-2, 3	30.93	8.67	
11H-2, 3	34.23	8.18	
12H-2, 3	37.53	8.33	8.81
13H-2, 3	40.83	8.40	
14H-1, 61	43.21	8.26	
15H-2, 3	45.05	8.31	8.08
16H-2, 3	48.35	8.11	
17H-2, 3	51.65	8.06	
18H-2, 3	54.95	7.76	7.81
19H-2, 3	58.25	8.07	
20H-2, 3	61.55	7.91	
21H-2, 3	64.85	7.78	7.70
22H-2, 3	68.15	7.62	
23H-2, 3	71.45	7.63	
24H-2, 3	74.75	7.65	7.80
25H-1, 141	77.93	7.89	7.85
26H-2, 3	81.35	7.90	

Respective count data are presented in the last two columns in logarithmic format.

Table T12. Samples taken for cell counts by flow cytometry and acridine orange direct count (AODC), Hole M0059E.

Core, section, interval (cm)	Top depth (mbsf)	Cytometer counts (log cells/cm^3)	AODC (log cells/cm^3)
347-M0059E-			
1H-2, 2	1.52	9.64	9.27
1H-2, 146	2.96		9.11
2H-2, 2	4.82	9.38	9.07
2H-2, 146	6.26		8.83
3H-2, 2	8.12	9.38	8.92
3H-2, 141	9.51		8.83
4H-2, 3	11.42		8.83
6H-2, 2	18.02	9.10	8.92
12H-2, 3	37.83	8.86	
15H-2, 3	47.73	8.70	
15H-2, 146	49.16		8.38
16H-2, 146	52.47		8.33
17H-2, 3	54.33		7.67
17H-2, 146	55.76		7.91
18H-2, 3	57.62	8.05	
18H-2, 146	59.05		7.92
19H-2, 3	60.93		8.06
19H-2, 146	62.36		8.20
20H-2, 3	64.23		8.03
20H-2, 146	65.66		7.87
21H-2, 2	67.52	7.64	
24H-2, 3	77.42		7.45
25H-2, 2	80.72	7.93	
26H-2, 3	84.02		7.80

Respective count data are presented in the last two columns in logarithmic format.

Table T13. Prokaryote cell numbers determined from drilling fluid obtained while coring at four different depths, Hole M0059E.

Top depth (mbsf)	Cell numbers (log cells/mL)
4	6.05
26	5.71
47	5.79
56	5.90

Table T14. Drilling fluid contamination, Hole M0059E.

Core	Depth (mbsf)	PFC (g/L)	LF fraction in sample	Contaminant (cells/cm^3)
347-M0059E-				
Core interior				
1H	1.45	9.05E–09	1.85E–03	1.40E+03
2H	4.75	1.64E–08	2.45E–02	1.86E+04
3H	8.05	4.98E–10	2.49E–04	1.89E+02
4H	11.35	BD	NA	NA
5H	14.65	BD	NA	NA
6H	17.95	8.66E–10	6.29E–06	4.77E+00
7H	21.25	1.07E–09	1.41E–04	1.07E+02
8H	24.55	BD	NA	NA
9H	27.85	4.24E–09	7.03E–04	5.33E+02
10H	31.15	BD	NA	NA
11H	34.45	5.14E–09	3.33E–05	2.53E+01
13H	41.05	2.09E–08	1.26E–03	9.54E+02
15H	47.65	7.37E–10	1.63E–05	1.24E+01
17H	54.25	1.24E–09	3.59E–05	2.72E+01
19H	60.85	BD	NA	NA
21H	66.00	2.05E–09	3.93E–05	2.99E+01
23H	74.05	7.06E–10	5.51E–04	4.18E+02
25H	80.65	BD	NA	NA
Core halfway				
1H	1.45	5.19E–10	1.06E–04	8.06E+01
2H	4.75	1.69E–09	2.52E–03	1.91E+03
3H	8.05	BD	NA	NA
4H	11.35	3.76E–10	2.57E–05	1.95E+01
5H	14.65	4.61E–07	4.02E–02	3.05E+04
6H	17.95	6.13E–10	4.46E–06	3.38E+00
7H	21.25	1.37E–10	1.79E–05	1.36E+01
8H	24.55	5.23E–10	2.99E–04	2.27E+02
9H	27.85	1.21E–07	2.01E–02	1.53E+04
10H	31.15	BD	NA	NA
11H	34.45	2.66E–07	1.72E–03	1.31E+03
13H	41.05	3.83E–09	2.30E–04	1.75E+02
15H	47.65	3.89E–10	8.62E–06	6.54E+00
17H	54.25	BD	NA	NA
19H	60.85	BD	NA	NA
21H	66.00	BD	NA	NA
23H	74.05	BD	NA	NA
25H	80.65	BD	NA	NA
Core exterior				
1H	1.45	3.00E–09	6.13E–04	4.65E+02
2H	4.75	3.59E–08	5.36E–02	4.07E+04
3H	8.05	1.78E–08	8.89E–03	6.75E+03
4H	11.35	2.56E–09	1.75E–04	1.33E+02
5H	14.65	4.12E–07	3.60E–02	2.73E+04
6H	17.95	2.33E–06	1.69E–02	1.29E+04
7H	21.25	1.11E–08	1.46E–03	1.11E+03
8H	24.55	3.35E–08	1.91E–02	1.45E+04
9H	27.85	3.08E–08	5.10E–03	3.87E+03
10H	31.15	3.47E–09	6.54E–05	4.96E+01
11H	34.45	5.36E–08	3.47E–04	2.63E+02
13H	41.05	BD	NA	NA
15H	47.65	2.26E–09	5.01E–05	3.80E+01
17H	54.25	1.20E–06	3.48E–02	2.64E+04
19H	60.85	2.35E–09	2.66E–03	2.02E+03
21H	66.00	7.22E–09	1.39E–04	1.05E+02
23H	74.05	4.91E–09	3.83E–03	2.91E+03
25H	80.65	7.16E–08	2.20E–04	1.67E+02
Liner fluid				
1H	1.45	4.89E–06	NA	NA
2H	4.75	6.70E–07	NA	NA
3H	8.05	2.00E–06	NA	NA
4H	11.35	1.46E–05	NA	NA
5H	14.65	1.15E–05	NA	NA
6H	17.95	1.38E–04	NA	NA
7H	21.25	7.62E–06	NA	NA
8H	24.55	1.75E–06	NA	NA
9H	27.85	6.03E–06	NA	NA
10H	31.15	5.31E–05	NA	NA
11H	34.45	1.54E–04	NA	NA
13H	41.05	1.67E–05	NA	NA
15H	47.65	4.52E–05	NA	NA
17H	54.25	3.45E–05	NA	NA
19H	60.85	8.84E–07	NA	NA
21H	66.00	5.21E–05	NA	NA
23H	74.05	1.28E–06	NA	NA
25H	80.65	3.26E–04	NA	NA
Drilling fluid				
1H	1.45	1.16E–05	NA	NA
8H	24.60	9.25E–06	NA	NA
8H		4.64E–05	NA	NA
8H		4.66E–05	NA	NA
14H	42.90	1.31E–06	NA	NA
14H		1.33E–06	NA	NA
14H		6.69E–06	NA	NA
17H	54.30	1.52E–06	NA	NA
17H		1.54E–06	NA	NA
17H		1.46E–04	NA	NA
25H	80.70	5.39E–06	NA	NA
25H		8.75E–05	NA	NA
27H	85.80	1.84E–04	NA	NA
27H		1.82E–04	NA	NA

Samples taken from interior, halfway, or exterior positions in piston cores, in liner fluid, and in drilling fluid. The contaminant cell numbers in samples represent an estimated potential maximum. PFC = perfluorocarbon tracer, LF = liner fluid. BD = below detection. NA = not applicable.

Table T15. Composite depth scale, Site M0059.

Core	Offset (m)	Top depth (mbsf)	Top depth (mcd)
347-M0059A-			
1H	0.21	0.00	0.21
2H	–0.11	3.30	3.19
3H	0.24	6.90	7.14
4H	0.67	10.20	10.87
5H	0.67	13.50	14.17
6H	0.76	16.80	17.56
7H	0.76	20.10	20.86
8H	0.93	23.40	24.33
9H	1.48	26.70	28.18
10H	1.48	30.00	31.48
11H	1.35	33.30	34.65
12H	1.35	36.60	37.95
13H	1.35	39.90	41.25
14H	0.74	43.20	43.94
15H	1.64	46.50	48.14
16H	1.83	49.80	51.63
17H	1.83	53.10	54.93
18H	2.06	55.30	57.36
19H	2.06	58.60	60.66
20H	1.31	61.90	63.21
21H	1.31	65.20	66.51
22H	1.44	68.50	69.94
23H	1.44	71.80	73.24
24H	0.65	75.10	75.75
25H	0.45	78.40	78.85
26H	0.45	81.70	82.15
27X	0.45	83.20	83.65
28X	0.52	83.20	83.72
347-M0059B-			
1H	1.30	60.00	61.30
2H	0.70	63.30	64.00
3H	0.52	66.60	67.12
4H	0.50	69.90	70.40
5H	0.76	73.20	73.96
6H	0.57	76.50	77.07
7H	0.67	79.80	80.47
8H	–0.36	83.10	82.74
9X	–0.36	85.80	85.44
10X	–0.36	89.30	88.94
11X	–0.36	90.40	90.04
12X	–0.36	91.40	91.04
13X	–0.36	92.90	92.54
14X	–0.36	93.00	92.64
15X	–0.36	94.16	93.80
16X	–0.36	100.00	99.64
17X	–0.36	101.37	101.01
18X	–0.36	104.97	104.61
19X	–0.36	107.28	106.92
20X	–0.36	107.43	107.07
21X	–0.36	109.63	109.27
22X	–0.36	111.03	110.67
23X	–0.36	111.03	110.67
24X	–0.36	111.05	110.69
25P	–0.36	117.30	116.94
27X	–0.36	169.03	168.67
29P	–0.36	203.53	203.17
347-M0059C-			
1H	–0.02	0.00	–0.02
2H	–0.02	3.00	2.98
3H	–0.14	6.30	6.16
4H	–0.14	9.60	9.46
5H	–0.14	12.90	12.76
6H	–0.53	16.20	15.67
7H	–0.33	19.50	19.17
8H	–0.53	22.80	22.27
9H	0.15	26.10	26.25
10H	0.15	29.40	29.55
11H	0.48	32.70	33.18
12H	0.15	36.00	36.15
13H	0.30	39.30	39.60
14H	–0.39	42.60	42.21
15H	0.45	43.52	43.97
16H	–0.24	46.82	46.58
17H	1.10	50.12	51.22
18H	1.10	53.42	54.52
19H	2.01	56.72	58.73
20H	2.01	60.02	62.03
21H	0.96	63.32	64.28
22H	0.68	66.62	67.30
23H	0.68	69.92	70.60
24H	0.68	73.22	73.90
25H	0.68	76.52	77.20
26H	0.68	79.82	80.50
27H	1.32	82.23	83.55
28S	1.32	84.11	85.43
30S	1.32	87.12	88.44
32S	1.32	90.12	91.44
34S	1.32	93.12	94.44
36S	1.32	96.12	97.44
38S	1.32	99.12	100.44
40S	1.32	102.12	103.44
42S	1.32	105.12	106.44
44S	1.32	108.12	109.44
46S	1.32	111.12	112.44
48S	1.32	114.12	115.44
50S	1.32	117.12	118.44
52S	1.32	120.12	121.44
54S	1.32	123.12	124.44
56S	1.32	124.62	125.94
58S	1.32	126.12	127.44
60S	1.32	127.62	128.94
61H	1.32	127.62	128.94
62H	1.32	130.62	131.94
63H	1.32	131.72	133.04
64H	1.32	134.72	136.04
66H	1.32	135.70	137.02
67H	1.32	138.70	140.02
70H	1.32	141.70	143.02
71H	1.32	144.00	145.32
72S	1.32	144.50	145.82
74S	1.32	145.00	146.32
76S	1.32	146.00	147.32
78S	1.32	148.00	149.32
80S	1.32	153.00	154.32
82S	1.32	154.00	155.32
84S	1.32	158.00	159.32
347-M0059D-			
1H	0.00	0.00	0.00
2H	0.00	1.80	1.80
3H	0.00	5.10	5.10
4H	0.00	8.40	8.40
5H	0.00	11.70	11.70
6H	0.00	15.00	15.00
7H	0.00	18.30	18.30
8H	0.00	21.60	21.60
9H	0.00	24.90	24.90
10H	0.00	28.20	28.20
11H	0.00	31.50	31.50
12H	0.00	34.80	34.80
13H	0.00	38.10	38.10
14H	0.00	41.40	41.40
15H	0.00	44.70	44.70
16H	0.00	48.00	48.00
17H	0.00	51.30	51.30
18H	0.00	54.60	54.60
19H	0.00	57.90	57.90
20H	0.00	61.20	61.20
21H	0.00	64.50	64.50
22H	0.00	67.80	67.80
23H	0.00	71.10	71.10
24H	0.00	74.40	74.40
25H	0.00	77.70	77.70
26H	0.00	81.00	81.00
27H	0.00	84.30	84.30
28S	0.00	86.47	86.47
347-M0059E-			
1H	–0.22	0.00	–0.22
2H	0.30	3.30	3.60
3H	0.37	6.60	6.97
4H	0.37	9.90	10.27
5H	0.37	13.20	13.57
6H	0.37	16.50	16.87
7H	0.37	19.80	20.17
8H	0.37	23.10	23.47
9H	–0.52	26.40	25.88
10H	–0.52	29.70	29.18
11H	–0.52	33.00	32.48
12H	–0.52	36.30	35.78
13H	–0.52	39.60	39.08
14H	–0.52	42.90	42.38
15H	–0.52	46.20	45.68
16H	–0.52	49.50	48.98
17H	0.49	52.80	53.29
18H	0.49	56.10	56.59
19H	0.49	59.40	59.89
20H	0.48	62.70	63.18
21H	–0.38	66.00	65.62
22H	–0.38	69.30	68.92
23H	–1.27	72.60	71.33
24H	–1.27	75.90	74.63
25H	–1.27	79.20	77.93
26H	–1.94	82.50	80.56
27H	–1.94	85.80	83.86
28X	–1.94	88.80	86.86
29X	–1.94	91.80	89.86
30X	–1.94	92.80	90.86
31X	–1.94	93.80	91.86
32X	–1.94	94.80	92.86
33X	–1.94	95.80	93.86
34X	–1.94	96.80	94.86
35X	–1.94	97.80	95.86
36X	–1.94	98.80	96.86
37X	–1.94	99.60	97.66

Table T16. Splice tie points, Site M0059.

Hole, core, section, interval (cm)	Depth (mbsf)	Depth (mcd)		Hole, core, section, interval (cm)
347-				347-
M0059D-1H-2, 19	1.49	1.70	Tie to	M0059A-1H-1, 149
M0059A-1H-2, 144	3.16	3.16	Tie to	M0059D-2H-1, 135
M0059D-2H-2, 93	4.34	4.23	Tie to	M0059A-2H-1, 104
M0059A-2H-2, 129	5.98	5.98	Tie to	M0059D-3H-1, 88
M0059D-3H-2, 153	7.89	8.13	Tie to	M0059A-3H-1, 99
M0059A-3H-2, 113	9.90	9.76	Tie to	M0059C-4H-1, 29
M0059C-4H-2, 123	11.53	12.20	Tie to	M0059A-4H-1, 133
M0059A-4H-2,91	13.27	13.27	Tie to	M0059D-5H-1,157
M0059D-5H-2, 144	13.98	14.64	Tie to	M0059A-5H-1, 47
M0059A-5H-2, 114	16.80	16.80	Tie to	M0059D-6H-2, 30
M0059D-6H-3, 35	17.59	18.35	Tie to	M0059A-6H-1, 79
M0059A-6H-2, 90	19.97	19.97	Tie to	M0059D-7H-2, 16
M0059D-7H-3, 26	20.80	21.56	Tie to	M0059A-7H-1, 70
M0059A-7H-1, 158	22.44	22.44	Tie to	M0059D-8H-1, 83
M0059D-8H-2, 143	23.60	24.54	Tie to	M0059A-8H-2, 20
M0059A-8H-2, 117	27.01	27.01	Tie to	M0059D-9H-2, 60
M0059D-9H-4, 13	26.88	28.35	Tie to	M0059A-9H-1, 17
M0059A-9H-2, 20	29.88	29.88	Tie to	M0059D-10H-2, 19
M0059D-10H-4, 15	31.60	31.60	Append	Appended
M0059D-11H-3, 33	33.48	34.83	Tie to	M0059A-11H-1, 18
M0059A-11H-3, 69	37.54	37.54	Tie to	M0059D-12H-2, 123
M0059D-12H-3, 27	36.72	38.07	Tie to	M0059A-12H-1, 12
M0059A-12H-1, 74	38.69	38.69	Tie to	M0059D-13H-1, 59
M0059D-13H-3, 46	40.21	41.56	Tie to	M0059A-13H-1, 31
M0059A-13H-1, 68	41.94	41.94	Tie to	M0059D-14H-1, 53
M0059D-14H-3, 22	43.89	44.62	Tie to	M0059A-14H-1, 68
M0059A-14H-2, 83	46.27	46.27	Tie to	M0059D-15H-1, 157
M0059D-15H-3, 31	48.23	47.71	Tie to	M0059E-15H-2, 32
M0059E-15H-2, 117	46.71	48.35	Tie to	M0059A-15H-1, 20
M0059A-15H-3, 29	51.96	51.43	Tie to	M0059E-16H-2, 88
M0059E-16H-2, 119	51.67	51.67	Tie to	M0059D-17H-1, 36
M0059D-17H-3, 61	53.80	54.90	Tie to	M0059C-18H-1, 38
M0059C-18H-1, 62	53.32	55.15	Tie to	M0059A-17H-1, 21
M0059A-17H-1, 58	55.51	55.51	Tie to	M0059D-18H-1, 91
M0059D-18H-3, 20	55.64	57.70	Tie to	M0059A-18H-1, 33
M0059A-18H-2, 63	59.50	59.50	Tie to	M0059D-19H-1, 159
M0059D-19H-4, 10	59.41	61.48	Tie to	M0059A-19H-1, 81
M0059A-19H-1, 156	60.93	62.23	Tie to	M0059B-1H-1, 93
M0059B-1H-2, 151	64.32	64.32	Tie to	M0059D-20H-3, 11
M0059D-20H-3, 33	63.22	64.54	Tie to	M0059A-20H-1, 132
M0059A-20H-4, 9	66.48	66.48	Tie to	M0059D-21H-2, 48
M0059D-21H-3, 21	66.20	67.52	Tie to	M0059A-21H-1, 100
M0059A-21H-4, 14	69.82	69.82	Tie to	M0059D-22H-2, 51
M0059D-22H-2, 158	69.45	70.89	Tie to	M0059A-22H-1, 94
M0059A-22H-3, 21	73.15	73.15	Tie to	M0059D-23H-2, 55
M0059D-23H-3, 28	73.43	74.19	Tie to	M0059B-5H-1, 22
M0059B-5H-3, 23	77.19	77.19	Tie to	M0059D-24H-2, 129
M0059D-24H-3, 26	77.09	77.67	Tie to	M0059B-6H-2, 59
M0059B-6H-2, 154	80.12	80.12	Tie to	M0059D-25H-1,
M0059D-25H-4, 11	80.33	81.00	Tie to	M0059B-7H-1, 52
M0059B-7H-2, 129	83.27	83.27	Tie to	M0059D-26H-2, 77
M0059D-26H-3, 11	84.48	84.12	Tie to	M0059B-8H-1, 138
M0059B-8H-2, 42	84.53	84.53	Tie to	M0059D-27H-1, 23

Table T17. Sound velocity data for lithostratigraphic units, Site M0059.

Unit	Thickness of unit (m)	Sound velocity (m/s)*	TWT (ms)	Depth (m)	Depth (mbsf)
Seafloor	37.1	1475	0.050	37.1	0
Ia	47.1	1588	0.111	84.2	47.1
Ib	4.58	1672	0.115	88.78	51.68
II	0.05	**1581**	0.1152	88.83	51.73
III	31.47	1581	0.155	120.3	83.2
IV	6.92	1581	0.640	127.22	90.12
V	9	**1698**	0.174	136.22	99.12
VI	58.88	1698	0.244	195.1	158

* = sound velocities are based on values measured during the OSP. There are no sound velocity measurements from Units II and V. Sound velocities for these units have been estimated (bold values) using sound velocity measurements from deeper lithostratigraphic units. TWT = two-way traveltime.